Development of a free-air ozone control system and estimation of the ozone impacts on regional wheat production

（開放系オゾン濃度制御システムの開発と
オゾンがコムギ生産に及ぼす広域的影響の推定）

Tang Haoye

タン　ハオイェ

Development of a free-air ozone control system and estimation of the ozone impacts on regional wheat production

（開放系オゾン濃度制御システムの開発と
オゾンがコムギ生産に及ぼす広域的影響の推定）

2013

Institute of Soil Science
Chinese Academy of Sciences
Tang Haoye

Supervisor: Prof. Kazuhiko Kobayashi

ACKNOWLEDGMENTS

I wish to express my sincere respect and appreciation to Prof. Kazuhiko Kobayashi for his continuous encouragement and scientific guidance during my study in his laboratory at the University of Tokyo. Special thanks are extended to the other members of my thesis review committee, Prof. Masaru Mizoguchi, Prof. Kensuke Okada, Dr. Akira Miyata and Dr. Masayuki Takigawa for their valuable comments to improve my dissertation.

My profound appreciation goes to the members in the Institute of Soil Science, Chinese Academy of Sciences (ISSAS), in Nanjing, China, especially Prof. Zhu Jianguo, my home advisor, and Prof. Liu Gang, Prof. Han Yong who work with me in the FACE-O_3 experiments, and Prof. Shen Renfang, the director of ISSAS for their supports as well as assistance during my PhD research.

I thank Dr. Feng Zhaozhong of the Research Center for Eco-Environmental Sciences, Chinese Academy of Sciences. He generously spared his time, shared the data, and willingly cooperated in my research work.

I also thank Prof. Hiroki Oue of Ehime University, Japan for providing me with valuable suggestions, and Prof. Zhang Gongxuan of Nanjing University of Science and Technology for technical supports.

My thanks extend to the Japan Society for the Promotion of Science for providing me with the RONPAKU Fellowship (CAS-11012) to obtain the doctoral degree. I also acknowledge the Bureau of International Co-operation Chinese Academy of Sciences for supporting and coordination.

I am indebted to the members of Prof. Kobayashi's laboratory, Mr. Zhang Guoyou, Ms. Shen Yinyue and others for constantly supporting my work and sharing the fun time with me during my stay in Japan.

And last but not least, my deepest senses of gratitude go to my family, my wife Yue Jin and my son Tang Ziyan in Nanjing for their constant care and support for my life.

Tang Haoye

Tokyo, May 2013

EXECUTIVE SUMMARY

Tropospheric ozone (O_3) is regarded as the atmospheric pollutant that is most likely to threaten crop production across the globe due to its phytotoxicity and prevalence over important agricultural regions of North America, Europe and Asia.

In **Chapter 1**, I reviewed the previous studies that investigated O_3 impacts on global crop production. Since 1980s, numerous experiments have been conducted using open-top chambers (OTC) in North America and Europe to investigate the negative effects of O_3 on vegetation. However, previous studies indicated that plant growth performance in the enclosures of OTC may differ from that in ambient fields. In the absence of fully open-air field-scale treatment, there have been large uncertainties as to whether the effects of O_3 observed in the experiments are realized in farmers' fields. Being both an important agricultural production area and a region with very high industrial activities, the Yangtze River Delta (YRD) in China suffers from serious O_3 pollution, whose impacts on crop production had however been unknown. It was therefore needed to investigate the effects of elevated O_3 concentrations ([O_3]) on crop production in this region under the field conditions.

Our experimental site is located at Jiangdu county, Jiangsu province in northern YRD. This region is among the main rice and wheat producing areas of China, but there have been no long-term observations of [O_3]. Therefore, a study was conducted on "*characterization of the ozone pollution in agricultural fields of northern Yangtze River Delta*" as presented in **Chapter 2**. Long-term observations of surface [O_3] were conducted during 2007–2011, and extremely high [O_3] was frequently observed in May and June with the highest hourly mean of 144 ppb. The monthly 7-h (9:00-16:00 Chinese Standard Time) mean of [O_3] showed a bimodal pattern with peaks in June and October, and the 3-month AOT40 (accumulated [O_3] above a 40 ppb threshold) greatly exceeded the critical level established in Europe for protecting crop species from O_3 damages. Analyses of the wind direction and air mass trajectories showed that pollutants were carried from the industrialized area of YRD by the prevailing

wind, causing an increased [O_3] in spring, and that, in summer, frequent incursions of maritime air mass diluted the high [O_3] in the polluted air mass. Furthermore, it was found that extensive open burning of crop residues in central eastern China made a significant contribution to the peak [O_3] in June. Our study has thus demonstrated the serious O_3 pollution and its major determinants in the agricultural areas of the northern YRD.

The occurrence of elevated [O_3] at present and its projected increase in the future make a big threat to crop production in YRD. To investigate the O_3 impact on crops in the field conditions, I and my colleagues developed a "*Free-Air Concentration Enrichment System with Ozone (FACE-O_3)*" as described in **Chapter 3**. Using this system, rice and wheat plants were grown in ambient [O_3] (A-O_3) or elevated [O_3] (E-O_3) without any enclosures. The target [O_3] for the E-O_3 treatment was set at a level by 50% higher than [O_3] for the A-O_3 level. Ozone generated from pure O_2 and mixed with compressed air was released into the E-O_3 plots from a 14 meter diameter octagon. The gas release was controlled for each E-O_3 plot with an algorithm based on wind direction, wind speed and [O_3] at the center of the plot. For 1-min mean [O_3], the achieved elevation was within ± 20% of the target for 94% of time, and within ± 10% of the target for 73% of time on average across the years from 2007 to 2010. Comparison of ozone exposure regimes as characterized by M7 (seasonal mean daily 7-h [O_3]) and AOT40 indicated that this FACE-O_3 system can maintain elevated [O_3] in open field with modest alteration to the [O_3] regime to an extent comparable to that by OTCs. The FACE-O_3 thus provides a reliable means to study the impacts of [O_3] elevation on crops in the real-world field.

In order to quantitatively estimate the crop yield loss due to O_3, a "*flux–response relationship of wheat yield loss in subtropical China*" was established in **Chapter 4**, using the observations in the FACE-O_3 experiments. A stomatal conductance (g_{sto}) model for wheat in Europe was re-parameterized to fit to the local conditions. Compared to European model parameterizations, the main changes were that the VPD (Vapour Pressure Deficit) and radiation response functions were made less and more

restrictive, respectively, and that the temperature function was omitted. The revised g_{sto} model performed well with an r^2 value of 0.76. The slope and intercept of the regression between observed and estimated g_{sto} were not significantly different from 1 and 0, respectively. An O_3 uptake threshold of 12 nmol m^{-2} s^{-1} was judged most reasonable for the O_3 flux–wheat yield response relationship in subtropical China. It was also suggested that the Chinese wheat cultivars investigated in our study were more sensitive to O_3 than European cultivars with a comparison based on either O_3 flux-based or O_3 concentration-based relationship.

The new flux–response relationship was applied to the "*evaluation of the ozone-induced wheat production loss in China and India for the years 2000 and 2020*" as presented in **Chapter 5**. With surface [O_3] simulated by a high resolution (40 × 40 km) chemical transport model coupled with the Regional Emission inventory in Asia (REAS), we evaluated O_3-induced wheat production loss in China and India for years 2000 and 2020 using dose–response functions based on AOT40 and POD_Y (phytotoxic O_3 dose, accumulated stomatal flux of O_3 above a threshold of Y nmol m^{-2} s^{-1}). Two O_3 dose metrics (90-days AOT40 and POD_6) were derived from European experiments, and the other two (75-days AOT40 and POD_{12}) were from the FACE-O_3 experiment. Relative yield loss (RYL) of wheat in 2000 was estimated to be 6.4–14.9% for China, and 8.2–22.3% for India. POD_6 predicted greater RYL, especially for the warm regions of India, whereas the 90-days AOT40 gave the lowest estimates. For the future projection, all the O_3 dose metrics gave comparable estimates of an increase in RYL from 2000 to 2020 in the ranges of 8.1–9.4% and 5.4–7.7% for China and India, respectively. The lower projected increase in RYL for India may be due to conservative estimation of the emission increase in 2020. Sensitivity tests of the model showed that the POD_Y-based estimates of RYL are highly sensitive to perturbations in the meteorological inputs, but that the estimated increase of RYL from 2000 to 2020 is much more robust.

The findings in the preceding chapters are synthesized and the implications of the findings are discussed in **Chapter 6**. The findings have shown that the O_3 pollution in

agricultural fields of northern YRD is serious, and that aggressive measures must be taken to restrict the open burning of crop residues in addition to the controls over the industrial and municipal emissions. The FACE-O_3 has been shown to be an ideal means for investigating the O_3 effects on crops in the real-world conditions. A g_{sto} model and O_3 flux–wheat yield response relationship were established with the FACE-O_3 experiment, and they were confirmed to be more suitable to predict O_3 risk for wheat in YRD rather than those from Europe. The wheat production loss projected for China and India due to the increasing [O_3] is substantial beyond the uncertainties, and there is an urgent need for curbing the rapid increase of surface [O_3] in these regions.

Further research is warranted for protecting crop production from the increasing threats of surface [O_3] in Asia. An improved assessment of ozone impact on crops over Asia would require a network of field experiments across the Asian countries. The interactions between O_3 pollution and climate change will have to be explored for future projections of the O_3 impacts, since the on-going climatic warming would accelerate the O_3 producing reactions in the troposphere whereas the rising atmospheric CO_2 concentration would restrict the O_3 flux via the stomatal closure. Another target of research would be agronomic countermeasures such as breeding and nutrient management against the crop yield losses caused by increasing surface [O_3]. Such studies have been impractical in the small land areas available in OTC and other existing facilities. The FACE-O_3 system established in this study would serve as a very powerful platform for the future research as mentioned above, and thereby contribute to an improved food security in Asia and the world in the future.

TABLE OF CONTENTS

LIST OF TABLES

LIST OF FIGURES

LIST OF ABBREVIATIONS

A-O_3	Ambient [O_3]
AATSR	Advanced Along-Track Scanning Radiometer
AOT40	Accumulated [O_3] above a threshold of 40 ppb
API	Air Pollution Index
ATSR	Along Track Scanning Radiometer
CAAQS	Chinese Ambient Air Quality Standards
CEC	Central Eastern China
CHASER	CHemical Atmospheric general circulation model for Study of atmospheric Environment and Radiative forcing
CTM	Chemical Transport Model
E-O_3	Elevated [O_3]
EDGAR	Emission Database for Global Atmospheric Research
EMEP	European Monitoring and Evaluation Programme
ESA	European Space Agency
FAO	Food and Agricultural Organization of the United Nations
FACE	Free-Air Concentration Enrichment
GDAS	Global Data Assimilation System
GEIA	Global Emissions Inventory Activity
GFED	Global Fire Emission Database
g_{sto}	Stomatal conductance
HYSPLIT	Hybrid Single Particle Lagrangian Integrated Trajectory
IPCC	Intergovernmental Panel on Climate Change
LAI	Leaf Area Index
LRTAP	International Cooperative Programme on Mapping and Modelling under the UNECE Convention on Long-Range Transboundary Air Pollution
M7	7-h seasonal mean [O_3] during daytime
M12	12-h seasonal mean [O_3] during daytime

MODIS	Moderate Resolution Imaging Spectroradiometer
NCEP	National Centers for Environmental Prediction
NCP	North China Plain
NOAA	National Oceanic and Atmospheric Administration
OTC	Open-top chamber
PFC	Policy Failure Case
PLA	Projected leaf area
POD_Y	Phytotoxic O_3 dose, accumulated stomatal flux of O_3 above a threshold of Y nmol m^{-2} s^{-1}
PRD	Pearl River Delta
PPFD	Photosynthetic Photon Flux Density
PSC	Policy Success Case
RADM	Regional Acid Deposition Model
REAS	Regional Emission inventory in Asia
REF	REFerence case
RH	Relative Humidity
ROS	Reactive Oxygen Species
RY	Relative Yield
RYL	Relative Yield Loss
S-O_3	Scaled-up O_3, with constant 24% increase of the A-O_3
SR	Short-wave Radiation
SUM06	Accumulated [O_3] when it exceeds 60 ppb
TAR	Target Achievement Ratio
W126	Accumulated [O_3] with a sigmoidal weighting function
WPL	Wheat Production Loss
WRF	Weather Research and Forecasting
YRD	Yangzi River Delta

CHAPTER 1

INTRODUCTION

1.1 Ground-level ozone pollution

Fresh air is one of the very basic requirements for human wellbeing. However, in many countries of the world, air pollution seriously threats both human being and the environment (Akimoto, 2003). Tropospheric ozone (O_3) is regarded as one of the most important global air pollutants due to its toxicity and prevalence over North America, Europe and East Asia, with impacts on human health, crop production and natural ecosystems (Ashmore, 2005; Booker et al., 2009; Fuhrer & Booker, 2003). It is also an important greenhouse gas with a radiative forcing power since 1750 being next only to carbon dioxide (CO_2) and methane (CH_4) (IPCC, 2007).

Unlike many other air pollutants, O_3 is not directly emitted into the atmosphere, but is a secondary product of a sequence of photochemical reactions involving carbon monoxide (CO), volatile organic compounds (VOC) and nitrogen oxides (NO_x). Due to rapid increase of these O_3 precursors in particular the increased emissions of NO_x from human activities after the Industrial Revolution, background O_3 concentrations ($[O_3]$) in the mid-latitudes of Northern Hemisphere has doubled to about 30–35 ppb between the late 19th century and 1980s, and have since continued to rise over the past several decades at a rate of 0.5–2% per year (Vingarzan, 2004). In the absence of appropriate controls over the O_3 precursors emission, global $[O_3]$ are projected to further increase by 20-25% by the middle of this century (The Royal Society, 2008).

East Asia is one of the most rapidly developing regions in the world. Asian NO_x emissions, which contributed only in a minor fraction to global emissions during the 1970s, have increased rapidly since then and surpassed emissions from North America and Europe in the mid-1990s (Akimoto, 2003). As the biggest developing country in the world with rapid economic growth, China plays the dominating role in East Asian NO_x emissions in the last two decades (Streets & Waldhoff, 2000). Ohara et al. (2007)

reported a 70% increase in NO_x emission from 6.5 Tg in 1990 to 11.2 Tg in 2000 over China. In contrast, NO_x emissions have significantly decreased from 18 Tg (1990) to 12 Tg (1999) in Europe, and have slightly increased from 2.8 Tg (1990) to 3.2 Tg (1997) in Japan (Naja & Akimoto, 2004; Van Aardenne et al., 1999; Vestreng, 2001). These enhanced NO_x emissions over China should have a significant influence on the tropospheric O_3 levels not only around the emission source areas, but also on a regional to continental scale (Yamaji et al., 2007). However, in comparison to North America, Europe, and Japan, the long-term observations of surface [O_3] have been sparse, if not absent, in China.

Surface O_3 has been shown to exhibit pronounced temporal and spatial variations in different geographic locations controlled by a number of processes including photochemical reaction, stratosphere–troposphere exchange, deposition, and transport (Monks, 2000). In view of the importance of O_3 to air quality and atmospheric chemistry, many previous studies have devoted great effort to obtain in-situ measurements of surface O_3 and investigate the factors and processes affecting O_3 formation, accumulation, and transport on local, regional and global scales (Jonson et al., 2006; Lefohn et al., 2010; Logan, 1989; Monks, 2000; Pochanart et al., 2002; Solomon et al., 2000; Tanimoto, 2009). In the Yangtze River Delta (YRD) of China, which is one of the world's largest continental-scale Metro–Agro–Plexes (Wang et al., 2007a), systematic measurements of [O_3] are only concentrated in and around the big cities (Geng et al., 2008; Tu et al., 2007; Wang et al., 2006), or at a few rural sites in the southern YRD (Cheung & Wang, 2001; Luo et al., 2000; Wang et al., 2001). These studies have improved the knowledge of O_3 behaviors in the YRD, but our better understandings of the temporal and spatial distribution of surface O_3 in this region are still far from complete, especially in the northern YRD, where no long-term observations of O_3 are currently available.

The northern region of the Yangtze River Delta is less developed than the southern counterpart, but is one of the most important agricultural production areas of China. More than 70% of the food crop production in Jiangsu province is concentrated in this

region. Modeling studies have shown that the inflows from severely polluted areas of both the North China Plain (NCP) (northwesterly) and industrialized areas of the YRD (southeasterly) may cause high O_3 episodes under favorable weather conditions in the northern YRD (Takigawa et al., 2009; Yamaji et al., 2008; Zhao et al., 2009). In addition to the industrial and municipal impacts, extensive open crop residue burning after harvest in the vast agricultural fields are also demonstrated to enhance emissions of precursors e.g. NO_x and CO, hence [O_3] in this region, especially in June (Li et al., 2007; Streets et al., 2003; Yamaji et al., 2010). These modelling studies have indicated a big O_3 threat to crop production in northern YRD, however, as mentioned before, long-term observations of surface [O_3] are yet to be conducted in this region. Therefore, before investigating the O_3 impacts on agricultural crop in this major grain production areas of China, one question must be answered: "*What is the current situation of O_3 pollution in the northern YRD, and what are the determinants of [O_3] variation in this region?*" (**Question 1**).

1.2 The effect of ozone on crop production

Ozone has various effects on terrestrial ecosystem, such as reduction in vegetation growth and carbon sequestration, altering nutrient-use efficiency, modifying species composition and altering plant disease susceptibility. But the most important and best-documented effect is reduction in crop yield (Ashmore, 2005; Fuhrer, 2003). Many determinants of yield including photosynthesis, leaf area index (LAI), biomass, partitioning ratio and individual grain mass are affected by O_3 (Ainsworth, 2008; Biswas et al., 2008; Clarke et al., 1990; Feng et al., 2008; Kobayashi et al., 1992; Morgan et al., 2006). The mechanisms behind the effect of long-term O_3 exposure on crop yield have been presented and discussed by Fuhrer and Booker (2003), Fiscus et al. (2005) and others. In essence, the phytotoxicity of O_3 on plants arises primarily as a result of the oxidative damage to the plasmalemma (Heath, 1987). After being taken up into the leaf interior through the stomata, O_3 can react with the aqueous matrix associated with the cell wall (i.e. the apoplast) to yield a suite of reactive oxygen species (ROS) and hydrogen peroxide (H_2O_2), which, in addition to O_3, result in the

oxidation of sensitive components of the plasmalemma, and subsequently the cytosol (Fiscus et al., 2005; Long & Naidu, 2002). It decreases photosynthesis by impairing rubisco activity or stomatal conductance, and/or indirectly via onset of premature senescence and thus protein (rubisco) and chlorophyll degradation, particularly during the flowering stage (Fiscus et al., 2005; Morgan et al., 2004). Ozone can further inhibit reproduction by affecting pollen germination and tube growth, fertilization and abscission or abortion of flowers, pods and individual ovules or seeds (Black et al. 2000). Finally, O_3 impairs phloem loading and reduces assimilate partitioning from other organs to grain (Fuhrer & Booker 2003).

There are abundant evidences that current levels of surface [O_3] in many areas of the world are sufficiently high to reduce yields of major staple crops such as rice (Ainsworth, 2008; Feng et al., 2003), wheat (Legge et al., 1995; Wahid et al., 1995; Wang et al., 2005), soybean (Nali et al., 2002; Morgan et al., 2003) and potato (Clarke et al., 1990). A meta-analysis of 406 experimental observations around the world revealed that surface [O_3] at current ambient level (31–50 ppb) have induced an average yield loss of 11.3% in the range from 5% to 19% for the six major food crops including wheat, rice, potato, barley, bean, and soybean, as compared with those in the base [O_3] (< 26 ppb) (Feng & Kobayashi, 2009). Another meta-analysis of 53 published studies investigating O_3 effects on wheat between 1980 and 2007 indicated that elevated [O_3] of 72 ppb on average (range of 30–200 ppb) have decreased grain yield by 29% and above ground biomass by 18% in wheat, when compared with plants grown in charcoal filtered air (13 ppb [O_3] on average) (Feng et al., 2008). Although there are large differences in crop sensitivity to O_3 both within and between species (Mills et al., 2007), and the extent of the O_3 effects varies with different studies (Feng et al., 2008; Feng & Kobayashi, 2009; Morgan et al., 2003), these findings confirm that increasing [O_3] has become a serious threat to global food security, urging a global solution.

However, as indicated by Ashmore (2005), current knowledge of O_3 damage to crops are mostly derived from observations and experiments in North America and

Europe, and the investigation of the impacts of O_3 on crop grown is very limited in other regions. During the last decade, an increasing attention is being given to impacts of O_3 on crop production in the developing countries characterised by rapid urbanisation and industrialisation. In the YRD of China, Feng et al. (2003) firstly reported the O_3 damage to crops, and estimated that the yield losses in 1999 due to O_3 pollution were to be 10.0% and 2.8% for wheat and rice, respectively, which was calculated from dose–response functions based on local open-top chamber (OTC) studies and [O_3] data in that region. Another observational studies of surface O_3 suggested a greater yield loss of 20–30% for wheat grown in the YRD in 1999–2000, based on the dose–response relationships derived from North America and Europe (Wang et al., 2005). With the growing concern about O_3 pollution, a few studies were successively conducted in this region to investigate the O_3 effects on wheat (Yao et al., 2008; Zhu et al., 2011), rice (Pang et al., 2009; Shi et al., 2009; Zhan et al., 2008), and oilseed rape (Wang et al., 2008a). Recently, Wang et al. (2012a) summarized their 5 years' results from OTC experiments conducted in YRD, and indicated that the wheat and rice yield losses in their study were even more serious than in previous reports both domestically and from abroad.

1.3 Methodology: OTC vs. FACE

Most of the studies mentioned above are based on experiments carried out in open-top chambers (OTC) (Heck et al., 1988; Jäger et al., 1992; Legge et al., 1995). Typically, the cylindrical open-topped and transparent-walled chambers used for O_3 effects studies are placed over field plots of soil-grown plants and supplied with filtered air (to provide exposure to below ambient [O_3]), non-filtered air, or non-filtered air with ozone added (to provide exposures to elevated [O_3]). Despite being partially open to the atmosphere and carefully designed, the OTC facilities inevitably modify the growth conditions of the plants (Colls et al., 1993). The enclosure of chamber could alter the direct and diffuse solar radiation, increase the air temperature and vapour pressure deficit (VPD), thus affect the energy balance of the crop, plant growth and phenology development (De Temmerman et al., 2002; Fuhrer,

1994; Jetten, 1992; Olszyk et al., 1980; Piikki et al., 2008). The forced ventilation of chambers might influence the bulk resistance, and hence the movement of gaseous pollutant from the atmosphere to the plant plasmalemma (Jetten, 1992). In particular, previous studies have indicated that, because of the forced turbulence, the O_3 flux in such chambers is normally higher than that outside, even though without modification of [O_3] in the chambers (Nussbaum & Fuhrer, 2000; Pleijel et al., 1994). Furthermore, other obvious effects of an OTC include that wind is removed, preventing wind damage and dispersal of pathogens and pests, and that rainfall interception is decreased and soil–plant-atmosphere coupling is altered (McLeod & Long, 1999). Such changes in microclimate, and hence in growth characteristic, in OTC experiments have suggested artificial alterations to the real response of the plants to O_3 under field conditions.

These so-called chamber effects can be avoided with the Free-Air Concentration Enrichment (FACE). FACE technology is almost unanimously considered to provide the best means to expose plants to the elevated atmospheric concentrations with minimal alteration of microclimate and the soil–plant–atmosphere continuum (Long et al., 2004). Field experiments with FACE also allow treatment of a much larger area of crop than is possible within OTC. This advantage minimizes the influence of the edge effects that have a greater influence in chambers, and makes the agronomic trials to be better represented (Long et al., 2006; McLeod & Long, 1999). The possibility of controlled enrichment of atmospheric concentration in the field was first investigated with CO_2 in the 1970s (Harper et al., 1973), and paralleled a number of studies made to fumigate field plots with air pollutants such as sulphur dioxide (McLeod et al, 1991; McLeod et al, 1995). Technologically updated FACE systems have been developed to expose small to large field plots to elevated CO_2 concentrations under different natural conditions as reviewed by Kimball et al. (2002) and Long et al. (2006). This technology was also used for studies on ecosystem warming (Bridgham et al., 1999; Kimball et al., 2008).

In recent years, FACE experiment with O_3 has been applied in soybean (Morgan et

al., 2004, 2006; Betzelberger et al., 2010). With a 23% increase in [O_3] from an average daytime ambient 56 ppb to a treatment 69 ppb over two growing seasons, soybean yields were decreased by 20% (Morgan et al., 2006). Importantly, these results suggest that when treated under open-air conditions yield losses in soybean may be even greater than the large losses already reported in earlier chamber studies. It is thus vital to consider the implications of these findings for other crops including rice and wheat, which are the largest and second largest food crops in the world (FAO, 2010), providing more than half of the calorific intake of the world's population and up to 70% of the calorific intake of the population of Asia (Kiple & Ornelas, 2000). To date, however, scarcely any observations have been made on yield loss in rice and wheat exposed to elevated [O_3] under fully open-air conditions. In assessing the food production and security in East Asia with the projected great increases in [O_3] and huge populations, an improved investigation of the impact of O_3 on rice and wheat using FACE is clearly essential. In the development of a FACE-O_3 system, a crucial question must be addressed as to "*How closely can the FACE-O_3 system represent the future elevated [O_3] situation in the real world?*" (**Question 2**). This is because the validity of the experimental findings will be highly dependent on the system performance in reproducing the real−world environment.

1.4 Dose–response relationship

To quantitatively estimate O_3 effects on crops, we have to establish a link between certain pollutant index and the plant responses of concern. Since the 1980s, extensive O_3 fumigation experiments were carried out with OTC in the US (National Crop Loss Assessment Network, NCLAN) and in Europe (European Open Top Chamber Programme, EOTCP). The aim of these experiments was to establish crop-specific dose–response relationships which relate quantifiable mean or accumulative [O_3] indices to a reduction in the crop yield (Heck et al., 1988; Jäger et al., 1992; Legge et al., 1995). These programmes resulted in the derivation of robust dose–response relationships using different O_3 indices for a number of key agricultural crops.

In the NCLAN experiments, concentration-based indices of M7 and M12 (7-h

(9:00–15:59) and 12-h (8:00–19:59) daily mean [O_3], respectively) were initially used to characterize crop exposure (Heck et al., 1988). However, in the post-experimental data analysis, cumulative indices e.g. SUM06 (accumulated [O_3] when it exceeds 60 ppb) and W126 (accumulated [O_3] with a sigmoidal weighting function, see EPA, (1996) for detail) were thought to better fit to the yield loss observations, and thus were favored by most experts (Lefohn & Foley, 1992; Mauzerall & Wang, 2001; Tingey et al., 1991). Being different from US, Europe adopted another cumulative exposure index, AOT40 (accumulated [O_3] over a threshold of 40 ppb), as it has been found to have a strong relationship with O_3-inducd yield loss of many crop species, such as wheat, potato and soybean in different countries during the last two decades (Betzelberger et al., 2010; Mills et al., 2007; Sarkar & Agrawal, 2010; Wang et al., 2012a). Nevertheless, analysis of experimental data for wheat collected over several seasons in southern Sweden showed that there was a wide variation in the slope of the relationships between AOT40 and relative yield in different years (Pleijel et al., 2000). When the relative yield was related to the modelled stomatal O_3 uptake over the same period, most of the experimental data fell closely around a common line. It has thus been established that the use of the stomatal O_3 flux-based index would be superior to the exposure-based one in accounting for the crop yield loss due to O_3 (Ashmore et al., 2004).

Stomatal O_3 flux depends not only on [O_3] at plant height, but also on stomatal conductance which depends on species or genotype as well as on phenological and climatic factors (Ashmore et al., 2004; Danielsson et al., 2003; Fuhrer, 2000; Karlsson et al., 2007). In the last decade, multiplicative stomatal conductance (g_{sto}) models (Jarvis, 1976) were adopted and parameterized to estimate O_3 flux through stomata in order to more accurately assess O_3-induced yield loss, because internal O_3 exposure (inducing metabolic effects) is more harmful than external O_3 exposure (causing damage to the leaf cuticle) to plants (Emberson et al., 2000; Danielsson et al., 2003; Pleijel et al., 2000, 2004, 2007). These models are based on the Jarvis-type multiplicative model, which simulates the leaf g_{sto} variation as a simple function of

phenology and short-term effects of environmental factors like radiation, temperature, VPD and O_3. By using g_{sto} models, numerous studies have indicated that detrimental effects of O_3 have stronger relationships with cumulative flux-based dose than the exposure-based dose (e.g. AOT40) in many species, such as wheat, potato and silver birch (Danielsson et al., 2003; Pleijel et al., 2004; Uddling et al., 2004). Taking into account its advantages, flux-based method has been adopted in the Mapping Manual of the LRTAP Convention (LRTAP Convention, 2004, 2010) to assess O_3 risk for vegetation in Europe. The biologically relevant flux-based O_3 index i.e. POD_Y (phytotoxic O_3 dose, accumulated stomatal flux of O_3 above a threshold of Y nmol m^{-2} s^{-1}) is suggested to be a better indicator of O_3 effects in the field than AOT40 (Mills et al., 2011b).

Wheat (*Triticum aestivum* L) is the second largest food crop with an annual production of more than 650 million metric tons (Mt) (FAO, 2010), but is also among the O_3-sensitive crop species (Mills et al., 2007; Feng & Kobayashi, 2009). Relationship between cumulative stomatal O_3 uptake and yield loss for European wheat cultivars has now been established using combined data from OTC experiments across a range of soils and climatic conditions, and was proved to produce a better fit to measured yield reductions as compared with AOT40-based function (Danielsson et al., 2003; Pleijel et al ., 2004, 2007). Since the wheat cultivar, phenology, climate and pollutant exposure pattern are much different between subtropical China and Europe, a question may arise: "*How can the wheat yield loss in China be best related to the stomatal O_3 flux?*" (**Question 3**). However, until now, little information has been available on O_3 flux and flux–response relationships for wheat as well as other crops in China (Oue et al., 2011). The existing estimates of O_3 impacts on regional wheat productivity in China have been entirely based on the exposure-based index like M7 and AOT40 (Aunan et al., 2000; Wang et al., 2005; Wang & Mauzerall, 2004). Such estimates could be biased (Klingberg et al., 2011; Mills et al., 2011a; Simpson et al., 2007), and there is an urgent need to develop a flux–response relationship for China and make a more credible assessment of the wheat yield loss due to O_3 pollution.

1.5 Regional evaluation

Demonstration of the O_3 impact on present-day and future global crop production need an assessment of the magnitude and spatial distribution of O_3-induced yield loss of major crops over the important agricultural regions around the world. This work is crucial for global food security as the grain demand is expected to increase globally by 50% from 2010 to 2030 due to an increase in global population, rising living standards, and the expansion of global biofuel production (World Bank, 2007). Integrated assessment of O_3-induced reductions in crop yield is primarily dependent on modelling procedures by regional/global air chemical transport models that can provide a geographically broad-scale prediction of present-day and future [O_3] under different emission scenarios. The modelled [O_3] fields will be combined with dose–response relationships, crop distribution and growing season, to obtain regional and/or global estimates of the crop yield loss.

Using similar integrated assessment approaches, Aunan et al. (2000) and Wang & Mauzerall (2004) evaluated the O_3-induced yield losses of major crops in China and East Asia (China, Japan and South Korea), respectively, for the base year 1999 and projected losses for 2020. Both studies concluded that present-day surface [O_3] already causes substantial crop losses in this region (in particular for O_3-sensitive crops such as wheat and soybean) and that significant additional losses may be expected to reach 30% by 2020 under the emission scenarios considered. On a global scale, recent assessments revealed that the global yields of key staple crops e.g. rice, maize, wheat, and soybean have been reduced by 2–16% due to present-day O_3 exposure in 2000 (Avnery et al. 2011a; Van Dingenen et al., 2009), and O_3-sensitive crops e.g. wheat and soybean could see a further 10% decline in yields by 2030 if global O_3 precursor emissions continue to increase under the pessimistic A2 scenario of IPCC (Avnery et al. 2011b). Furthermore, these studies also indicated that there is a considerable regional variability in the projected global yield losses, and China and India in particular are on the cusp of substantial reductions in wheat production (Van Dingenen et al., 2009; Avnery et al. 2011a, b).

The above studies are important steps towards assessing O_3 risk to agricultural production regionally and globally, and provide evidences of potential aggravated reductions in crop yield in the near future. However, it is important to recognize the many limitations in these estimates. Firstly, they employ air chemical transport models and emission inventories with coarse temporal/spatial resolutions to predict O_3 exposure and most studies take no account of conversion of [O_3] at a reference height to canopy height. Secondly, they apply the dose–response functions derived from US or European OTC experiments, which have been suggested to under-predict the yield loss for Asian cultivars (Emberson et al., 2009; Wang et al., 2012a) and for the crops under open-air condition (Morgan et al., 2006). Most importantly, the use of exposure-based relationships, that relate yield loss to external [O_3] rather than the stomatal O_3 flux, may lead to systematic errors in the evaluation of the magnitude of the impacts on yield, and their spatial distribution.

In fact, the new flux-based approach has been applied in Europe for mapping the O_3 flux risk for vegetation, and exhibited considerably different geographical pattern as compared to that of exposure index i.e. AOT40 (Klingberg et al., 2011; Mills et al., 2011a; Simpson et al., 2007). Comparison of the estimated wheat yield loss between flux-based and AOT40-baesd methods for five grid cells representing each of five European climate zones also indicated a higher flux-based yield loss by an average factor of 1.5, varying with different climatic zones (Holland et al., 2006). However, such studies are yet to be done using flux-based approach to assess O_3 impact on crops in Asia.

As mentioned before, wheat is one of the most important food crop in the world. Nearly two-thirds of the world population depends on this crop for their primary diet. Being the two most populous countries, China and India are also the largest and second largest wheat producers in the world with an annual production of 115 Mt and 80 Mt, respectively (FAO, 2010), which being combined together account for 30% of the global wheat production and 67% of wheat production in Asia. The economic and social implications of the tremendous yield reduction in wheat of these two countries

could be very serious, not only for Asia, but for the world. As there is a large uncertainty in the previous studies (Aunan et al., 2000; Avnery et al. 2011a, b; Van Dingenen et al., 2009; Wang & Mauzerall, 2004), a more credible answer to this question "*How much of the wheat production in China and India have been/will be reduced due to present-day/future O_3*" (**Question 4**) by evaluation using flux-based method derived from FACE experiment in Asia is highly expected. Only with this solution, we can sent the correct signals to policy makers for taking measures to curb the rapid increase of surface [O_3] in this region.

1.6 Rationale and objectives of the present study

In years 2007–2012, I and my colleagues developed a Free-Air Concentration Enrichment system with ozone (FACE-O_3) at Jiangdu county, Jiangsu province in northern YRD. Long-term surface [O_3] observations were conducted in this system to obtain the up-to-date information of O_3 pollution in this region. Productivity of wheat and rice under elevated [O_3] and ambient [O_3] in the open-air field was observed to investigate the O_3 effects. With the findings of the FACE-O_3 experiment, the O_3 flux–response relationship for wheat was established to predict the yield loss. This relationship as well as other flux-based and exposure-based relationships derived from European OTC experiments were combined with a high resolution chemical transport model (CTM) to give a regional evaluation of O_3-induced wheat production loss in China and India at present and in the future.

In this thesis, the afore-mentioned questions are addressed in the relevant chapters.

The Question 1: "*What is the current situation of O_3 pollution in the northern YRD, and what are the determinants of [O_3] variation in this region?*" was addressed in Chapter 2 by a comprehensive analysis of five years' surface [O_3] observational data in northern YRD during 2007–2011. Meteorological data and backward air mass trajectories were used to analyze the influence of the Asian summer monsoon and associated long-range air mass transports on [O_3]. Measured [O_3] during high and low fire activity periods demarcated by satellite fire hotspot observations were compared

with each other to identify the contribution of biomass burning to [O_3] at the study site. Furthermore, the observed surface [O_3] data were also used for model evaluation of the CTM which was applied to regional wheat yield loss evaluation.

Chapter 3 addressed the Question 2: "*How closely can the FACE-O_3 system represent the future elevated [O_3] situation in the real world*?**"** with a series of systematic evaluations of the FACE-O_3 control performance. The temporal performance was measured by the fraction of [O_3] stayed within ± 20% and ± 10% of the target [O_3] and the mean ratio of measured [O_3] to target [O_3] during rice and wheat experiments across 2007–2010. The spatial performance was studied with the seasonal M7 and AOT40 distributions over the elevated [O_3] plots. Because artificial addition of ozone may alter the O_3 regimes in the experimental plots as compared with that in the real world. I also compared the O_3 regimes as characterized by the M7–AOT40 relationship between elevated, ambient, and scaled-up [O_3], as well as between FACE and OTC experiments.

Chapter 4 addressed the Question 3: "*How can the wheat yield loss in China be best related to the stomatal O_3 flux?***"** Firstly, a g_{sto} model of wheat in YRD region was developed and parameterized by using g_{sto} measurements from the FACE-O_3 experiment. With this g_{sto} model, relationships between cumulative stomatal O_3 uptake and wheat yield loss were derived and the performance of different cut-off flux thresholds was evaluated. The slope of the established O_3 flux–response relationship was compared with that from European OTC experiments to find whether there is significant difference in the flux–response of wheat yield loss to O_3 between YRD and European studies. The new flux–response relationship could be applied to O_3 risk assessment in subtropical regions of Asia.

The Question 4: "*How much of the wheat production in China and India have been/will be reduced due to present-day/future O_3*?" was addressed in Chapter 5 by a projection of O_3-induced wheat production loss in China and India for years 2000 and 2020 with both exposure-based and flux-based approaches. Present and future surface [O_3] were simulated by a high resolution (40 × 40 km) global–regional CTM system

coupled with the Regional Emission inventory in Asia (REAS). The estimates by using different O_3 dose metrics and corresponding dose–response relationships derived from European OTC and FACE-O_3 experiments were compared, and the possible reasons for their different performance were analyzed. Because the calculations of stomatal O_3 uptake are strongly dependent on the quality of the meteorological input data, the uncertainty from the possible biases in the meteorological inputs for flux-based evaluations was also analyzed.

Finally, Chapter 6 summarizes the results and limitations of the study, and discusses broader implication of the findings of this study. Therein, I tried to find an answer to the ultimate question: "*How can we protect the crop production in Asia from the deleterious impact of ozone pollution in the near future*?" See Fig. 1.1. for the entire structure of this dissertation.

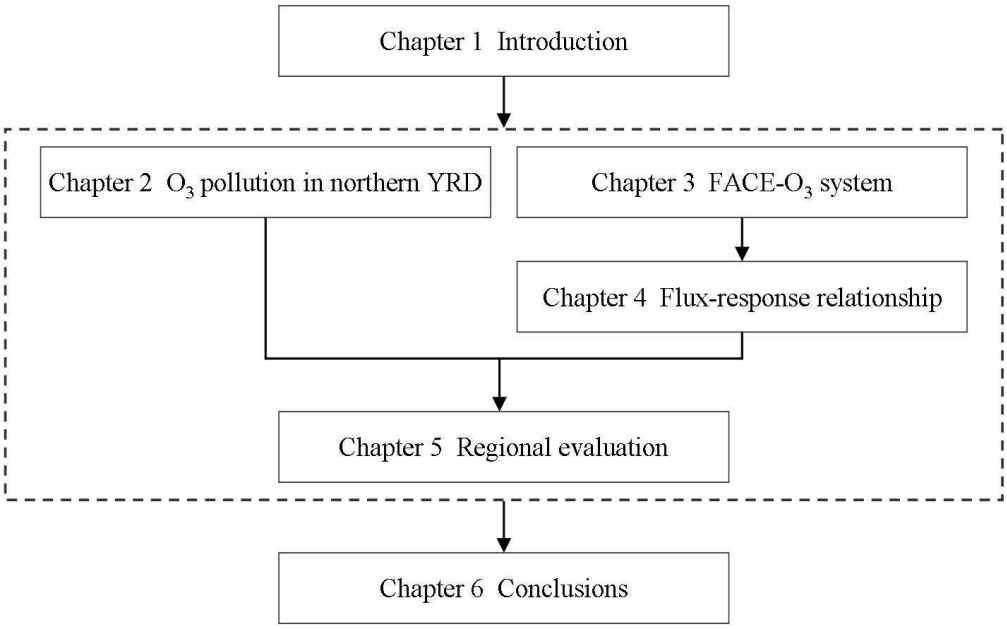

Fig. 1.1 Structure of the dissertation.

CHAPTER 2

CHARACTERIZATION OF THE OZONE POLLUTION IN AGRICULTURAL FIELDS OF NORTHERN YANGTZE RIVER DELTA

2.1. Introduction

China has experienced phenomenal economic growth in the past several decades. The economic expansion as well as rapid urbanization, industrialization and development of transportation have resulted in increasing consumption of fossil fuels, leading to increasing emissions of primary O_3 precursors, e.g. NO_x, CO and VOC (Ohara et al., 2007; Streets & Waldhoff, 2000). High concentrations of O_3 are thus associated with hot sunny weather and occur over many populated and industrial areas (Geng et al., 2008; Lam et a., 2005; Tu et al., 2007; Wang et al., 2006; Zhao et al., 2009). Neighbouring agricultural regions, especially downwind regions, are typically enveloped by regional pollution. One of these areas projected to be seriously affected is northern YRD, which is between the two of the most heavily polluted areas in China, southern YRD (on the southeast) and North China Plain (on the northwest).

In addition to the industrial and municipal impacts, extensive open crop residue burning after harvest in the vast agricultural fields is also demonstrated to further deteriorate the air quality over central eastern China (CEC) (Li et al., 2007; Streets et al., 2003; Yamaji et al., 2010). A modelling study has reported that the open crop residue burning increased the concentrations of primary pollutant e.g. CO, black carbon and organic carbon by 62–80%, and hence O_3 by 23% at Mount Tai (1534 m a.s.l.) in Shandong province (Yamaji et al., 2010), which is to the north of YRD.

On the other hand, the Asian summer monsoon is suggested to have significant effects on seasonal variability of O_3 in eastern China (He et al., 2008; Luo et al., 2000; Wang et al., 2001). The summer monsoon, with its typical maritime inflow, could reduce O_3 levels in many different ways, such as dilution of O_3 and its precursors by mixing between cleaner layers of the atmosphere, removal of pollutants by rainfall,

and reduction of photochemical production of O_3 by increased cloudiness (He et al., 2008; Wang et al., 2008b). Long-term measurements of [O_3] and its precursors (such as CO), coupled with backward trajectory analyses have elucidated the influence of long-range transport of air mass on [O_3] variations at many remote sites (Pochanart et al., 2002, 2003; Sikder et al., 2011; Suthawaree et al., 2008); however, these analyses did not include the northern YRD.

Being one of the most important crop producing areas in China, the northern YRD faces the big threat of increasing [O_3]. However, without multi-years in-situ observation on [O_3] coupled with investigation on its determinants makes it difficult to make a general statement on O_3 pollution in this region and set up prevention strategies. Therefore, in this chapter, we present results of surface O_3 monitoring at an agricultural site during 2007–2011. The objectives of this study are: (1) to characterize the seasonal variations of [O_3] in the northern YRD; (2) to analyze the influence of the Asian summer monsoon and associated long-range air mass transports on [O_3]; and (3) to identify the contribution of biomass burning to [O_3] at the study site.

2.2. Materials and methods

2.2.1. Site and meteorology description

Ground-based measurements were conducted at a rural site (119°45’ E, 32°35’ N, 5 m a.s.l.) in Xiaoji town, Jiangdu county, Jiangsu province, China. This site is located in an agricultural plain north of the Yangtze River (Fig. 2.1). It is 130 km northeast and 250 km northwest of the major population centers of Nanjing and Shanghai, respectively. Several small villages are sparsely spread within a 10 km range, but no industrial pollution sources exist nearby. From Jiangdu to the north are underdeveloped areas of Jiangsu province, and also one of the most important crop production regions in China. The main crops are wheat grown in winter and spring and rice grown in summer and autumn. According to the China Agriculture Yearbook 2010, the rice and wheat production in Jiangsu province are 18 and 11 million metric tons, respectively, and the northern regions take more than 70% of the contributions.

Being in the subtropical marine climatic zone, Jiangdu site is influenced by the Asian monsoon with a mean annual precipitation of 1100–1200 mm, a mean annual temperature of 16 °C, a total number of annual sunshine hours > 2000, and a frost-free period of > 230 days. Figure 2.2 shows the monthly variations of short-wave solar radiation (SR), air temperature (T), precipitation and relative humidity (RH) at Jiangdu site across the five years from 2007 to 2011. On average, more than 65% of the annual precipitation was concentrated in the three months from June to August. Although T was highest during the summer months, the high frequency of rainy and cloudy days sharply decreased SR and increased RH from June to September, both of which are unfavorable to photochemical production of O_3. In May, by comparison, the weather condition was conducive to O_3 production with increasing T and SR, little precipitation, and low RH. The most humid and driest months at Jiangdu site were found to be August and May, respectively.

2.2.2. Measurements of O_3 concentrations

Ground-based ambient [O_3] was continuously measured in alternating fashion at 5 heights (0.25 m, 0.5 m, 1 m, 2 m, and canopy height fluctuating from 0.3 m to 1.2 m with the crop growth) in the crop field using a UV photometry analyzer (Thermo Electron 49i, Thermo Scientific Co., USA). The O_3 analyzer was calibrated against a transfer standard (Thermo Electron 49i-PS, Thermo Scientific Co., USA) on an approximately monthly basis. The meteorological variables (T, RH, SR, precipitation, wind speed and direction) at 3 m above the ground were measured every 10 min at a weather station (AG3000, Campbell Sci., North Logan, Utah, USA) located at the same site. Raw data of [O_3] were recorded every 2 min from March 2007 to December 2011. Spurious data caused by an occasional miscalibration or system malfunction were removed manually. Failure of electricity sometimes occurred, resulting in additional gaps in the dataset. Therefore, the percentage of time in which accurate data was captured was about 93% for the whole study period from March 2007 to December 2011. The 2-min raw data at 2 m height were used to calculate the hourly average [O_3], which is used for the analyses in this study.

2.2.3. Satellite observations of biomass burning

The biomass burning in CEC is mainly open crop residue burning after harvest, concentrated in the months of May and June (Streets et al., 2003; Yamaji et al., 2010). Data of fire hotspot/activity were derived from the Moderate Resolution Imaging Spectroradiometer (MODIS) (MOD14 Level 2, Terra and Aqua) active fire data products (http://modis-fire.umd.edu/download/) (Davies, et al., 2009). The daily fire activity over central eastern China within the domain of 28º N–40º N and 112º E–124º E (12.0º × 12.0º) was counted during the study period of 2007–2011. The MODIS data includes daily global scale scanning with a greater detection rate than the Along Track Scanning Radiometer (ATSR) satellite data developed by the European Space Agency (ESA), which only operates during nighttime and completes global coverage every three days (Barbero et al., 2011). The daytime scanning of MODIS, however, includes the possibilities of false detection due to solar reflection by the land surface (Kaufman et al., 1998). Nevertheless, such false fires can be rejected by the use of an improved detection algorithm provided with MODIS fire data sets (Giglio et al., 2003). Thus, in the present study, we only used fires with detection confidence above 50%, which we presumed to be a reasonable mid-point between the accuracy and efficiency in detecting the small-scale and incomplete combustion of crop residues.

To demarcate the high and low fire activity periods over the study region, median values in May and June fire spot numbers over 2007–2011 are used as the criteria. *High fire activity periods* in May and June over 2007–2011 are defined as those periods when the fire count averaged across the previous 3 days exceeded the median value while the remaining periods are defined as *low fire activity periods*. In order to distinguish the impact of local meteorological conditions on O_3 production, the high and low fire activity periods are further subdivided into *sunny days* and *rainy days* with a simple criterion of daily precipitation being zero or not. According to these definitions, the total number of *high fire activity days* during the study period was 80 days in May and 112 days in June, with 69 and 92 of those days being *sunny days*, in May and June, respectively.

2.2.4. Air mass trajectory analysis

To identify the origins and transport pathways of the air masses arriving at the study site, 72-h backward trajectories were calculated by using the Hybrid Single Particle Lagrangian Integrated Trajectory (HYSPLIT) model Version 4.8 developed by the Air Resources Laboratory of the National Oceanic and Atmospheric Administration (NOAA), USA (Draxier & Hess, 1988). The meteorological input for the trajectory model was the GDAS (Global Data Assimilation System) data, which was processed by the National Centers for Environmental Predictions (NCEP) with 6-h temporal resolution, approximately 190 km horizontal resolution, and 13 vertical layers. For the whole O_3 monitoring period (from March 2007 to December 2011), backward trajectories arriving at 500 m above sea level were calculated twice a day, i.e., at 00:00 and 12:00 Chinese Standard Time (CST), with a time step of 1 h for HYSPLIT.

The accuracy and limitations of trajectory calculations have been investigated in several studies (Stohl. 1998; Kahl, 1996). In order to reduce the uncertainties of the trajectory analysis, one trajectory at the exact location of the Jiangdu site and four others displaced by ± 0.5º of latitude and longitude from the site were calculated at each arrival time. If the five trajectories did not follow the same flowing pattern, the trajectories at the time were not used for further analysis. The residual trajectories were assigned to 6 clusters using an automated K-means clustering algorithm (by maximizing between-group variance and minimizing within-group variance). The mean trajectory of each cluster was then calculated from its trajectory members and presented in Fig. 2.7. In order to control for self-consistency within the daily trajectory group, the two trajectories (arrival time at 0:00 and 12:00 CST) were pooled for each day. The daily trajectory groups whose two individual trajectories belonged to the same cluster were then matched with the daytime (9:00–16:00 CST) ozone data, and used for the analyses of $[O_3]$ variations in different air mass groups.

2.3. Results

2.3.1. The O_3 concentration level at Jiangdu site

The time series of daily 1-h maximum of [O_3] and 30-day running average of [O_3] observed at the study site during the period from March 2007 to December 2011 are presented in Fig 2.3. The pattern of seasonal change in [O_3] is obvious with lows in winter and highs in late spring and early summer. Compared with the Chinese Ambient Air Quality Standards (CAAQS, revised GB 3095–1996 of Chinese National Air Quality Standards), hourly O_3 levels at Jiangdu exceeding Grade II (0.2 mg/m^3, approximately 102 ppb at 1 atmospheric pressure and 25 °C) occurred in several months, with the highest frequencies in May and June. In total, there were 217 h during which the O_3 levels exceeded the Grade II value across the entire observation period. During year 2009, the Grade II value was exceeded for 11, 47 and 5 h in May, June and July, respectively, with the highest value of 144 ppb occurring in June. Across the 5 years, the daily mean (0:00-24:00 CST) of [O_3] ranged from 2.9 to 67.5 ppb with an average of 22.1 ppb and standard deviation (SD) of 19.3 ppb. The daily 7-h mean (9:00–16:00 CST) of [O_3] ranged from 6.3 to 117.7 ppb with an average of 36.2 ppb and SD of 20.0 ppb. The highest monthly mean [O_3] occurred in June 2009, with the values of 24-h mean and 7-h mean being 38.1 ppb and 67.3 ppb, respectively.

2.3.2. Intra-annual variations

Like many rural sites, [O_3] in Jiangdu shows typical diurnal cycles related to photochemistry, with maxima in the afternoon and minima in the early morning. The averaged amplitude of diurnal variation of [O_3] was about 40 ppb in summer as compared to only 20 ppb in winter, reflecting the more active photochemical production of O_3 in the summertime (Fig. 2.4). As the boundary layer is expected to get shallower and O_3 titration becomes stronger at night, nighttime observations may be sensitive to soil emissions over the field. Thus, for the analysis of seasonal variation of O_3 presented below, we focused on observations during the daytime (900–1600, CST), the typical period of elevated [O_3].

The average seasonal cycles of [O_3] at the study site are shown in Fig. 2.5 with the monthly statistical summary across 2007–2011. The monthly 7-h mean [O_3] increased gradually from 22 ppb in January to the peak value of 55 ppb in June, then decreased rapidly to exhibit a trough of 32 ppb around August. After attaining the second peak of about 39 ppb in October, the [O_3] gradually decreased toward the end of year. This bimodal pattern of O_3 has been widely reported in eastern China (Luo et al., 2000; Wang et al., 2001). The [O_3] peak in late spring and early summer reflects the contribution of photochemical production during the period of favorable weather conditions (increasing T and SR, in conjunction with low precipitation), and the drop of [O_3] during the period from July to September indicates the significant influences of Asian summer monsoon in this region (He et al., 2008; Wang et al., 2008b).

It should be noted that the hourly mean [O_3] shows the largest variability in June as indicated by the largest range of the box chart (Fig. 2.5). Although the mean value of hourly [O_3] in June (55.3 ppb) was higher than that in May (52.2 ppb), the median value of hourly [O_3] was slightly lower in June (48.8 ppb) than that in May (50.6 ppb). These features of the summary statistics may reflect the more episodic peaks of high [O_3] in June than in other months.

2.3.2.1. The influence of wind direction

In order to analyze the influence of wind on [O_3] seasonal variation, the dependence of seasonal average [O_3] on wind direction is presented in Fig. 2.6. Seasons are defined as follows: spring is March, April and May, summer is June, July and August, autumn is September, October and November, and winter is December, January and February. As can be seen in Fig. 2.6, the greatest concentrations of O_3 in spring are mainly associated with the wind from SSE, SE, and ESE, with the average [O_3] across these three sectors being 54.4 ppb, which is 36% higher than the average across all wind directions (39.9 ppb). For the summer and autumn months, however, no obvious association was found between greater concentrations of O_3 and the prevailing wind direction. In the winter, [O_3] tended to be a little greater in the wind direction of NE in comparison to other wind directions.

2.3.2.2. The influence of long-range transport

By clustering the backward trajectories over 2007–2011, we have identified six groups of air mass transport from different origins and/or having distinctly different transport paths; their mean trajectories are shown in Fig. 2.7. The seasonal and total frequencies of each air mass group arriving at the study site across the 5 year period are tabulated in Table 2.1, and the monthly variation of daytime (9:00-16:00 CST) [O_3] matched with each air mass group is shown in Fig. 2.8.

Cluster 1 (C1) and Cluster 2 (C2) represent air masses that originated from inland areas of Russia or Mongolia, and have passed through northern China quickly before reaching the study site. These two groups of air mass were dominant in winter (accounting for 55.6% of all the air trajectories), but were seldom observed in summer (accounting for 2.4% of all the air trajectories). Cluster 3 (C3) comprises the air mass coming from continental areas of northern China, whereas Cluster 4 (C4) represents the un-oriented loop trajectories meandering over the YRD at short distances. C3 and C4 accounted for 22.5% and 23.1% of all the air trajectories, respectively. The maritime air masses of Cluster 5 (C5) and Cluster 6 (C6) occurred predominantly in summer (about 70% of C5 and 90% of C6, respectively) with C5 originating in Japan, Korea and the surrounding ocean, and C6 originating in the South China Sea.

The [O_3] in C1 was a little lower than that in C2, although both originated from relatively clean inland areas (Pochanart et al., 2003) and showed similar transport paths. It should be noted that [O_3] of C1 was much higher in spring (36.8 ppb) than in autumn (28.2 ppb) and winter (26.3 ppb). As the air mass of C1 was mainly transported from low or middle troposphere (about 4000 m above ground level, see Fig. 2.7), the higher [O_3] in spring could be associated with the maximum stratosphere-troposphere exchange in spring (Monks, 2000). Since C3 and C4 represent air masses originating from highly polluted areas of northern China and YRD, it is not surprised that significantly higher [O_3] was observed in these groups of air masses compared to other groups (Fig. 2.8). The maritime air masses of C5 and C6 showed low [O_3] with monthly means of 29.5–37.9 ppb (C5) and 21.1–33.2 ppb (C6).

2.3.2.3. The influence of biomass burning

Across the 5 years of 2007–2011, the greatest monthly fire spot count from MODIS was consistently observed in June, with an average of 6955. The monthly fire spot count in May was the second highest, but the average was 2360, only 35% of that in June. It should be noted that the number of fire spots detected in 2008 was much lower than those in other years; in June of that year, the number was only 4359. Across the 5-year study period, the spatial distributions of fire spots over central eastern China were similar each year, with the highest density of the spots being located in the regions northwest of Jiangdu (see Fig. 2.9 of year 2010 for example).

The average value of daytime (9:00-16:00 CST) [O_3], T, SR and RH during different fire activity and weather condition periods in May and June over 2007–2011 are shown in Fig. 2.10. During the period of high fire activities, [O_3] was higher than that during low fire activities by 10% and 7% on sunny days and rainy days, respectively, in May, and by 39% and 27% on sunny days and rainy days, respectively, in June. On the other hand, no significant differences in T, SR or RH were found between the high fire activity and low fire activity periods for both sunny and rainy days.

2.3.3. Inter-annual variation and its determinants

The seasonal pattern of [O_3] at the study site changed slightly from year to year. In 2007 and 2008, the monthly 7-h mean [O_3] peaked in May, whereas in other years the peak was found in June. This year-to-year variation in the seasonal pattern may be related to the inter-annual variation of meteorology and precursor emissions such as biomass burning.

Monthly 7-h mean [O_3] in June for 2007, 2008 and 2010 was 52.4, 42.2 and 51.2 ppb, respectively, and much lower than in 2009 (62.6 ppb) and 2011 (65.3 ppb). The inter-annual variation in the mean 7-h [O_3] was correlated with that of maritime air mass (C5, C6) occurrences in June: 45.7%, 52.5% and 55.0% for 2007, 2008 and 2010, respectively, as compared with 23.1% and 26.7% for 2009 and 2010,

respectively (Fig. 9). The lowest value of 7-h mean [O_3] in June among the five years occurred in 2008 (42.2 ppb), and can be associated with the lowest number of fire spots (4359), which is almost 40% lower than the average value of fire counts for June in other years.

2.4. Discussion

2.4.1. The O_3 concentration level at the study site

Our measurements of [O_3] at the Jiangdu site showed an hourly [O_3] exceeding the CAAQS Grade II (approximately 102 ppb) for 217 h during the study period from March 2007 to December 2011. The frequent occurrence of high [O_3] (above 102 ppb) is comparable to the results of measurements in and surrounding big cities in China (Geng et al., 2008; Lam et al., 2005; Shan et al., 2008; Tu et al., 2007), and confirms the existence of serious O_3 pollution in this major agricultural area.

In comparison with the major field measurement campaigns at several rural sites in the YRD during 1999–2000 (Cheung & Wang et al., 2001; Wang et al., 2001; Wang et al., 2006), the annual mean of [O_3] over all 5 years at our study site (22.1 ± 19.3 ppb) was a little lower than those in the reported results (22.5–35.3 ppb). Although the geographic location of the measurement and increase in NO_x emission during this past decade (Xu et al., 2008) should be considered in this comparison, the difference in the underlying surface of the measurement site may also have made some contributions. Since our measurements were conducted within a crop field, the O_3 uptake by vegetation as well as deposition onto soil underlying the vegetation should be considerable (Emberson et al., 2000; LRTAP Convention, 2010).

With respect to the detrimental effects of O_3 on crops, the 3-month AOT40 for a typical wheat season (March, April and May) and rice season (July, August, and September) were 7.5 ± 2.5 ppm h and 6.3 ± 2.7 ppm h, respectively, on average across the five years from 2007 to 2011. These AOT40 values correspond to 150% (wheat) and 110% (rice) exceedance of the critical level of 3 ppm h for protecting crops as proposed by the European Monitoring and Evaluation Programme (EMEP). It is

worth noting additionally that the calculation of AOT40 values did not include June which had the highest [O_3] level, and that the potential impact of O_3 on crop production in this region may become even larger with shifting cropping calendars due to global climate change (Teixeira et al., 2011).

2.4.2. Climate and atmospheric transport as major determinants of [O_3]

In spring, [O_3] tended to be higher with the prevailing wind at the study site (Fig. 2.6). One reasonable explanation could be that the levels of industrialization and urbanization are distinctly higher in the region that is southeast of the study site (see the NO_2 column distribution in Fig. 2.1), and, hence, the wind coming from these directions would bring more pollutants to the study site. In addition, the wind coming from the southeast in spring is usually associated with higher temperature and intense solar radiation in Jiangdu, which is conducive to O_3 production. In contrast, in summer, there was no obvious association between high [O_3] and wind direction, due possibly to the increase of strong convective weather, especially with the influence of rainfall. Numerous rainy days during summer may have weakened the effects of the horizontal transport process by scavenging the O_3 precursors (i.e., wet deposition), and suppressed the photochemical production of O_3 (Shan et al., 2008). [O_3] is generally lower in winter than in other seasons for all wind directions, because O_3 production becomes weak and high NO accumulation in the YRD may consume O_3 through chemical reactions (Geng et al., 2008). When NE winds transported fresh maritime air to Jiangdu leading to a dilution of NO, [O_3] rose compared to other wind directions.

Besides the analyses of the dependence of [O_3] on wind direction, the trajectory analysis also indicated that the transport from the YRD makes the most contribution to the high [O_3] through the regional looped air mass group (C4). Additionally, the transport from the middle troposphere may aggravate the ozone pollution in the YRD, particularly in summer. Satellite observations have revealed elevated levels of ozone in the middle troposphere over East Asia (Nakatani et al., 2012), and Middle East and North Africa (Liu et al., 2009) during the Asian summer monsoon. The [O_3] for C5

and C6 trajectories were much higher than the [O_3] reported for maritime air masses from the northwest Pacific Ocean (Pochanart et al., 2002) and South China Sea (Wang et al., 2009a) due to the inevitable pollution from inland areas on their way to Jiangdu. Yet, the frequent incursion of maritime air mass contributed to the depression of O_3 in summer, especially in July, August and September. It should be noted that the low levels of [O_3] in maritime air groups cannot be solely attributed to the clean air with less O_3 and its precursors from ocean because the inflow of maritime air mass are usually associated with rainy and cloudy weather, which are very adverse conditions for the photochemical production of O_3.

The variation of the maritime air masses also contributes to the inter-annual variation in [O_3] as seen in [O_3] in the month of June, whose year-to-year change was consistent with occurrences of maritime air masses. This can be explained in part by the strong dilution of O_3 and its precursors with clean air masses of marine origin. Another important aspect is that the summer monsoonal circulation can also determine the local and regional weather through processes such as weakening atmospheric stability, driving large scale circulations, and increasing humidity and cloud formation. All of these weather conditions have major impacts on the mixing scale of various pollutants and the formation of O_3 in central eastern China (He et al., 2008; Zhao et al., 2009). Since year-to-year fluctuations of anthropogenic emissions are usually small across a few years (Ohara et al., 2007), it is mostly the meteorological pattern that contributes to a heavy O_3 episode at the local or regional scale in a specific year (Xu et al., 2011).

2.4.3. Contribution of biomass burning to [O_3]

Biomass burning has been recognized as an important source of several trace species (such as CO, NO_x, and black and organic carbon particles), and contributes to the air quality degradation at local to global scales (Galanter et al., 2000; Andreae & Merlet, 2001; Streets et al., 2003). The contribution of biomass burning to elevated [O_3] in the boundary layer has been documented by observational and modeling studies at various sites (Kumar et al., 2011; Li et al., 2007; Yamaji et al., 2010). In this

study, the increase of [O_3] during high fire activity periods was estimated to be 39% on sunny days and 27% on rainy days, in June, and 10% on sunny days and 7% on rainy days, in May. Since the main meteorological factors did not differ significantly between the high and low fire activity periods, the increase of [O_3] could be attributed to the burning of crop residues after harvest. The estimated [O_3] increase in June at Jiangdu is comparable to that at Mount Tai (1534 m a.s.l.) in Shandong Province (26%) (Yamaji et al., 2010); however, in May, the value at our site was much lower than at Mount Tai. The difference between May and June is presumably due to the much higher fire activity in June than that in May. In fact, the meteorological conditions may be more favorable to photochemical O_3 production in May (highest SR, lowest RH and less precipitation) than in June. The fact that, during the low fire activity periods on sunny days, [O_3] in May (53.5 ppb) was higher than in June (45.4 ppb), supports our assumption (Fig. 2.10a). The extensive biomass burning in June provides abundant O_3 precursors, and strengthens the O_3 production under favorable weather conditions on the sunny days. In addition, the 27% increase of [O_3] in June on rainy days, when the in-situ photochemical production is suppressed, may imply an enhancement of background [O_3] caused by biomass burning within this region.

Since the measurements of O_3 precursors (both gases and aerosols) released by the biomass burning were not available at our study site, we used the air pollution index (API, obtained from China National Environmental Monitoring Center http://www.cnemc.cn/) to assess the level of air pollution caused by the open crop residual burning (Xue et al., 2012). The API is calculated from observed data of three trace species (PM10, NO_2, and SO_2) using certain formulae. During the period of high fire activity in May and June over 2007–2011, the average API in Yangzhou was 107 ± 35 (mean ± SD), which is significantly higher than the value of 61 ± 18 (mean ± SD) during the period of low fire activity. Yangzhou is a city located about 40 km southwest of the Jiangdu site. Given these factors, a large enhancement of those trace species as well as other O_3 precursors (such as CO, PANs) due to the biomass burning is thus strongly suggested for this region.

In contrast to the maximum [O_3] observed in May at Lin'an (119°44' E, 30°18' N, 139 m a.s.l., see Fig. 2.1 for location) in the southern YRD (Wang et al., 2001; Xu et al., 2009), [O_3] exhibits a peak in June at Jiangdu. Since Jiangdu is located in the north of the YRD, a larger number of open crop residue burnings could cause much greater O_3 enhancement in Jiangdu than in Lin'an following the harvest of winter wheat in the North China Plain, which is China's largest wheat production area.

The contribution of biomass burning to surface [O_3] is also evident in the inter-annual variation of [O_3]. In June 2008, concurrent with the lowest number of fire spot counts, the monthly mean 7-h [O_3] was also the lowest among the five years of the study. This significant decrease of fire spots could be explained by the enactment of a strict policy against open straw burning in preparation for the Beijing Olympic Games in 2008. A series of aggressive measures to reduce pollutant emissions for the Olympic Games have been proven to have significantly reduced the boundary layer O_3 and other pollutants over a large region of the North China Plain and central eastern China in 2008 (Wang et al., 2009b).

2.5. Conclusions

Our 5 years (2007–2011) of measurements showed a frequent occurrence of high hourly [O_3] exceeding the CAAQS Grade II (approx. 102 ppb) in May and June at our study site in Jiangdu. The 3 month AOT40 greatly exceeded the critical level for protecting crop species from O_3 damage. Since the measurements were conducted within the context of typical agricultural land use, the observed [O_3] levels should reasonably represent the situation for a large part of the northern YRD, and the data implies a serious threat of O_3 pollution to the crop production in this region, which is considered one of the major agricultural regions in China.

The monthly 7-h mean of [O_3] showed a bimodal pattern in the seasonal change with peaks in June (54.6 ± 25.3 ppb) and October (39.4 ± 18.0 ppb). The seasonal change pattern was mainly due to the meteorological conditions. The prevailing wind from the industrialized area of the YRD may have contributed to the rise of [O_3] in

spring, whereas the monsoonal climate in summer led to more rainy and cloudy days with weather conditions adverse to photochemical O_3 production. Furthermore, the backward trajectory analysis suggested that the frequent incursions of maritime air mass diluted the high [O_3] in the polluted air masses and contributed to the depression of [O_3] in the summertime. The variation in maritime air mass incursion was also partially responsible for the inter-annual variation of [O_3].

Our study also found that the extensive open crop residue burning in central eastern China was a significant contributor to the peak [O_3] in June. The enhancement of [O_3] by the open crop residue burning was estimated to be 39% on sunny days and 27% on rainy days in June. The worse air quality as indicated by higher API during the high fire activity periods also suggested a large emission of O_3 precursors from biomass burning within the study region. The lowest [O_3] in June among the 5-year period occurred in 2008, and could be attributed to the lack of residue burning events along with the greater incursion of maritime air mass in that year. Further studies with observational data on other trace species (such as CO, NO_x) are warranted for a comprehensive investigation of the processes affecting O_3 formation and accumulation in our study region.

Table 2.1 Seasonal frequency of each air mass group reaching the study site in Jiangdu in 2007-2011. For the back-trajectory clusters of C1 to C6, see Fig. 2.7.

Season	Frequency (%)					
	C1	C2	C3	C4	C5	C6
Spring	12.8	17.9	25.7	26.6	6.3	—
Summer	—	2.4	10.1	32.8	31.2	11.5
Autumn	15.6	14.2	37.6	14.7	7.1	1.3
Winter	22.1	33.5	16.8	18.3	—	—
Whole year	12.6	17.0	22.5	23.1	11.1	3.2

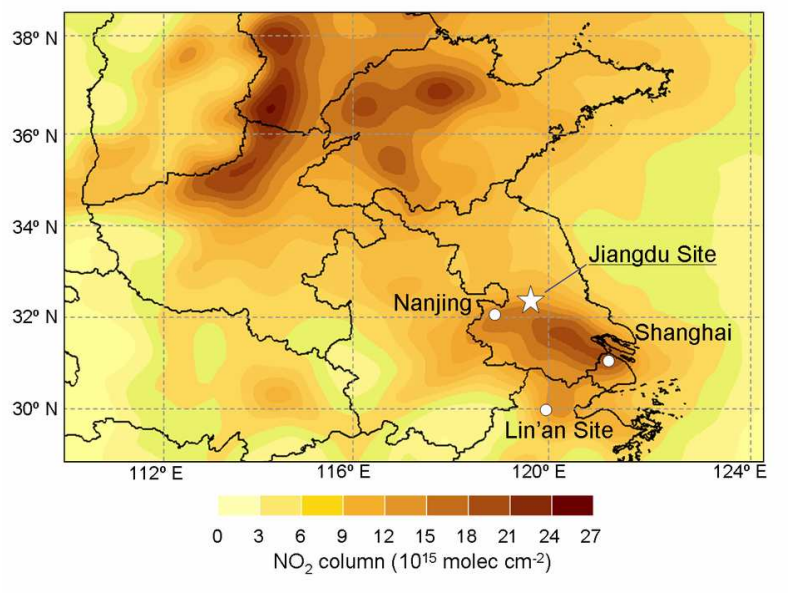

Fig. 2.1 Tropospheric NO_2 column distribution (averaged over 2007-2010) over central eastern China and Yangtze Delta. The study site in Jiangdu is indicated as a pentacle, and the Shanghai city, Nanjing city and the Lin'an site are indicated as circles. NO_2 column Data were obtained from EOS Aura Ozone Monitoring Instrument (OMI) in NASA's Aura Validation Data Center (http://avdc.gsfc.nasa.gov/Data/Aura/OMI/OMNO2/).

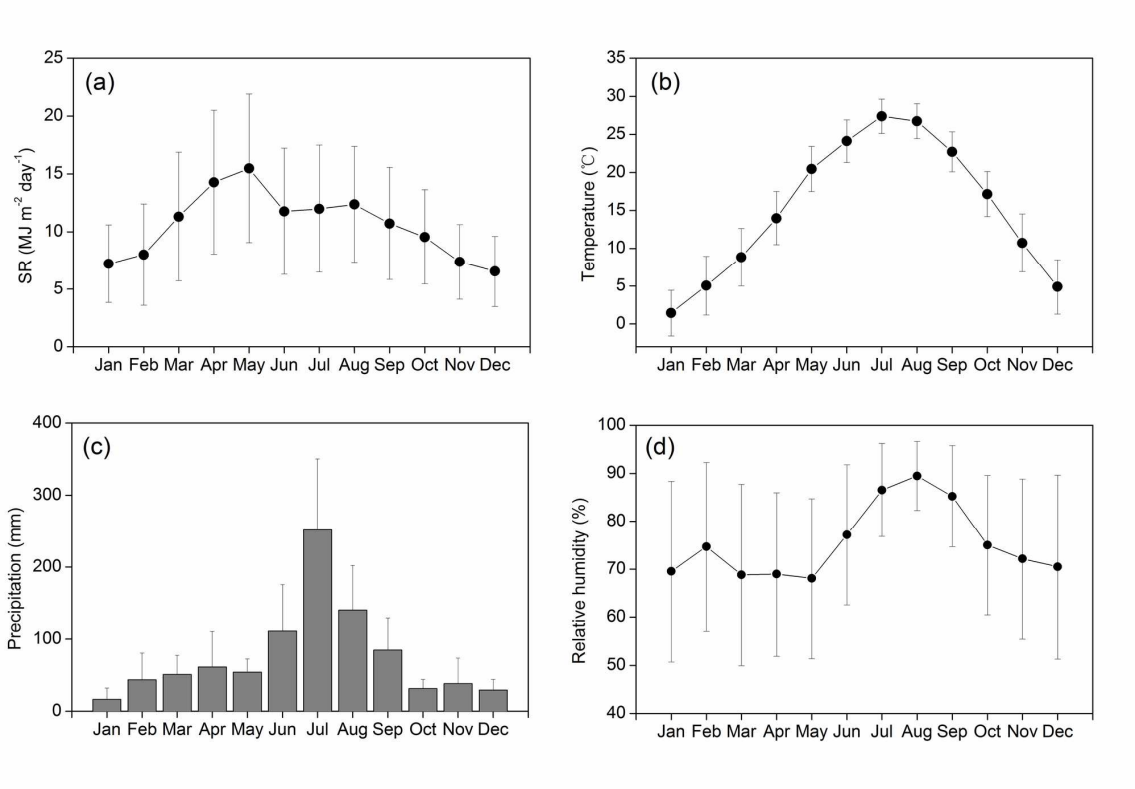

Fig. 2.2 Monthly variations of mean daily short-wave solar radiation (a), air temperature (b), precipitation (c), and relative humidity (d) over 2007-2011 at the Jiangdu site.

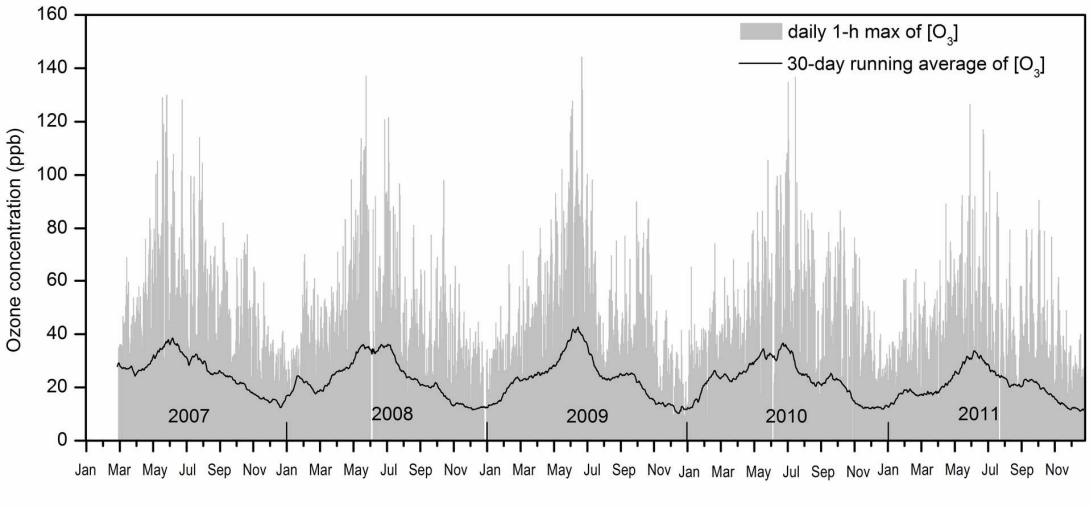

Fig. 2.3 Time series of daily 1-h maximum of [O_3] and 30-day running average of [O_3] observed at the Jiangdu site from March 2007 to December 2011.

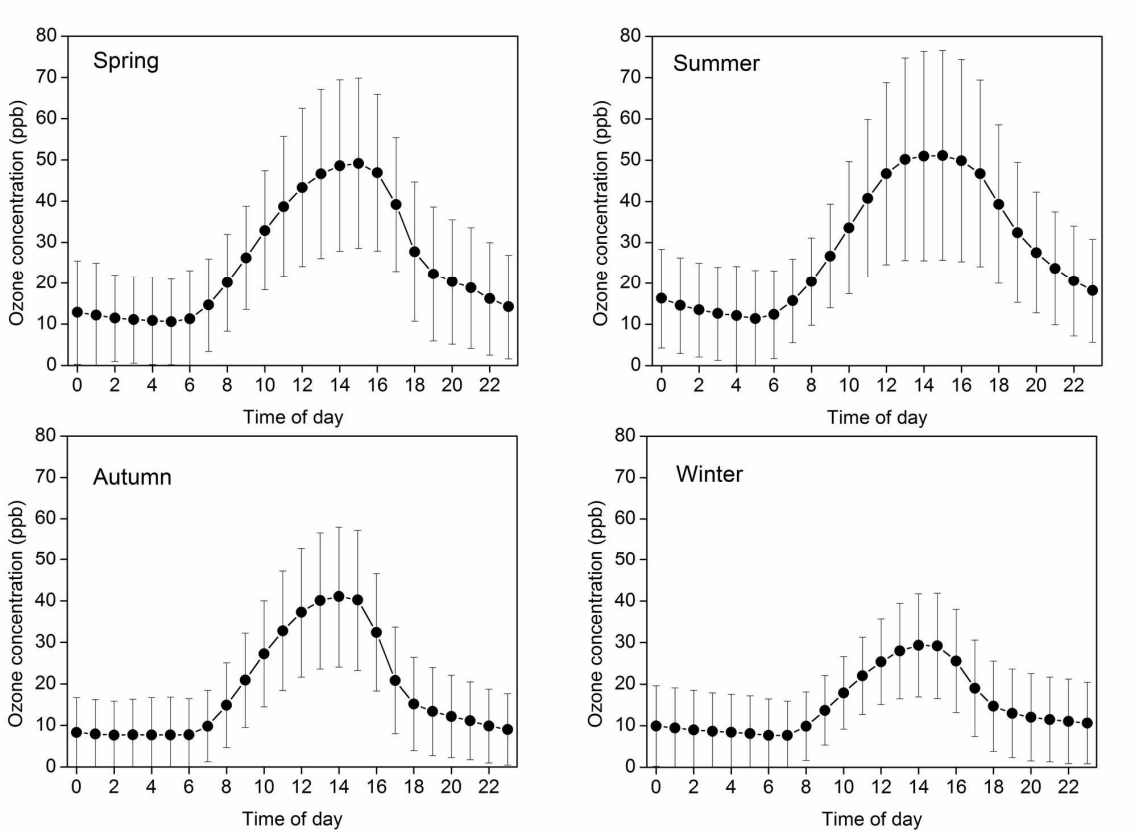

Fig. 2.4 Average diurnal variation of [O_3] for each season at the Jiangdu site.

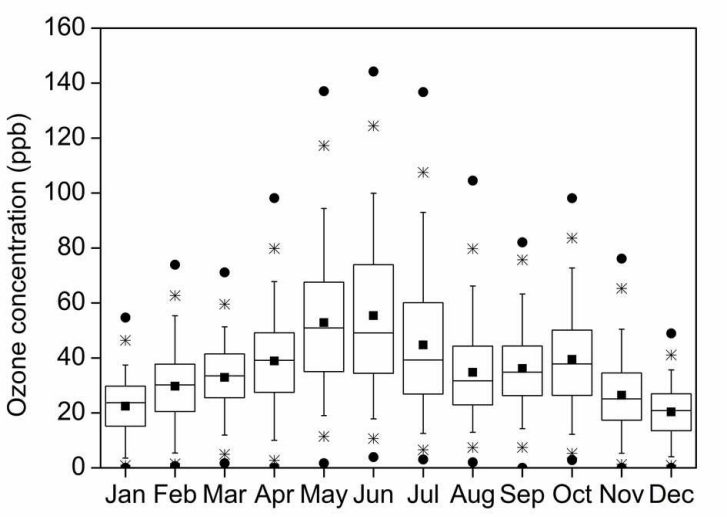

Fig. 2.5 Monthly summaries of daytime (9:00-16:00 CST) 7-h mean [O_3] across the 5 years at the Jiangdu site. For each month, the lower star, lower whisker, bottom of the box, middle line, top of the box, upper whisker, and upper star represent 1^{st}, 5^{th}, 25^{th}, 50^{th} (median), 75^{th}, 95^{th}, and 99^{th} percentile, respectively. The solid square in the middle indicates the monthly mean. The bottom dot and the top dot indicate the lowest and the highest hourly mean values, respectively, for that month.

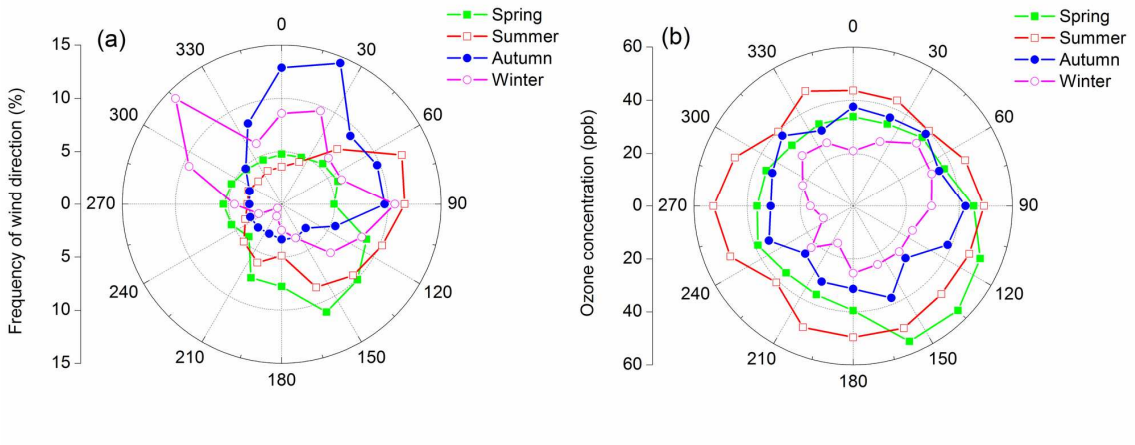

Fig. 2.6 Relative frequency (a) and daytime (9:00-16:00 CST) 7-h mean [O_3] (b) for different wind directions and seasons at the Jiangdu site.

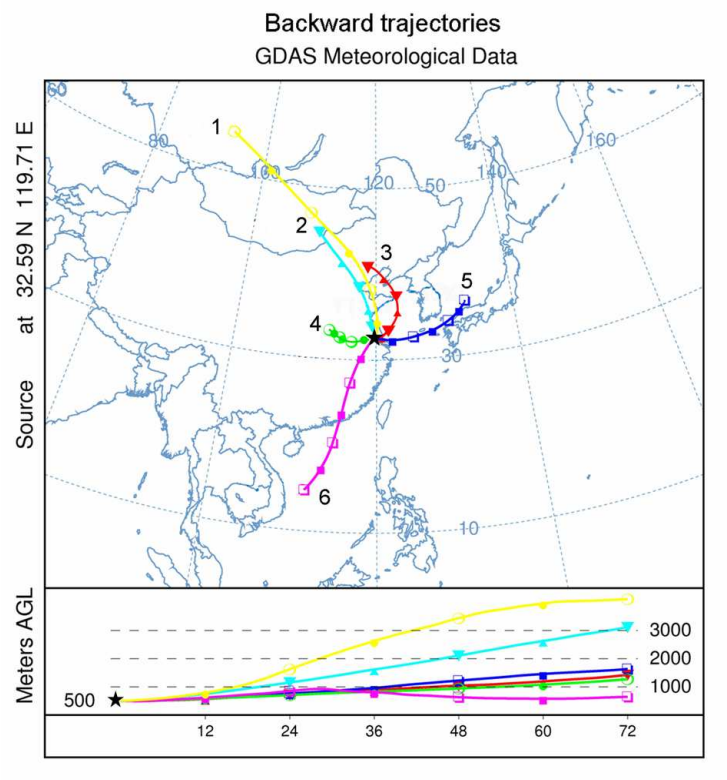

Fig. 2.7 Mean backward trajectories for the trajectory clusters: C1 to C6, over 2007-2011. See text for explanation of the trajectory clusters.

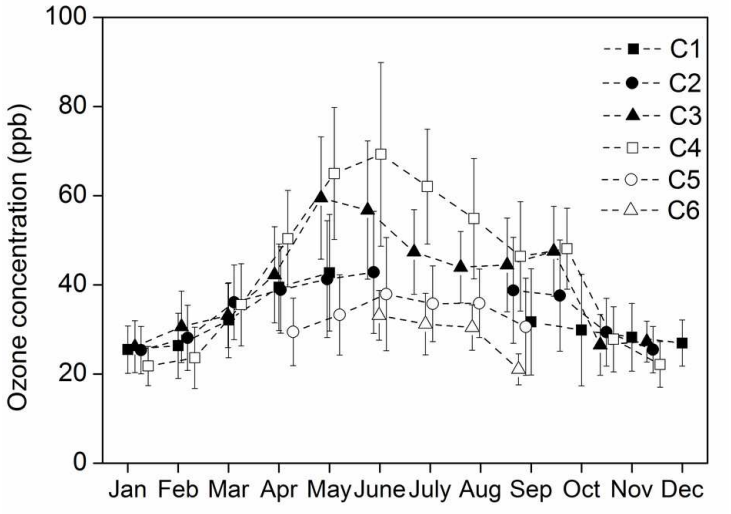

Fig. 2.8 Monthly variation of daytime (9:00-16:00 CST) 7-h mean [O_3] by the trajectory clusters at the Jiangdu site.

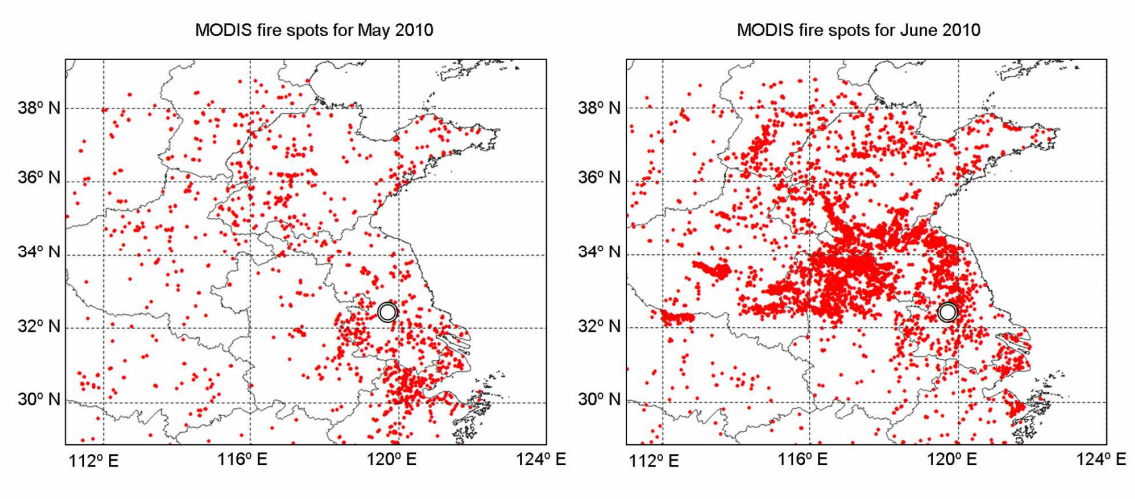

Fig. 2.9 Spatial distribution of fire spots detected from MODIS over central eastern China for May 2010 (left-hand panel) and June 2010 (right-hand panel). The Jiangdu site is indicated as an open circle.

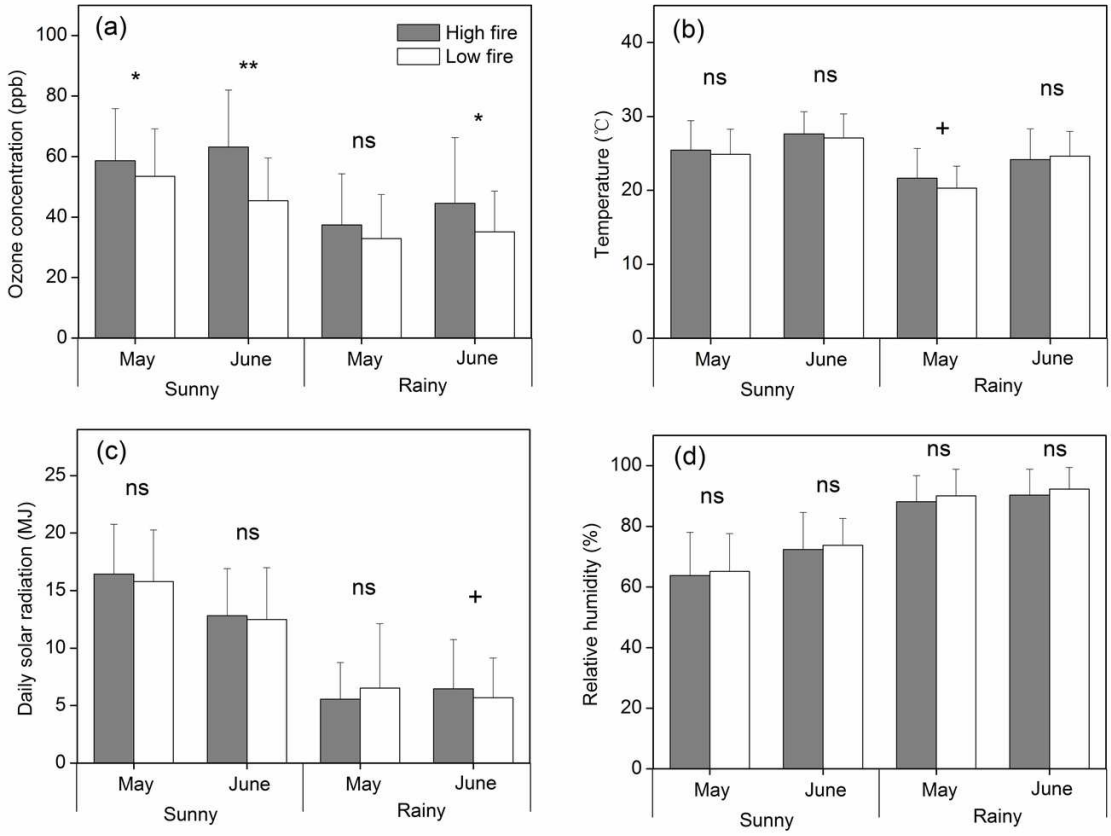

Fig. 2.10 Comparison between high fire activity days and low fire activity days in May and June for the daytime (9:00-16:00 CST) 7-h mean [O_3] (a) and meteorological parameters: temperature (b), daily solar radiation (c) and relative humidity (d) at the Jiangdu site. Vertical bars indicated one standard error. ANOVA results are shown with ns, +, * and ** indicating no significance, $P < 0.1$, $P < 0.05$ and $P < 0.01$, respectively.

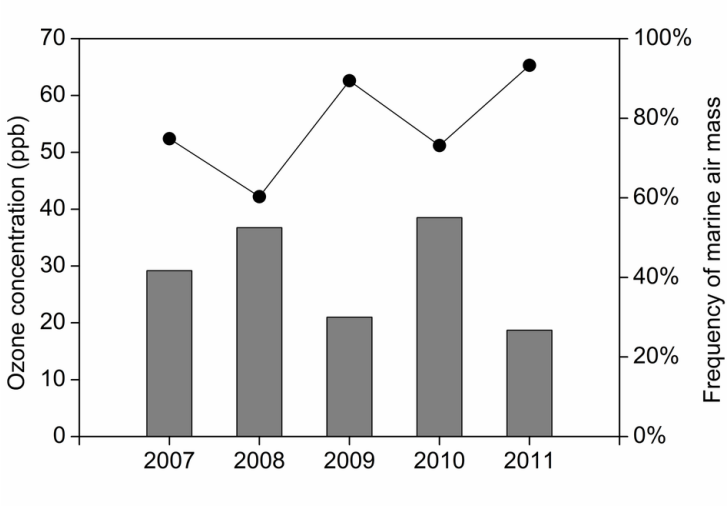

Fig. 2.11 Inter-annual variations of monthly daytime (9:00-16:00 CST) 7-h mean [O_3] (solid circles line, left-*y* axis) and frequency of marine air mass (grey bars, right-*y* axis) at the Jiangdu site in June.

CHAPTER 3

DEVELOPMENT OF A FREE-AIR CONCENTRATION ENRICHMENT SYSTEM WITH OZONE (FACE-O_3)

3.1. Introduction

The current levels of [O_3] observed at our study site are sufficiently high to make damage to crops in YRD. To be worse, models predict that troposphere [O_3] in Northern Hemisphere could further increase by 20–25% between 2015 and 2050 if current emission trends continue, parts of eastern China will suffer some of the highest surface [O_3] (Meehl et al., 2007). Food security in China could then be seriously threatened by the increasing O_3. Therefore, it is necessary to investigate the potential crop loss under future situation with elevated [O_3] levels.

For this purpose, numerous experiments with O_3 fumigation have been conducted worldwide using open-top chambers (OTC) (Feng et al., 2003; Heck et al., 1988; Jäger et al., 1992; Wang et al., 2012a). However, as reviewed in Chapter 1, previous studies have indicated that plant growth performance would differ between OTCs and ambient fields (Fuhrer, 1994a; Piikki et al., 2008). Enclosures can substantially modify the plant canopy microclimate (McLeod & Long, 1999), affect leaf gas exchange and pollutant uptake, and, hence, alter the plant responses to O_3. The so-called chamber effects can be avoided with FACE approach. FACE experiment is conducted in fully open-air field with minimum alteration to the soil-crop-atmosphere continuum (Long et al., 2004), and hence better represents the future environment with elevated [O_3] than other existing experimental approaches.

It should be noted, any artificial addition of ozone, even with FACE approach, may alter the O_3 regimes in the experimental plots from that in the real world. It is often argued that a small number of peaks in [O_3] are more important in determining the crop losses than the majority of lower [O_3] (Krupa et al., 1994; Meyer et al., 1997). Such an argument has been embodied in the O_3 dose metrics, e.g. AOT40 or SUM06

(Fuhrer et al., 1997; Lefohn et al., 1988; Mills et al., 2007; Pleijel et al., 1995), which put greater weights on higher concentrations in calculating the O_3 dose, whereas un-weighted means, e.g. daily 7-hour means (M7), are also used to characterize the O_3 regime (Adams et al., 1989; Lesser et al., 1990; Ishii et al., 2004). If, for example, the O_3 regime in an experiment is *peakier* than that in the real world in the future, the yield loss prediction based on the experiment could give smaller yield loss with AOT40 than that with M7. Such an inconsistency between O_3 dose metrics has indeed been noted in the crop yield loss estimation (Aunan et al., 2000; Avnery et al., 2011a, b; Van Dingenen et al., 2009; Wang & Mauzerall, 2004), although other sources of deviation, e.g. difference in the experimental data bases (Emberson et al., 2009), are also possible.

To investigate the O_3 impact on wheat and rice production in East Asia under future situation, a FACE-O_3 system was established in Jiangsu province, China. With this system, field experiments have been conducted with wheat and rice for several consecutive seasons. In this chapter, a comprehensive description of the FACE-O_3 system was presented. The specific objectives of this study are: (1) to evaluate the system's control performance and (2) to characterize the O_3 regime in the FACE-O_3 in relation to that in current ambient air and a projected future [O_3].

3.2. Materials and methods

3.2.1. FACE-O_3 system

3.2.1.1. System layout

The FACE-O_3 system was set up in 2007 at Jiangdu site in Jiangsu province of China. A detailed description of the geographical and meteorological conditions of this site is given in Chapter 2. The field experiment was conducted with two [O_3] levels: elevated [O_3] (hereinafter called E-O_3) and ambient [O_3] (hereinafter called A-O_3). There were three replicates for each [O_3] level at the start of the experiment in 2007, and four replicates since the 2008 rice season. Any one of the E-O_3 plots was separated from the other plots by at least 70 m to avoid cross-contamination.

For wheat season, O_3 fumigation usually began in early March and continued until harvest in late May or early June. For rice season, O_3 fumigation usually began at the beginning of July after rice transplanting, and continued through to harvest in late October. In each day, the O_3 enrichment was conducted from 9:00 a.m. Chinese Standard Time (CST) to sunset, but was suspended when: (1) leaves were wet: leaf-wetness sensor was used to shut down the O_3 fumigation, or (2) ambient [O_3] was lower than 20 ppb.

Rather than a fixed increase, ozone was added as a fixed proportion of the instantaneous background [O_3] in this system. The target [O_3] for the E-O_3 plots was 50% higher than that in A-O_3 plots at the start of the experiment, and was raised to 60% since 2008 rice season. To prevent extraordinarily high [O_3] from damaging the plants, the maximum of target [O_3] was set at 250 ppb, which was, however, never reached during the experiments. Across 2007–2010 experiments, the maximum 1-min mean [O_3] in E-O_3 was 186 ppb, when [O_3] was 126 ppb in A-O_3, throughout the wheat seasons, and it was 191 ppb, when [O_3] was 137 ppb in A-O_3, throughout the rice seasons. Because of the discontinuation of the fumigation as mentioned before, actual seasonal mean [O_3] elevation above A-O_3 was about 24%, which is close to the IPCC projected mean increase in tropospheric [O_3] for 2050 (Meehl et al., 2007).

The FACE-O_3 system consists of three main units as shown in Fig. 3.1, the detailed descriptions of each unit are presented below.

3.2.1.2. Ozone air supply unit

In the FACE-O_3 system, ozone was produced by an O_3 generator (KCF-BT0.2, Jiangsu Koner Ozone Co., Ltd., China) using pure O_2. Atmospheric air can be used as the gas source also, but the efficiency is lower than when pure O_2 is used. In addition, nitrogen oxides, including nitrogen pentoxide will be generated in that case, they are strongly phytotoxic and must be scrubbed out of the air before release. Therefore, pure O_2 gasified from liquid oxygen was fed into generation cells of the O_3 generator. These cells were constructed of stainless steel, filled with glass electrodes. A high

voltage was applied to the electrodes to produced ozone. The O_3 generator was capable of producing 200 g h^{-1} ozone at a maximum concentration of 100 mg L^{-1}, that could supply six E-O_3 plots at most (we installed four E-O_3 plots by now). A dedicated mass flow control valve (CMQ-V, Yamatake Co., Japan) regulated the flow rate of the generated O_3-enriched gas (ca. 5% O_3 and 95% O_2) for each E-O_3 plot.

The ozone air, which is produced at low pressure and low volumes, must be diluted and pressurized with a carrier gas in order to work with the high-pressure fumigation system. With a bypass venturi injector manufactured by ourselves, a more than 50% pressure drop across the venturi forces ozone gas at the suction port to be mixed into the air stream (at a pressure of ca. 390 kPa), while the bypass assembly maintains pressure on the downstream side (at a pressure of ca. 150 kPa). The high-pressure air stream was provided by an air compressor (GF30+FF, Wuxi Atlas Co., Ltd., China) and passed through filters to remove oil, water and solid particles. Using this approach, a maximum mixture of 15 L min^{-1} (which is the maximum range of the mass flow control valve i.e. CMQ-V, Yamatake Co., Japan) O_3-enriched gas was diluted with approximately 700 L min^{-1} compressed air, and the mixed ozone air was delivery through flexible PTFE tubes to the treatment plots.

3.2.1.3. Ozone release unit

The ozone release unit was mainly based on the method of Okada et al. (2001), but with use of compressed air enriched in ozone replacing compressed CO_2 in the earlier study. In each E-O_3 plot, we installed an octagonal ring of 14 m diameter consisting of eight 6 m long ABS horizontal pipes (ca. 150 m^2). The pipes were manually drilled with tiny holes (approx. 0.3 mm in diameter) at a spacing of 4 cm facing the center of the ring. Emission of O_3 gas was controlled with an on/off valve for each of the 8 pipes. When the O_3 gas was released through the tiny holes at high pressure, a turbulent mixing helps the dilution of the released gas with the surrounding air before being transported across the ring by wind. The O_3 release ring was maintained at approximately 0.5 m above the canopy top throughout the growing season.

In each E-O_3 plot, a dedicated data logger-controller (Campbell CR10X, Campbell Scientific Co., USA) served for data acquisition and control. Wind speed and direction were monitored with a cup anemometer and a wind vane (Model 03001 Wind sentry, RM Young Co., USA) at 1 sec intervals at a height of 2.5 m above the ground. Instantaneous [O_3] was measured at canopy height by an O_3 analyzer (Thermo Electron 49i, Thermo Scientific Co., USA) at the center of the plot every 1 sec, and averaged across 20 sec for control purpose. With the wind speed and [O_3], the data logger-controller used a PID (Proportional Integral Differential) algorithm to calculate the O_3 flow required to obtain the set level of O_3 enrichment. This flow demand was converted to DC (0–5 V) signal input and sent to the mass flow control valve to regulate the O_3 flow rate every 20 sec. The PID coefficients were empirically determined and the same values were used throughout the whole season. Because large and rapid changes in O_3 flow regulation might result in sharp fluctuations in [O_3], upper and lower limits were set for the DC signal input to prevent such changes. The limits were a linear function of the 5-min averages of wind speed.

The data logger-controller also actuated the on/off valves of emission pipes every 5 sec to release O_3 from the most upwind pipe and the two adjacent pipes at the 5-sec mean wind speed higher than 0.3 m s^{-1}. At the wind speed below 0.3 m s^{-1}, the detection limit of the wind sensor, O_3 was released from every other pipe (four pipes at a time) alternated for every 5 sec.

3.2.1.4. Control and monitoring unit

In addition to [O_3] measurements at the central point of each E-O_3 for system control, the spatial distribution of [O_3] was monitored in one of the E-O_3 plots throughout the experimental period. In that E-O_3 plot, [O_3] at the canopy height was measured at 13 sampling points, one of which was located at the center and the others being located equidistantly in two concentric circles of 6 m diameter (four location) and 12 m diameter (eight location). Furthermore, ambient [O_3] at canopy height was monitored with separate O_3 analyzers in two of the A-O_3 plots at a 2-min interval.

Every 10 min, a control computer accessed all the data logger-controllers in A-O_3 and E-O_3 plots to collect the latest [O_3]. Among the ambient [O_3] values, the lower one was taken as the background [O_3], from which the target [O_3] was calculated. This target [O_3] was sent to each of the data logger-controllers in the E-O_3 plots for the next 10 min control. A dedicated software programed using the language VB (Visual Basic 6.0, Microsoft Corporation, USA) coupled with SQL database (SQL Server 2000, Microsoft Corporation, USA) was used to analyze and store the collected data automatically, and displayed the real-time status of each units and system performance on the control computer.

3.2.2. Analysis of the FACE-O_3 performance

In this study, 1-min average [O_3] at the E-O_3 plot center was used to assess the temporal control across the experimental seasons. The data were aggregated for all E-O_3 plots during the actual operational time over four wheat and rice seasons from 2007 to 2010. The performance was measured by the fraction of [O_3] stayed within ± 20% and ± 10% of the target. Another indicator of the TAR (target achievement ratio), which has been defined as the ratio of measured [O_3] to target [O_3] (Okada et al., 2001), was also used to evaluate the system performance. The spatial variability of [O_3] was studied with the observations on wheat and rice experiments in 2009. The seasonal M7 and AOT40 were calculated at the 13 locations, and interpolated using Kriging method to assess the distribution of mean and cumulative O_3 exposure doses across the whole experimental period.

3.2.3. Characterization of the O_3 exposure regime in FACE-O_3

Two widely used O_3 exposure dose metrics: M7 (900-1600 h CST) and AOT40 (accumulated [O_3] over a threshold of 40 ppb) were calculated across the 3 months from March through to May for wheat and from July through to September for rice, respectively. When no O_3 release was performed, ambient [O_3] was used for the O_3 exposure dose calculation in E-O_3 plots. There were some [O_3] data missing in the period before O_3 fumigation in 2007 wheat season, and from August 9^{th} to 19^{th} in

2008 rice season. For the former period, averages of the ambient [O_3] in the same period of 2008–2010 were used; and for the latter period, [O_3] at another O_3 monitoring site ca. 1 km away from the FACE site was used to fill the data gap.

The O_3 regimes in E-O_3 plots as characterized by M7 and AOT40 were compared with those in the A-O_3 plots as well as the constant 24% increase of the A-O_3, which is referred to as the scaled-up O_3 (S-O_3). A linear model was fit to the relationship between M7 and AOT40, and the difference in the model parameters between A-O_3, E-O_3, and S-O_3 were tested for the statistical significance using JMP software (SAS Institute, USA).

The M7-AOT40 relationship was also compared between the FACE and OTC experiments, for which Fig. 1 of Mills et al. (2007) was digitized by using GRAFULA software (Weisk SoftHaus, Russia). The M7-AOT40 relationship was compared between FACE and OTCs in the same way as noted above.

3.3. Results

3.3.1. Temporal performance of the FACE-O_3 system

Table 3.1 shows the temporal performance of the system with 1-min average [O_3] across four consecutive wheat and rice seasons from 2007 to 2010. Because of the suspension of the O_3 fumigation under the conditions mentioned before, and of system maintenance sometimes, the actual operational time was around 50% of the fumigation period from 9:00 to sunset in experimental duration for each crop season. The elevated [O_3] was within ± 20% of the target for more than 90% of time across all the eight crop seasons, whereas the frequency within ± 10% of the target varied by season around the average of 73%. The lower fraction of [O_3] within ± 10% of target in 2008 and 2009 rice seasons was mostly due to intermittent failure of O_3 generation under unfavorable environmental conditions with high humidity and high temperature in August. This malfunction also caused the lower mean TAR in these seasons. The system performance was improved for the 2010 rice season, when an ameliorated cooling system for O_3 generators was installed.

Control of [O_3] on a daily basis is shown in Fig. 3.2 for one of the E-O_3 plots on May 17th, 2007. The mean TAR for the 20-s samples was 1.00, while minute to minute values ranged from 0.76 to 1.35. The large fluctuation of elevated [O_3] occurred when the wind speed dropped suddenly in the late afternoon. Across the whole day, about 85% and 97% of [O_3] samples were within ± 10% and ± 20% of the target, respectively.

In FACE, wind plays the crucial role in dispersing the fumigant across the plot. The system performance clearly depended on wind speed (Fig. 3.3): the best performance was achieved at wind speeds from 1 m s^{-1} to 4 m s^{-1}, which were recorded for 71% of the operational time. At lower wind speeds (< 0.3 m s^{-1}), the [O_3] variation was larger as mixing of gases became poorer. On the other hand, when wind speeds exceeded 4 m s^{-1}, it was difficult to maintain the target [O_3] because the O_3 supply became insufficient, which, however, occurred for only 3.6% of the operational time. The system performance also varied with time of day in association with the change in ambient [O_3] (Fig. 3.4). This could be partly due to the sharp rise and drop of ambient [O_3] caused by rapid photochemical reactions as well as increase in vertical mixing in early morning and by the lower wind speed in late afternoon.

3.3.2. Spatial performance of the FACE-O_3 system

Fig. 3.5 depicts the percentage deviation of M7 and AOT40 from the values at the center across the three months for wheat and rice seasons in 2009. At the center of the plots, M7 was 43.1 ppb (A-O_3) and 54.5 ppb (E-O_3) for wheat, and 35.9 ppb (A-O_3) and 43.5 ppb (E-O_3) for rice on average across the three months. The corresponding values for AOT40 were 7.8 ppb h (A-O_3) and 16.8 ppb h (E-O_3) for wheat, and 4.5 ppb h (A-O_3) and 10.9 ppb h (E-O_3) for rice. The spatial variability was small in wheat, as the deviation from the value at the center did not exceed 5% and 12% in M7 (Fig. 3.5a) and AOT40 (Fig. 3.5b), respectively. In rice season, by comparison, the southeast corner of the plot had noticeably higher O_3 exposure than the other areas with the maximum deviation from the center being +12% for M7 (Fig. 3.5c) and +36% for AOT40 (Fig. 3.5d). The large deviation could be due to the greater canopy

height of the rice cultivars (see Shi et al., 2009 for details of the cultivars) planted at this part in the ring. The air sampling ports were located at a constant elevation relative to the canopy height, and, hence, the sampling port over the taller varieties was in fact taking air samples at a position higher than those for other sampling ports.

3.3.3. O_3 regimes as compared between elevated, ambient, and scaled-up [O_3]

The seasonal M7 for A-O_3 was in the range from 35.9 to 45.0 ppb, and that for the E-O_3 was in the range from 45.8 to 54.5 ppb (Table 3.2). The seasonal AOT40 for the A-O_3 and E-O_3 ranged between 4.5 and 8.9 ppm h, and 10.9 and 17.5 ppm h, respectively, across the 2007–2010 seasons. Because of the discontinuity in O_3 fumigation, the effective increase in M7 was between 18.7% and 27.7% with an average of 23.7%, over eight crop seasons. This [O_3] elevation resulted in an increase of seasonal AOT40 in the range from 76.0% to 176.2% with an average of 115.1%.

The [O_3] regime in E-O_3 plots was compared with those of A-O_3 and S-O_3, of which the latter represents a constant 23.7% elevation of [O_3] above A-O_3, with respect to the relationship between M7 and AOT40. The two O_3 dose metrics were closely related with each other when separate lines were fitted for each of the O_3 levels (Fig. 3.6). The ANOVA of the model parameters showed no significant difference between the O_3 levels in the slope of the lines (P = 0.537) but a significant difference in the intercepts (P = 0.003). Therefore, we fit the linear model with a common slope and separate intercepts to the M7–AOT40 relationship across the three O_3 levels, of which E-O_3 had a greater intercept than the other two levels (Table 3.3).

3.3.4. O_3 regimes as compared between FACE and OTCs

The comparison of results from FACE experiment with those from OTC experiments was done in the same way as that between the O_3 levels. Despite the difference in the experimental methods and locations, FACE did not significantly differ from OTCs in the slope or intercept of the regression lines (P = 0.419 for intercept, P = 0.113 for slope, respectively), allowing these two database to be pooled together to fit a line (Fig. 3.7).

3.4. Discussion

Over the four years of experiments with wheat and rice, the system was able to maintain the elevated [O_3] within ± 20% of target for more than 90% of time. Against a stricter criterion, the performance was better with wheat than rice: elevated [O_3] stayed within ± 10% of target for 79% of time for wheat, while the corresponding figure was 66% for rice. This inferior performance with rice than wheat could be accounted for by the difference in environmental and plant attributes.

As wind has a strong influence on [O_3] control, the larger fraction of wind speed below 1 m s^{-1} in rice season (31% of time across four years) than in wheat season (17% of time across four years) should have contributed to the poorer [O_3] control performance in rice than wheat seasons. In addition, the humid and hot climate in the rice seasons caused the more frequent system failures. Furthermore, the difference in canopy height was as much as 0.4 m between the rice cultivars, whereas it was not significant between the wheat cultivars (Zhu et al., 2011). This uneven canopy height in rice should have a noticeable impact on the O_3 diffusion from the edge of the plot to the control point at the center, and thereby the spatial distribution of [O_3] within the plot as we discuss later.

In comparison with the performance of other free-air O_3 enrichment systems, our result is similar to the Soy FACE, which had 90% of [O_3] samples within ± 20% of target and 74% of [O_3] samples within ± 10% of target (Morgan et al., 2004), and better than a chamber-less system in grassland which had up to 71% of [O_3] samples within ± 20% of target (Erbs & Fangmeier, 2005). With respect to FACE in rice paddy, our system performance is comparable to a CO_2 FACE, for which a report showed approximately 90% and 60% of the CO_2 samples being within± 20% and ± 10%, respectively, of target (Okada et al., 2001), in spite of the much higher variability of ambient [O_3] than [CO_2]. It is noteworthy that our performance analysis is based on the results in total of eight crop seasons, whereas most of the previous reports are for only one crop season.

The spatial variability of M7 in our system was only less than 5% for wheat and 13% for rice (Fig. 3.5). In a small free-air O_3 exposure facility with a diameter of 2 m, the deviation of weekly average [O_3] within central 1 m^2 was in the range between –30% and +10% (Erbs & Fangmeier, 2005). A better performance has been reported by Volk et al. (2003), who kept the difference of seasonal M24 (24-h mean [O_3]) across the 7 m diameter plot relative to the plot center less than 5%. Our results are considered to be better than the former report and comparable to the latter one at least for wheat season, despite the much greater variability in M7 than M24.

As noted above, the spatial variability was greater with rice than wheat partly because of the difference in canopy height between the cultivars. The air sampling ports above the taller rice cultivars were indeed located higher than the other ports. Because of the vertical gradient of [O_3] in the FACE ring (McLeod, 1995), [O_3] above the taller canopy should be higher than that above the shorter ones as reported in a CO_2 FACE (Mollah et al., 2009). This was not the case with wheat, in which the cultivars had similar plant height.

It should be noted, in the spatial variability on a relative basis (Fig. 3.5), that the denominator or M7 at the center includes the natural background [O_3] which has to be subtracted to evaluate the impacts of anthropogenic O_3. In this respect AOT40, having a concentration threshold clearly above the natural background, would better represent the spatial variability of impacts of elevated [O_3] on crops. The large gradients of AOT40: 12% for wheat and 36% for rice, indicate the need to consider the confounding effects of subplot allocation to different cultivars within the E-O_3 plots. In our FACE-O_3, the subplot allocation was randomized for each experimental plot, and therefore the subplot effect was evaluated separately. With wheat, the subplot effect was not significant (Zhu et al., 2011), whereas the effect is yet to be determined with rice.

One of our aims in this study was to characterize the O_3 exposure regime in E-O_3. The greater intercept for E-O_3 than those for A-O_3 and S-O_3 in the relationships between M7 and AOT40 (Table 3.3) means a smaller M7 in E-O_3 at the same AOT40

than that in S-O_3, a 24% increase of M7. For AOT40 elevated to 15 ppm h, for example, E-O_3 in FACE-O_3 is associated with a 24% increase in M7 above ambient level, but in fact it represents a constant increase of M7 by 31%, i.e. about 30% greater increase in daytime mean [O_3] than the apparent increase. This does *not* mean an estimation bias of the crop loss in FACE-O_3, however. The error is incurred when the increase in [O_3] is characterized by an un-weighted mean such as M7, which is then converted to AOT40 without accounting for the deviation of the O_3 regime in FACE from that in the ambient air. The resultant AOT40 and yield loss estimate based on the yield loss sensitivity (e.g. that reported by Zhu et al., 2011) shall *underestimate* the actual O_3 dose and the resultant crop yield loss. When AOT40 is calculated directly from the hourly mean [O_3] rather than the conversion, there shall be no estimation bias.

The cause of the difference between the M7-AOT40 relationships among E-O_3, A-O_3, and S-O_3 is evident in Fig. 3.8, which shows the cumulative frequency distribution of hourly mean [O_3] for the respective O_3 levels during the daytime of the experimental seasons from 2007 to 2010. The S-O_3 has more [O_3] exceeding 40 ppb than E-O_3 does as the cumulative frequency at 40 ppb is 53.6% for S-O_3 in contrast to 45.3% for E-O_3. On the other hand, E-O_3 had greater frequency than S-O_3 at [O_3] higher than 60 ppb. Having lower frequency in low [O_3] and higher frequency in high [O_3], the O_3 regime in E-O_3 is peakier than S-O_3, and, hence, has a greater AOT40 for the same M7. Such distortion can be attributed to the discontinuity of O_3 release under the afore-mentioned conditions that are associated with low [O_3].

It is interesting to note that the M7-AOT40 relationship was similar between FACE and OTCs, which suggests that the O_3 regime in FACE was not very different from that in OTCs. This also suggests a bias in yield loss estimation based on the OTC results in combination with the conversion from un-weighted O_3 dose metrics to weighted one. The bias may not be very large, but non-negligible. As noted before, the bias can be avoided by calculating the weighted O_3 dose from hourly data rather than the conversion from un-weighted dose.

3.5. Conclusions

Our results showed that the free-air exposure system described in this chapter is suitable for [O_3] enrichment in rice and wheat. Temporal and spatial performances were comparable to or better than the existing systems. The [O_3] regime in the FACE-O_3 plots was peakier than a constant fractional increase in [O_3], and thereby had greater AOT40 for the same seasonal M7. The shift in AOT40 is only modest, however, and the [O_3] regime in the E-O_3 was consistent with that in the open-top chamber experiments.

The FACE-O_3 thus provides a reliable means to study the impacts of [O_3] elevation on crops without any alterations to the canopy microclimate. The findings therein, e.g. Shi et al. (2009) for rice and Zhu et al. (2011) for wheat, have clearly demonstrated the negative effects of elevated [O_3] on crop performance. Subsequent studies are warranted for up-scaling the findings in the FACE experiments to the crop loss prediction at national and international levels.

Table 3.1 The experimental period, system operational time, the frequency of elevated [O_3] within ±20% and ±10% of the target [O_3] and the mean TAR with standard deviations of each crop season. Calculation is based on 1-minute mean [O_3] at the center point aggregated across the E-O_3 plots during the operational time.

Year	Crop season	Experimental period	Fraction of operational time	Frequency of elevated [O_3] within ± 20% of target	Frequency of elevated [O_3] within ± 10% of target	Mean TAR
2007	Wheat	14 Apr. - 31 May	57.6%	95.6%	79.4%	0.96 ± 0.11
	Rice	1 July - 17 Oct.	50.9%	92.3%	71.6%	0.97 ± 0.10
2008	Wheat	1 Mar. - 31 May	49.7%	93.1%	77.1%	0.99 ± 0.13
	Rice	1 July – 13 Oct.	40.3%	90.3%	58.2%	0.92 ± 0.09
2009	Wheat	1 Mar. – 3 June	48.4%	96.5%	80.8%	0.98 ± 0.10
	Rice	1 July – 15 Oct.	40.0%	91.1%	60.7%	0.93 ± 0.07
2010	Wheat	1 Mar. – 3 June	51.1%	95.4%	78.8%	0.96 ± 0.08
	Rice	1 July – 8 Oct.	47.9%	93.6%	73.3%	0.97 ± 0.09

Table 3.2 The 7 h mean [O_3] (M7, 900-1600 h) and the accumulated daytime hourly [O_3] above threshold of 40 ppb (AOT40) during 3 months (from March to May for wheat season and from July to September for rice season) in A-O_3 and E-O_3 for each crop season.

Year	Crop season	M7 (ppb)		AOT40 (ppm h)	
		A-O_3	E-O_3	A-O_3	E-O_3
2007	Wheat	45.0	53.4	8.9	15.7
	Rice	41.9	51.8	7.7	15.4
2008	Wheat	43.7	54.1	8.8	17.4
	Rice	37.2	45.8	5.7	12.2
2009	Wheat	43.1	54.5	7.8	16.8
	Rice	35.9	43.5	4.5	10.9
2010	Wheat	37.9	48.4	5.0	13.7
	Rice	41.1	51.5	8.9	17.5

Table 3.3 The relationships between AOT40 and M7 for E-O_3 (elevated [O_3]), A-O_3 (ambient [O_3]) and S-O_3 (scaled-up [O_3] with 23.7% increment over A-O_3 in daytime).

[O_3] level	Number of points	Function (y = AOT40 in ppm h, x = M7 in ppb)	r^2
E-O_3	8	$y = 0.5845x - 14.50$	0.876
A-O_3	8	$y = 0.5845x - 16.66$	0.845
S-O_3	8	$y = 0.5845x - 16.17$	0.909

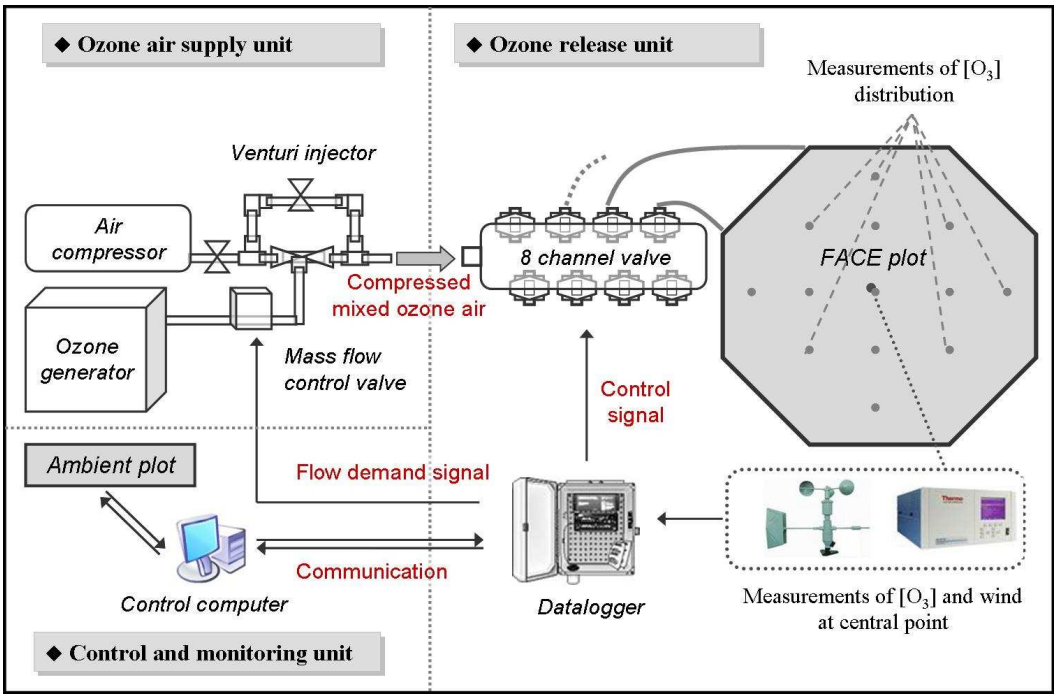

Fig. 3.1 The scheme of FACE-O_3 system (with one E-O_3 plot).

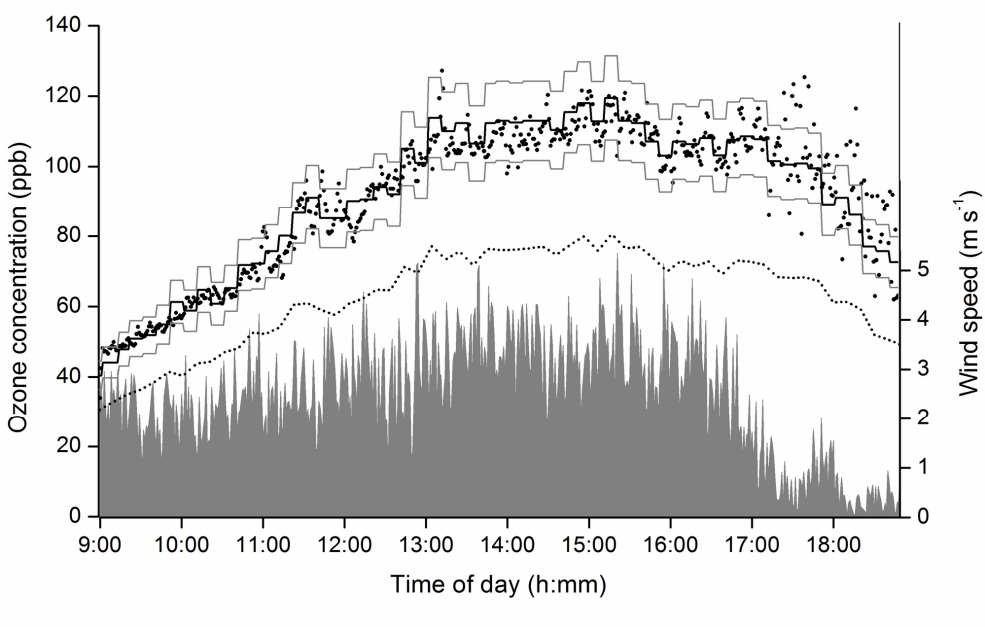

Fig. 3.2 Diurnal record of 20-s average [O_3] (solid circles; recorded every 1 min, left *y*-axis), ambient [O_3] (dotted line, left *y*-axis), target [O_3] and ± 10% of target [O_3] (black and gray lines, respectively, left *y*-axis) and 1 min mean wind speed (gray filled pattern, right *y*-axis) in one E-O_3 plot on May 17th 2007.

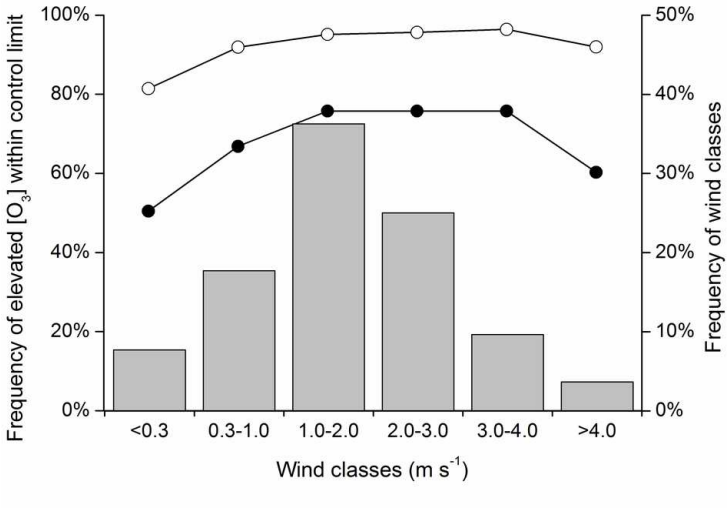

Fig. 3.3 Relationship between wind classes (gray bars, right *y*-axis) and the frequency of elevated [O_3] within ± 20% of the target [O_3] (open circles line, left *y*-axis), ± 10% of the target [O_3] (solid circles line, left *y*-axis). Data were aggregated across the E-O_3 plots in the operational time over four wheat and rice seasons.

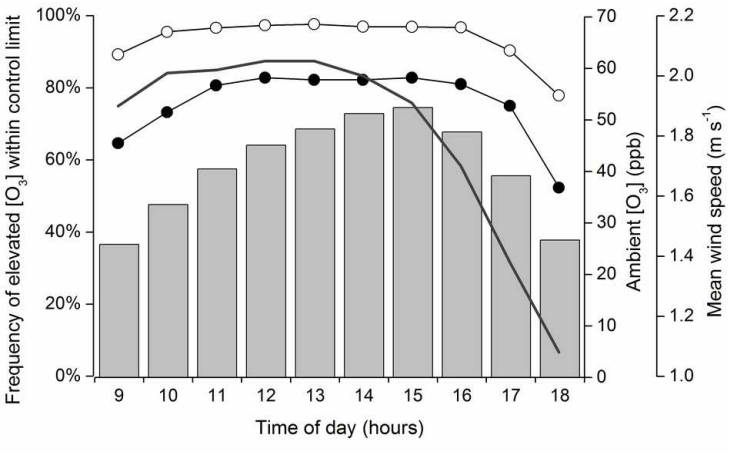

Fig. 3.4 Diurnal changes of frequency of elevated [O_3] within ± 20% of target (open circles line, left *y*-axis), that within ± 10% of target (solid circles line, left *y*-axis), ambient [O_3] (gray bars, right *y*-axis), and mean wind speed (gray thick line, far right *y*-axis). Data were aggregated across the E-O_3 plots in the operational time over four wheat and rice seasons.

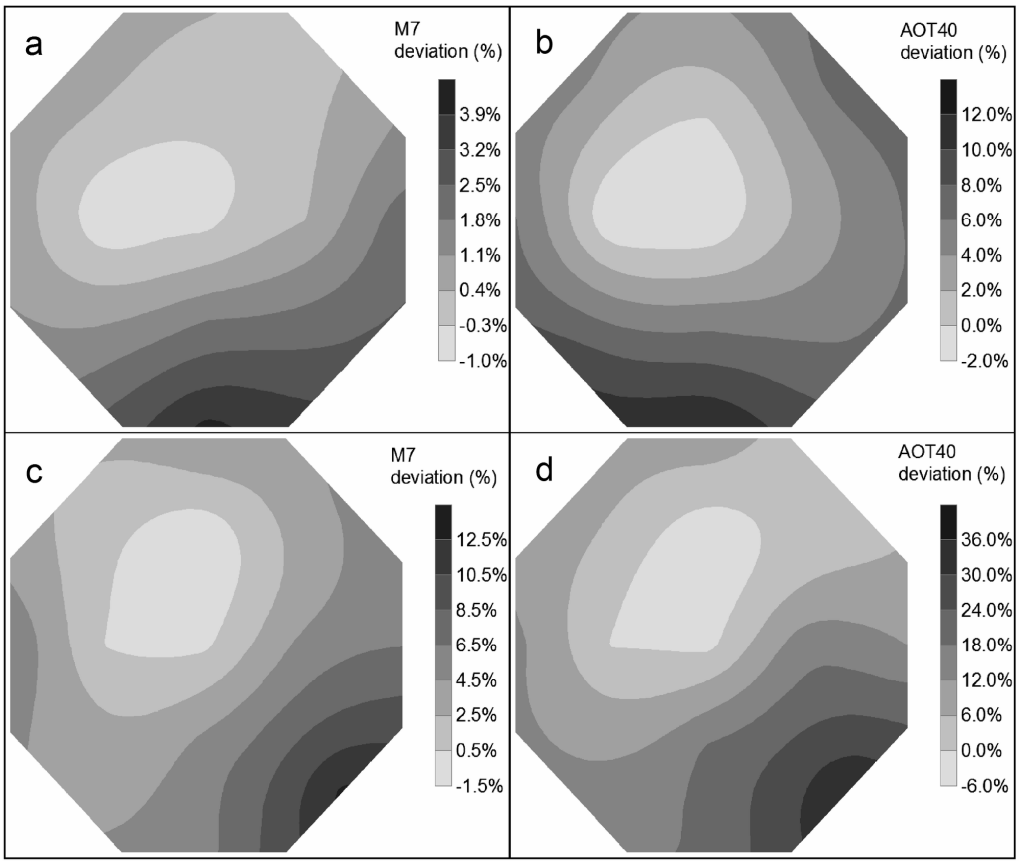

Fig. 3.5 Spatial variability of seasonal M7 and AOT40 for three months from March to May in wheat season (a, b), and from July to September in rice season (c, d) in 2009. The spatial pattern was estimated by Kriging the percentage deviation of the O_3 exposure doses at 13 sampling points from those at the center.

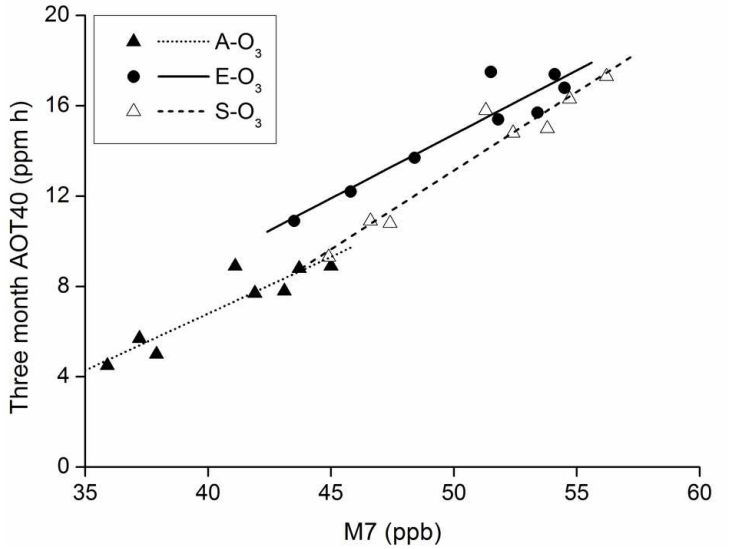

Fig. 3.6 Comparison of M7-AOT40 relationships among A-O_3 (ambient [O_3], dotted line), E-O_3 (elevated [O_3], solid line) and S-O_3 (scaled-up [O_3] with constant 23.7% increase of A-O_3 for daytime, broken line).

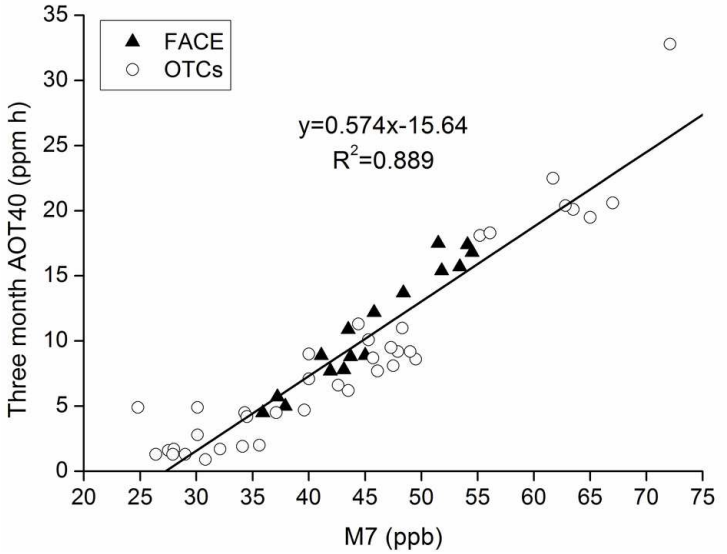

Fig. 3.7 The M7-AOT40 relationships for FACE in this study and OTCs reported by Mills et al. (2007).

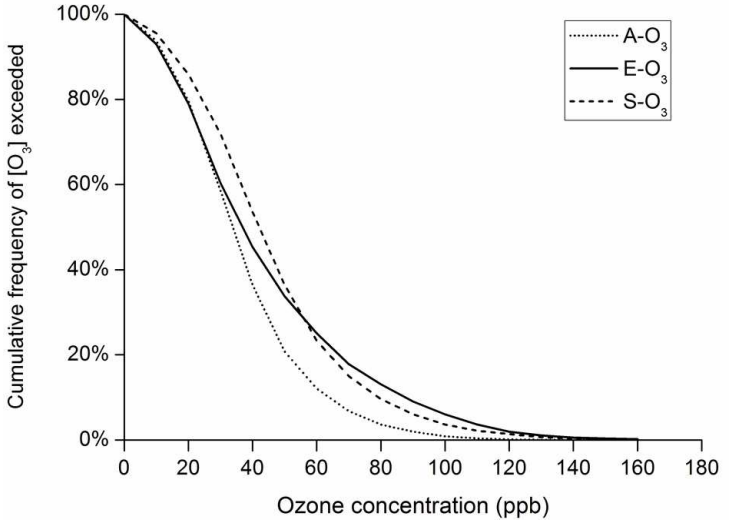

Fig. 3.8 Cumulative frequency distributions of hourly mean [O_3] for A-O_3 (ambient [O_3], dotted line), E-O_3 (elevated [O_3], solid line) and S-O_3 (scaled-up [O_3] with constant 23.7% increment over A-O_3 for daytime, broken line) during the daytime of experimental period from 2007 to 2010.

CHAPTER 4

A FLUX–RESPONSE RELATIONSHIP OF WHEAT YIELD LOSS IN SUBTROPICAL CHINA

4.1. Introduction

With the FACE-O_3 system introduced in Chapter 3, many research groups have put forth great effort to investigate the O_3 impact on rice (Pang et al., 2009; Shi et al., 2009; Wang et al., 2012b, c) and wheat (Feng et al., 2010, 2011; Zhu et al., 2011) in YRD. In comparison with rice, wheat is suggested to be more sensitive to O_3 (Mills et al., 2007). A meta-analysis revealed that surface [O_3] at current ambient level between 31 and 59 ppb (43 ppb on average) have induced an average yield loss of 18% in wheat relative to plants grown in charcoal filtered air (Feng et al., 2008). Under an elevated O_3 level (E-O_3, 57.3 ppb) in our FACE-O_3 experiment, a mean 25% enhancement above the ambient [O_3] (A-O_3, 45.7 ppb.) significantly reduced wheat yield by 20%, across three consecutive growth seasons from 2007 to 2009 (Zhu et al., 2011). It is thus vital to consider the implications of O_3 damage in other locations where wheat is a critical component for food supply. To do this work, we have to establish a dose–response relationship which relates a quantifiable O_3 index to the reduction in the crop yield.

Among O_3 exposure indices, AOT40 (accumulated [O_3] over a threshold of 40 ppb) has been used widely during the last two decades as it has been found to have a strong relationship with relative yield of many crop species (Betzelberger et al., 2010; Mills et al., 2007; Sarkar & Agrawal, 2010). Notably, the AOT40 index reflects the external [O_3] in the air nearby the plants during daylight hours. Thus, it does not consider biological and climatic factors influencing stomatal O_3 flux, which is suggested to be more closely related to damage to crops (Emberson et al., 2000; Danielsson et al., 2003; Pleijel et al., 2000). The flux–response relationship of wheat yield loss has been established in Europe, and was proved to produce a better fit to measured yield reductions compare with AOT40-based relationship (Danielsson et al., 2003; Pleijel et

al ., 2004, 2007). However, such work is yet to be done in China.

In addition, our previous study in FACE-O_3 indicated a larger slope of the AOT40–response function of wheat yield loss as compared with European results (Zhu et al., 2011). Since the flux-based index can take into account the factors of climate, phenology associated with O_3 fumigation pattern, it is interesting to compare the wheat yield loss sensitivity to O_3 between Asian FACE and European OTC experiments with flux–response relationship.

Therefore, the objectives of the present chapter were (1) to parameterize a stomatal conductance (g_{sto}) model of winter wheat grown in a subtropical region using g_{sto} measurements from fully open-air O_3 fumigation experiments (FACE-O_3); (2) to derive the relationship between stomatal O_3 uptake and yield loss and evaluate the performance of different cut-off flux thresholds; and (3) to compare the slope of current O_3 flux–response relationship with that from a recently updated European cultivars (Mills et al., 2011b).

4.2. Materials and methods

4.2.1. Site description, ozone fumigation and plant material

The wheat experiments were conducted at Jiangdu site in YRD. The location of the site and detailed information on environmental conditions such as temperature, precipitation are solar radiation were presented in Chapter 2. The design of the FACE-O_3 experiment and the performance of the [O_3] in E-O_3 were described in detail in Chapter 3.

We used four modern cultivars of winter wheat (*Triticum aestivum* L.): Yannong 19 (Y19), Yangmai 16 (Y16), Yangmai 15 (Y15) and Yangfumai 2 (Y2) in four consecutive growing seasons: 2006–2007, 2007–2008, 2008–2009 and 2009–2010. Standard cultivation practices common to the region were followed in all experimental plots. Seeds were hand sown with a basic seeding density of 2.25 million·ha^{-1} and a row spacing of 25 cm on 5 November 2006, 15 November 2007, 19 November 2008 and 8 November 2009. An inorganic fertilizer was applied at a rate of

210 kg N ha^{-1} with the same amount and timing during the four growing seasons. Details of the fertilizer application regime can be found in Zhu et al. (2011). The sub-plots (11 m^2 each) of the four cultivars were distributed randomly in each plot of A-O_3 and E-O_3. At maturity, the grain yield was determined in a 2 m^2 patch in the middle of each sub-plot (excluding plants near the borders). The grain yields of the experiments from the first three years have been published (Zhu et al., 2011).

4.2.2. Biological and environmental measurements

The g_{sto} of flag leaves was measured *in situ* with an open gas exchange LI-6400 photosynthesis system (LICOR, Lincoln, Nebraska, USA) in the 2008–2009 growing season. Diurnal variation in g_{sto} of flag leaves was measured in Y16 four times in A-O_3 and three times in E-O_3 every 90 minutes from 8:00 a.m. to 5:00 p.m. Additionally, light-saturated g_{sto} was measured five times in Y2 and Y16 for both A-O_3 and E-O_3. During the measurements, the range of g_{sto} was 0.07 ~ 0.43 mol O_3 m^{-2} s^{-1}, and hourly means of environmental variables such as photosynthetic photon flux density (PPFD), temperature (T) and vapor pressure deficit (VPD) was 210 ~1800 μmol m^{-2} s^{-1}, 16.8 ~ 33.2 °C and 0.0 ~ 3.5 kPa, respectively. Y16 data were used for model parameterization while both Y16 and Y2 data were used for model evaluation because no difference for g_{sto} between Y2 and Y16 was found before O_3-induced significant senescence occurred in the late grain filling stage (Feng et al., 2011). The total number of leaves measured was 504. The averaged g_{sto} of 3–5 replicate leaves measured in each plot in one measurement round was used to validate and adjust the g_{sto} model by Pleijel et al. (2007) and LRTAP (2010) for wheat grown in subtropical climate.

The environmental variables (PPFD, wind speed and direction, air T and relative humidity) at 3 m above the ground were measured every 10 minutes at a weather station (Campbell Sci. North Logan, Utah, USA) located in the middle of the experimental site. The [O_3] in each A-O_3 and E-O_3 plot was monitored every 20 sec. by an O_3 analyzer (Thermo Electron 49i, Thermo Scientific Co., USA) at the plant canopy height (approximately 1 m). Hourly means of environmental variables were

used in O_3 flux calculations. The range of PPFD, T and VPD was 100 ~1800 μmol m^{-2} s^{-1}, 13.0 ~ 33.2 °C and 0.0 ~ 3.5 kPa, respectively, during the period of O_3 flux accumulation (see below).

4.2.3. The multiplicative stomatal conductance model

The present study used a multiplicative stomatal conductance algorithm adapted from LRTAP (2010):

$$g_{sto} = g_{max} \times \min(f_{phen}, f_{O3}) \times f_{light} \times \max(f_{min}, f_{VPD}), \quad (1)$$

where g_{sto} is the actual stomatal conductance of O_3 (mmol O_3 m^{-2} projected leaf area (PLA) s^{-1}), g_{max} is the maximum stomatal conductance (mmol O_3 m^{-2} PLA s^{-1}), and f_{min} is the relative minimum stomatal conductance (fraction of g_{max}). g_{max} was estimated from measurements when there were no limiting effects of VPD, PPFD and O_3 on g_{sto} around anthesis. The factors f_{phen}, f_{O3}, f_{light}, f_{VPD} are response functions expressed in relative terms (i.e. they take values between 0 and 1), representing the influences of phenology, O_3, radiation and leaf-to-air VPD, respectively. Notably, the temperature response function was omitted from the original LRTAP (2010) model because T and VPD were highly correlated during daytime at this site (VPD = 0.117×T – 1.787, r^2 = 0.77, n = 378, P < 0.0001) and hence the influence of T could not be separated from that of VPD. The limitation of soil water on g_{sto} was not considered because water availability is sufficient for wheat growth in this region (Oue et al., 2011). Parameters of the g_{sto} response functions are provided in Table 4.1.

f_{phen} is calculated based on accumulation of thermal time:

when $(f_{phen\_f} - f_{phen\_e}) \leq tt \leq f_{phen\_f}$

$$f_{phen} = 1 + \frac{(1 - f_{phen\_b})}{f_{phen\_e}} \times tt \quad (2)$$

when $f_{phen\_f} < tt \leq (f_{phen\_f} + f_{phen\_g})$

$$f_{phen} = 1 \quad (3)$$

when ($f_{\text{phen\_f}} + f_{\text{phen\_g}}$) < $tt \leq (f_{\text{phen\_f}} + f_{\text{phen\_h}})$

$$f_{phen} = 1 - \frac{(tt - f_{phen\_g})}{(f_{phen\_h} - f_{phen\_g})} \times f_{phen\_a} \quad (4)$$

when ($f_{\text{phen\_f}} + f_{\text{phen\_h}}$) < $tt \leq (f_{\text{phen\_f}} + f_{\text{phen\_i}})$

$$f_{phen} = f_{phen\_b} - \frac{(tt - f_{phen\_h})}{(f_{phen\_i} - f_{phen\_h})} \times f_{phen\_b} \quad (5)$$

where tt is the effective temperature sum in °C days from mid-anthesis, using a base temperature of 0 °C and $f_{\text{phen\_a}}$ to $f_{\text{phen\_i}}$ are parameters given in Table 4.1. Three parameters of f_{phen} were changed compared to the European parameterizations (Table 4.1) in order to better fit local observations: (1) higher $f_{\text{phen\_g}}$ as there was no clear aging process in flag leaves during early grain filling (Feng et al., 2011); (2) smaller difference between $f_{\text{phen\_i}}$ and $f_{\text{phen\_h}}$ as the flag leaves lost chlorophyll content (senescence) rapidly (in a few days) during the last part of grain filling (Feng et al., 2011); (3) the maturity of wheat in this region is usually reached about 600–650 °C days after anthesis. Accumulation of O_3 flux starts at f_e °C days before anthesis and ends at f_i °C days after anthesis.

Response functions for radiation, VPD and O_3 were as follows:

$$f_{light} = 1 - \exp((-light_a) \times \text{PPFD}) \quad (6)$$

where the unit of PPFD is μmol m^{-2} s^{-1}.

$$f_{VPD} = \min\left\{1, \max\left[f_{\min}, \frac{(1 - f_{\min})(VPD_{\min} - VPD)}{(VPD_{\min} - VPD_{\max})} + f_{\min} \right]\right\} \quad (7)$$

where the unit of VPD is kPa.

$$f_{O_3} = \left(1 + \left(\frac{POD_0}{f_{ozone\_a}} \right)^{f_{ozone\_b}} \right)^{-1} \quad (8)$$

where POD_0 is the accumulated hourly stomatal O_3 flux above a flux threshold of 0

nmol O_3 m^{-2} PLA s^{-1} from f_e °C days before anthesis to f_i °C days after anthesis. f_{ozone_a} represents the POD_0 value at which f_{O3} equals 0.5, while f_{ozone_b} represents the steepness of the decline of f_{O3} around this value of POD_0 (the higher the f_{ozone_b} value, the steeper the decline).

In this study, f_{light} and the VPD_{min} parameter of f_{VPD} were re-parameterized based on field observations of g_{sto} using the iterative least squares method, after the *a priori* changes to f_{phen} and g_{max} described above had been made. Parameterizations of f_{light} and the VPD_{min} parameter of f_{VPD} were made simultaneously, as PPFD and VPD, and their influences on g_{sto}, are not strongly correlated. Originally, also the f_{O3} was included in the fitting process, but as the onset of significant O_3-induced reduction in g_{sto} observed agreed well with predictions by the f_{ozone_a} parameter of the LRTAP (2010) parameterization, the original f_{O3} of LRTAP (2010) was retained. The interdependence between parameter values from the least squares fitting and calculated POD_0 was determined by coupling model fitting with seasonal POD_0 calculation in an iterative process; i.e. parameter fitting and POD_0 calculation were repeated in cycles until all changes were similar to the previous cycle. Initial POD_0 calculation was made using parameters of f_{light} and f_{VPD} taken from LRTAP (2010).

4.2.4. Stomatal ozone flux

Following LRTAP (2010), stomatal O_3 flux to an unshaded and horizontal leaf (F_{st}, nmol O_3 m^{-2} PLA s^{-1}) was calculated as

$$F_{st} = [O_3] \times \frac{1}{r_b + r_c} \times \frac{g_{sto}}{g_{sto} + g_{ext}} \qquad (9)$$

where $[O_3]$ was the O_3 concentration at plant height, r_c was the leaf surface resistance ($r_c = 1/(g_{sto}+g_{ext})$), r_b was the leaf boundary layer resistance ($r_b = 1/g_b$, g_b is the leaf boundary layer conductance for O_3) and g_{ext} is the external leaf conductance. The value for g_{ext} (16.4 mmol m^{-2} s^{-1}) was chosen in consistency with LRTAP (2010). The value for g_b was calculated based on the conductance for mass transfer in laminar forced convection (Campbell & Norman, 1998):

$$g_b = 0.125 \times (\sqrt{\frac{u}{w}}) \times 1000 \quad (\text{mmol } O_3 \text{ m}^{-2} \text{ PLA s}^{-1}), \qquad (10)$$

where u is the wind speed at canopy height (scaled from a measurement height of 3 m using the logarithmic wind law; Campbell & Norman, 1998), and w is the maximum leaf width. Actually, the four cultivars differed little with respect to w (0.019 m in Y19, 0.021 m for both Y2 and Y16, 0.023 m in Y15). Considering that the average of 0.021 m across all cultivars is very close to 0.020 m, which is the leaf dimension used in LRTAP (2010), we used a fixed value of 0.020 m in the calculations.

Phytotoxic O_3 dose (POD_Y) per unit leaf area (mmol m^{-2} PLA) was defined as the accumulated F_{st} above a flux threshold of Y nmol O_3 m^{-2} PLA s^{-1} over a period from 200 °C days before anthesis to 600 °C days after anthesis, corresponding to the parameterization of the g_{sto} phenology function (Table 4.1).

4.2.5. Yield–response regressions

Regression analysis of yield in relation to O_3 exposure was based on the principles suggested by Fuhrer (1994b). First, a linear regression for each variety and each year was made. The grain yield mean of each treatment was then divided by the intercept of each regression to derive the relative yield (RY) representing a hypothetical yield at zero O_3 dose. The RY from each variety for each year and treatment thus becomes comparable on a common, relative scale. RY was then regressed against the O_3 dose metrics.

In this study, POD_Y–response relationships were determined with values of Y ranging from 0 to 24 nmol O_3 m^{-2} PLA s^{-1}. Moreover, relationships between RY and the concentration-based accumulated O_3 exposure over a threshold of X ppb during daylight hours (AOTX) were also determined for a broad range of X (0–100 ppb). In this study, unlike several other assessments where AOTX was calculated for a three-month period, AOTX was calculated for the same period as the POD_Y index, i.e. the integration period from the 200 °C days before anthesis to 600 °C days after anthesis.

To investigate differences between the European and Chinese cultivars, as well as among the four Chinese cultivars, with respect to RY sensitivity to O_3, the slopes of linear POD_6–RY and AOT40–RY relationships were statistically compared using ANOVA in the SAS software version 9.3.1 (SAS Institute, Cary, NC, USA).

4.3. Results

4.3.1. Stomatal conductance model

The Pleijel et al. (2007) model parameterization significantly underestimated observed g_{sto} (Fig. 4.1a), while the LRTAP (2010) parameterization underestimated low but not high g_{sto} (Fig. 4.1b). These regressions between observed and predicted g_{sto} had slopes significantly different from 1 and significant intercepts of approximately 30% of g_{max} for both regressions made using these European model parameterizations.

Table 4.1 specifies the model parameterizations of Pleijel et al. (2007), LRTAP (2010) and this study. In the current study, thermal time was calculated from 200 °C days before anthesis to 600 °C days after anthesis with a sum of 800 °C days, which was 100 and 170 °C days less than that in the LRTAP (2010) and Pleijel et al. (2007) model parameterizations, respectively. The minimum f_{VPD} was extended to VPD of 5.3 kPa through the extrapolation of available observations (up to 3.5 kPa), while it occurred at a VPD of 3.2 kPa in the other two parameterizations. The temperature effect was omitted due to overlapping effects with high VPD, as discussed below. The f_{light} parameterized was more restrictive than the European parameterizations. The sum of squares of the residuals (observed g_{sto} minus predicted g_{sto}) was much reduced from 1.07 to 0.44 when both f_{VPD} and f_{light} were changed compared to that of the LRTAP (2010) model parameterization.

Using the new algorithm representing a locally adapted parameterization, predicted g_{sto} fitted very well with measured g_{sto} (r^2 = 0.76, Fig. 4.1c). The regression line was very close to and not significantly different from the 1:1 line with the slope and intercept of 0.92 (with a 95% confidence interval (CI) of 0.81 to 1.03) and 0.024 (with

a 95% CI of –0.009 to 0.057), respectively. Compared with the original parameterization of LRTAP (2010), the residuals in the current parameterization were distributed more evenly at high VPD (≥ 2.5 kPa) and high temperature (≥ 26 °C) (Fig. 4.2a, b).

4.3.2. Ozone uptake and yield response

The r^2-value of the regression of RY on POD_Y across four cultivars increased with O_3 uptake threshold up to Y = 18 nmol O_3 m^{-2} PLA s^{-1} and then decreased (Fig. 4.3a). Similar results were found in the regression of RY on AOTX and with a highest r^2 at a concentration threshold of 75 ppb (Fig. 4.3b). High r^2 values were found in the range of thresholds of 11–20 nmol O_3 m^{-2} PLA s^{-1} for POD_Y (with r^2 of 0.77 ~ 0.83) and 55–85 ppb for AOTX (with r^2 of 0.77 ~ 0.83). Dose–response relationships based on AOTX had same maximum r^2 value as flux-based relationships (Fig. 4.3a, b). RY in the ambient O_3 treatment (RY_A) estimated from the relationship between yield and POD_Y varied from 0.42 when Y = 0 nmol O_3 m^{-2} PLA s^{-1} to 0.99 when Y = 24 nmol O_3 m^{-2} PLA s^{-1} (Fig. 4.3a). RY_A estimated from the regression of RY on AOTX increased from 0.47 at X = 0 ppb to 0.97 at X = 85 ppb (Fig. 4.3b). The choice of a reasonable O_3 flux and concentration threshold is treated in the Discussion section.

Regressions of RY on POD_6 estimated by European model parameterizations had higher r^2 values than the current model parameterizations (Fig. 4.4a, b, c), although the g_{sto} predicted by European model parameterizations deviated significantly from the 1:1 line (Fig. 4.1a, b). However, the current parameterizations yielded a medium yield response to $POD_{6,}$ as shown a slope ranking between the Pleijel et al. (2007) and the LRTAP (2010) parameterizations. The O_3 flux obtained from the current g_{sto} model parameterization was higher than that from the Pleijel et al. (2007) parameterization, largely as a result of less limiting f_{VPD} and lack of f_T (Table 4.1). Also the LRTAP (2010) parameterization predicted higher O_3 fluxes than the Pleijel et al. (2007) parameterization, mostly due to its higher g_{max} value (Table 4.1). The increase in r^2 with increasing Y was caused in part by A-O_3 data points being clustered at lower POD_Y values with higher Y (Fig. 4.4c, d, e). Moreover, Y2 showed

significantly higher relative yield sensitivity to POD_Y than the other three cultivars ($P < 0.05$) only when $Y \geq 13$ nmol O_3 m^{-2} PLA s^{-1}.

4.4. Discussion

Stomatal flux-based O_3 indices have been recommended for risk assessment within the framework of air quality policy implementation to protect plants against ground-level O_3 in Europe (LRTAP, 2010). Stomata constitute the principal control point of entrance of O_3 into the leaf and thus have been assumed to be the most important factor for improving O_3 risk assessment. In this study, recently revised multiplicative g_{sto} model parameterizations (Pleijel et al., 2007; LRTAP, 2010) were applied to wheat grown in a subtropical climate. Predicted g_{sto}, especially by the Pleijel et al. (2007) parameterization, was much lower than field observations. The slope and intercepts of the regression between measured and predicted g_{sto} in both models were significantly different from 1 and 0, respectively (Fig. 4.1a, b). It can be inferred that g_{sto} model parameterizations from temperate Europe must be revised based on local observations before application in a subtropical region.

In comparison to LRTAP (2010), the parameterizations of relative response functions for phenology, radiation and VPD were adjusted based on local observations to enhance the performance of the g_{sto} model. The new parameterization for phenology changed the model performance little, the sum of the squares of the residual increasing to 1.11 as compared to 1.07 using the LRTAP (2010) parameterization. However, the new parameterization, which was made a priori and was not part of the least squares model fitting, better represents the development of wheat in subtropical China. Among the adjusted functions, f_{VPD} was one of the most important. The modified f_{VPD} is less limiting to g_{sto} (full closure at 5.3 kPa) compared to the LRTAP (2010; full closure at 3.2 kPa) parameterization. This modification reflects that stomata of winter wheat remained open at high VPD during early grain filling in the present study. High g_{sto} of wheat at high VPD has also been found in Mediterranean conditions (LRTAP, 2010). High T and high VPD mostly co-occur in subtropical China and they were highly correlated during daytime at this site. As a

consequence, independent g_{sto} response functions for T and VPD could not be reliably determined. In our model, stomatal closure at high T and high VPD was attributed to (and parameterized for) VPD only. Thus the T response function was omitted.

Also f_{light} was adjusted to better fit with observations. The f_{light} parameterized here was similar to the one determined for spring wheat in Sweden by Uddling and Pleijel (2006) where they used a similar f_{phen} with three response stages. Adjusting both f_{VPD} and f_{light} constituted the main improvements of the original LRTAP (2010) model with a much smaller sum of squares of the residual after adapting it to the conditions of subtropical China. Based on the current model parameterization, the regression between predicted and observed g_{sto} was very close to the 1:1 line with a high r^2-value (0.76), suggesting that the adjusted parameterization for the multiplicative g_{sto} model worked well for the site where conductance was observed. Furthermore, model residuals from the current parameterizations were much smaller at high VPD or high T relative to the parameterization of the LRTAP (2010) (Fig. 4.2a, b).

Unlike charcoal-filtered air (CF) in open-top chambers, open-air fumigation experiments so far lack treatments with O_3 concentration below ambient. Estimation of RY at zero O_3 dose was made by extrapolation of linear regressions (Fuhrer, 1994b) based on only two treatments (A-O_3 and E-O_3). As a result, values of RY changed with O_3 uptake thresholds (Fig. 4.3a, b). Since no treatments with O_3 concentration below ambient were available, the determination of the best O_3 exposure or flux threshold is fundamentally uncertain. Furthermore, the fact that each experiment contained only two treatments will favor comparatively high flux thresholds, since high thresholds will cause convergence of A-O_3 data points towards zero exposure and RY of one, thus promoting high r^2. As the choice of X and Y threshold value for AOTX and POD$_Y$ is crucial for the risk assessment result (Fig. 4.3a, b), we also looked at other criteria than r^2-values in search of suitable cutoff thresholds. Results from field EDU application and a meta-analysis of data from open-top chambers indicate that the ambient [O_3] found at the experimental site would be likely to cause yield loss about 10% to 12% (Wang et al., 2007b; Feng & Kobayashi, 2009). Such yield loss in

A-O_3 was predicted with $POD_{12–13}$ and AOT50–55 in this study (Fig. 4.3a, b). Considering both the likely yield loss at A-O_3 and the r^2-value, we recommend using an O_3 uptake threshold of 12 nmol O_3 m^{-2} PLA s^{-1} to predict O_3-induced yield loss in subtropical regions. In European studies, a flux threshold of 6 nmol O_3 m^{-2} PLA s^{-1} was selected as it had the highest r^2-value of POD_Y–RY relationships with different values of *Y* (Pleijel et al., 2007; LRTAP, 2010) and response extrapolation was small or not necessary as most European experiments included CF treatments. Although the most reasonable flux threshold in the current study was higher than that in European studies (Pleijel et al., 2007; Mills et al., 2011b), it cannot simply be concluded that wheat cultivated in subtropical regions have a higher defense capacity to detoxify O_3 than European cultivars, because different model parameterizations were used.

Assuming that POD_Y estimated by the LRTAP (2010) and the present g_{sto} model parameterizations are suitable for Europe and subtropical China, respectively, the slopes of POD_6–RY obtained here and for Europe can be compared to assess O_3 sensitivity of wheat grown in China and Europe. There was significant difference (P = 0.041) in the slope of POD_6-RY between this study (slope: –0.058 with a 95% CI of –0.077 to –0.040) and a recent European synthesis by Mills et al. (2011b) (slope: –0.038). Similarly, the slope of AOT40–RY in this study (–0.024, with a 95% CI of –0.032 to –0.017) was significantly (P = 0.020) larger than that in European experiments (Mills et al., 2007), despite a shorter accumulation period in our study. Our study thus suggests that the cultivars used in the present study are more sensitive to O_3 than European cultivars. The study of Emberson et al. (2009) also indicated the Asian cultivars of wheat to be more sensitive to O_3 relative to North American cultivars. In this study, Y2 showed a higher relative yield sensitivity to O_3 than the other three cultivars at high *Y* above 13 nmol O_3 m^{-2} PLA s^{-1} ($P < 0.05$), different from Zhu et al. (2011) where no significant interaction of O_3 × cultivars on the yield was found. O_3 sensitivity variation between cultivars, as well as climate variability among years within a region, might also be important in a regional risk assessment.

It has been shown that POD_Y provides stronger relationships with effects than

external exposure such as AOT40 (Danielsson et al., 2003; Pleijel et al., 2004; Uddling et al., 2004) and that flux-based risk maps provide better fit to effects found in the field than AOT40-based risk maps (Mills et al., 2011a). In this study, the high r^2-values of dose–response relationships were obtained for $POD_{11\text{-}20}$ (r^2 = 0.77 to 0.83) and AOT55-85 (r^2 = 0.77 to 0.83) (Fig. 4.3a, b). When considering the reasonable cut-off thresholds Y = 12–13 nmol O_3 m^{-2} PLA s^{-1} and X = 50–55 ppb (corresponding to yield reduction in A-O_3 of ~10%; see text above), the r^2-value of $POD_{12–13}$–RY (0.80–0.81) was somewhat higher than that of AOT50–55 –RY (0.72–0.77) (Fig. 4.3a, b). The similar performance of flux-based and concentration-based O_3 metrics could be attributed to the fact that the data are from one site with similar climatic conditions in different years (Zhu et al., 2011) and that mild T and available soil water in subtropical regions favor high g_{sto} throughout the growing season.

Admittedly, there exist some uncertainties in the current g_{sto} model parameterizations, e.g. the baseline temperature for temperature sum calculation and the parameters of the f_{phen} . Measurements of g_{sto} from more than one site in subtropical regions are needed to improve the current parameterization. However, the O_3 flux-response relationship based on the current g_{sto} model parameterization allows for improved O_3 risk assessment in a subtropical climate relative to the AOT40 approach, and thus benefits Chinese air pollution policy, which can now be based on locally derived flux-response functions instead of those derived in other parts of the world. A mapping for the O_3 risk assessment on wheat production can be expected on the basis of current O_3 flux–response relationship.

4.5. Conclusions

After adjusting the multiplicative g_{sto} model of LRTAP (2010), the new model fitted well with field measurements of g_{sto} conducted in subtropical China. The main differences of the present model compared with the g_{sto} model parameterization used for Europe, were that the VPD response function was made less restrictive, the radiation function was made more restrictive, and the temperature function was omitted. The European model parameterizations systematically underestimated g_{sto}.

An O_3 uptake threshold of 12 nmol O_3 m^{-2} PLA s^{-1} was judged as reasonable for an O_3 flux-response relationship for wheat in subtropical China. Both flux-based and concentration-based response relationships indicated that the cultivars used were more sensitive to O_3 than European cultivars. The O_3 flux–response relationship obtained here will benefit regional O_3 risk assessment on wheat production.

Table 4.1 Summary of the parameterization of the multiplicative stomatal conductance model for wheat flag leaves in different models.

Parameter	unit	Pleijel et al., 2007	LRTAP, 2010	This study
g_{max}	mmol O_3 m^{-2} PLA s^{-1}	450	500	450
f_{min}	fraction	0.01	0.01	0.01
f_{phen_a}	fraction	0.2	0.3	0.3
f_{phen_b}	fraction	0.8	0.7	0.7
f_{phen_e}	°C days	270	200	200
f_{phen_f}	°C days	0	0	0
f_{phen_g}	°C days	-	100	350
f_{phen_h}	°C days	-	525	500
f_{phen_i}	°C days	700	700	600
Light_a	constant	0.0105	0.0105	0.0029
T_{min}	°C	12	12	-
T_{opt}	°C	26	26	-
T_{max}	°C	40	40	-
VPD_{max}	kPa	1.2	1.2	1.2
VPD_{min}	kPa	3.2	3.2	5.3
∑VPD	kPa	8	8	8
PAWt	%	50	50	-
f_{ozone_a}	POD_0, mmol m^{-2}	11.5	14	14
f_{ozone_b}	exponent	10	8	8
Height	m	1	1	1
Leaf dimension	m	0.02	0.02	0.02

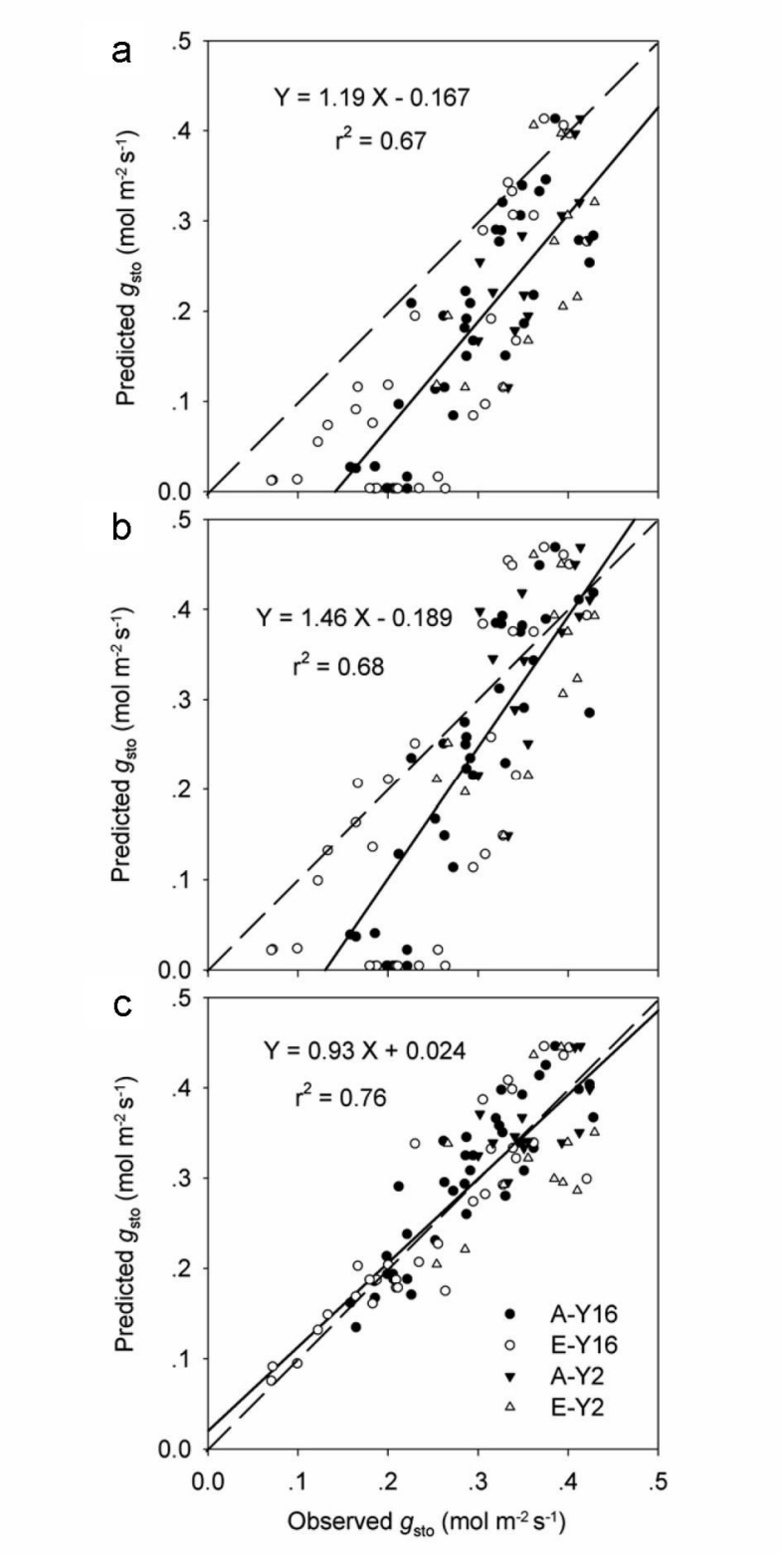

Fig. 4.1 Predicted versus observed stomatal conductance (g_{sto}) using the Pleijel et al. (2007) (a), the LRTAP (2010) (b), and this study's model parameterizations (c). Solid lines represent regressions and broken lines theoretical 1:1 relationships.

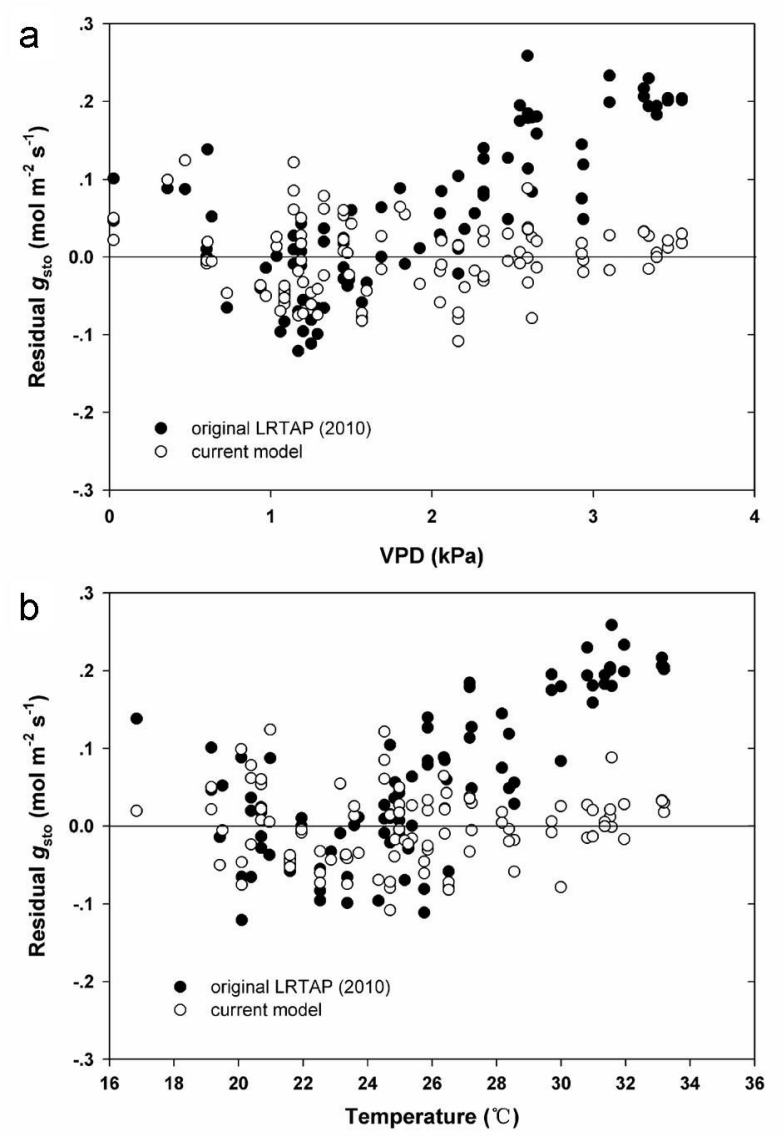

Fig. 4.2 Residual (observed minus predicted) stomatal conductance (g_{sto}) in flag leaves of wheat in relation to vapor depression deficit of air (VPD) (a) and in relation to air temperature (b). Predictions of g_{sto} were made with the model parameterization of LRTAP (2010) (filled circles) or with current model parameterization (open circles).

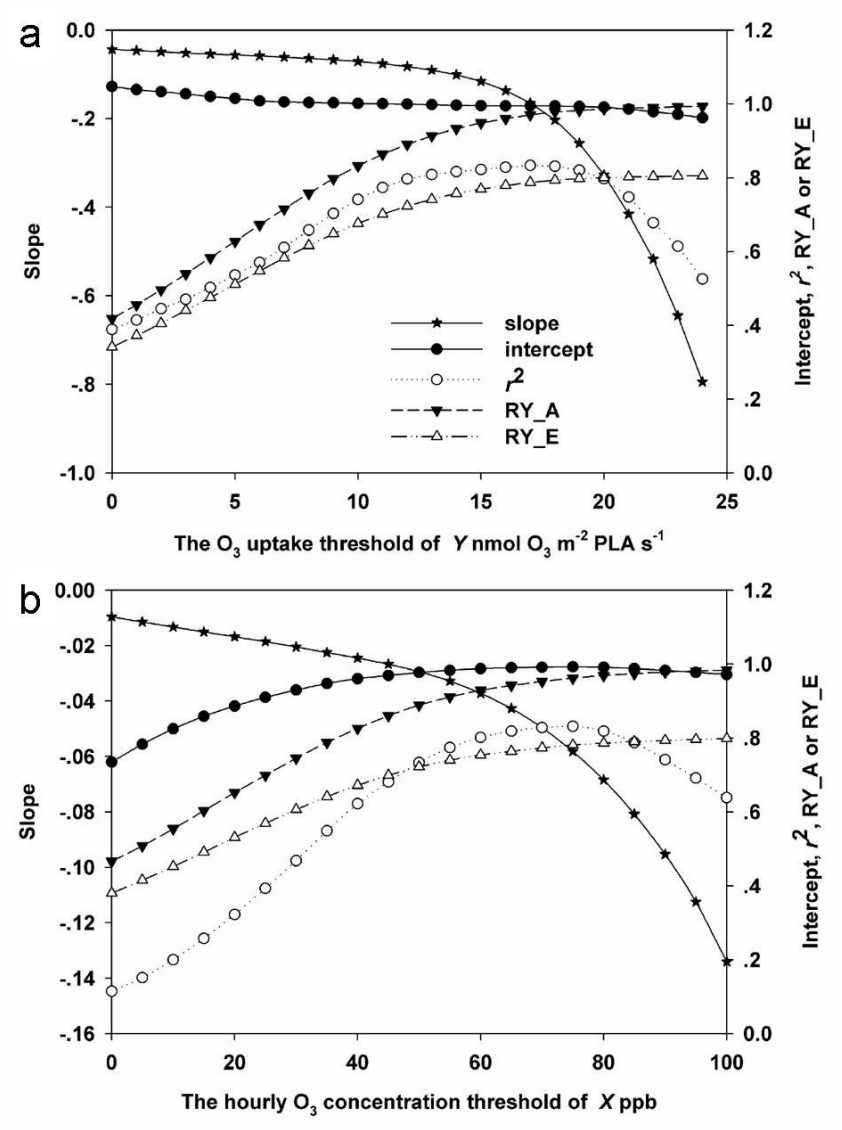

Fig. 4.3 Coefficient of determination (r^2), slope and intercept of regressions between relative yield (RY; *y*-axis) and estimated accumulated stomatal ozone uptake over a cut-off threshold of *Y* nmol O_3 m^{-2} s^{-1} (POD_Y, *x*-axis) (a) or between relative yield (RY; *y*-axis) and accumulated ozone exposure over an hourly cut-off threshold concentration of *X* ppb during daylight hours (AOT*X*) (b). Also shown are values of RY at ambient (RY_A) and elevated O_3 (RY_E) in relation to a hypothetical control at zero POD_Y or a hypothetical control at zero AOT*X* determined by linear extrapolation (Fuhrer, 1994b).

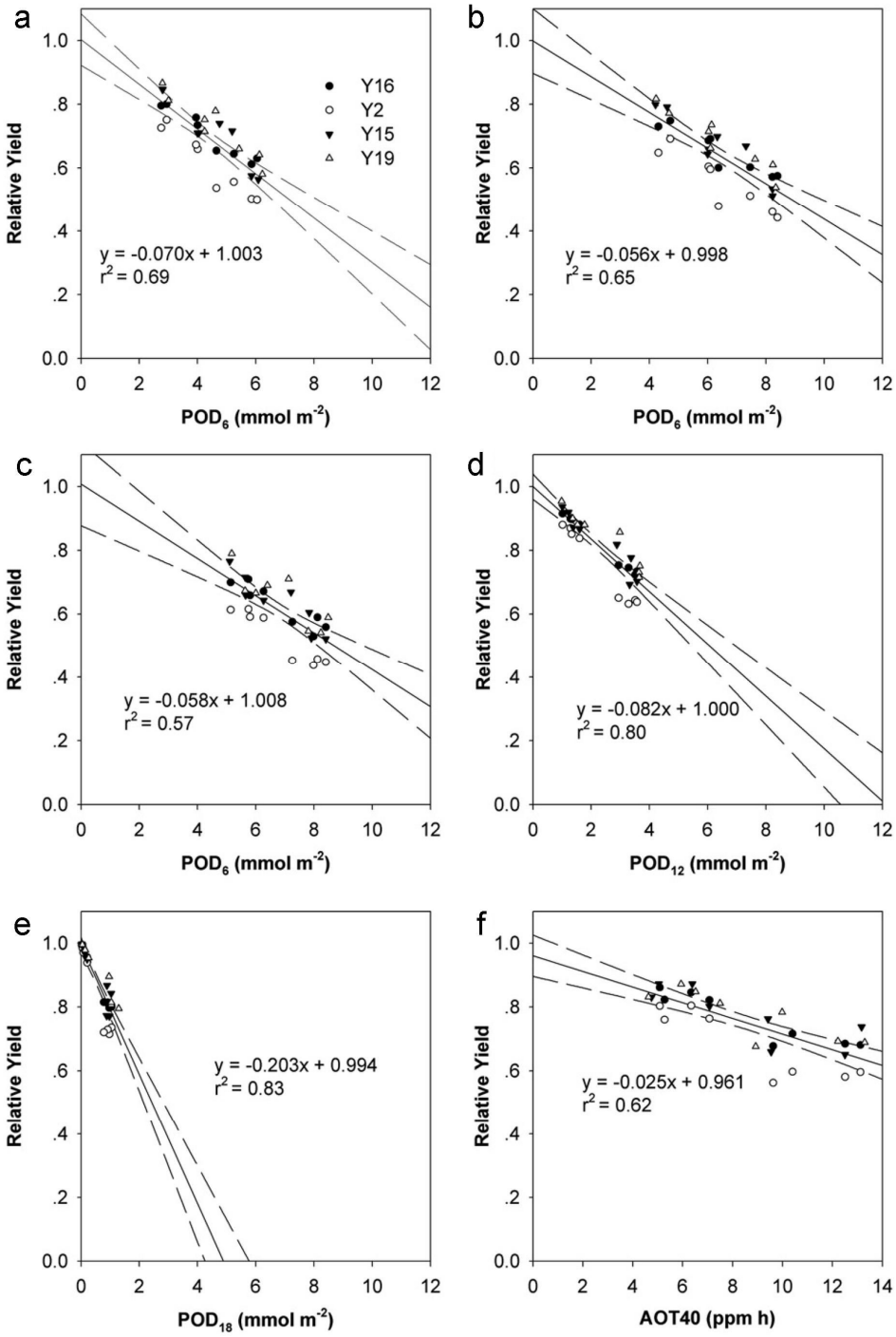

Fig. 4.4 Relative yield (RY) of wheat in relation to the accumulated ozone uptake above an uptake threshold of 6 nmol m^{-2} s^{-1} (POD_6) based on the Pleijel et al. (2007) (a) and the LRTAP (2010) model parameterizations (b), as well as POD_6 (c), POD_{12} (d) and POD_{18} (e) based on the model parameterization of this study, and (f) the accumulated ozone exposure over a threshold of 40 ppb during daylight hours (AOT40). Broken lines show the 95% confidence limits of the regression.

CHAPTER 5

EVALUATION OF THE OZONE-INDUCED WHEAT PRODUCTION LOSS IN CHINA AND INDIA FOR THE YEARS 2000 AND 2020

5.1. Introduction

Field experiments have demonstrated that atmospheric O_3 can damage crops, leading to significant yield reduction (Feng et al., 2009; Krupa et al., 1998). The resulting economic loss and threat to future food security has become an issue of concern in the world (Adams et al., 1987; Avnery et al. 2011a; Van Dingenen et al., 2009), especially for the developing nations as both population and O_3 precursor emissions are projected to increase over the next few decades (Akimoto, 2003; Cofala et al., 2006; Riahi et al., 2007; Streets et al., 2000). China and India are the two biggest developing countries with numerous undernourished people, they are also the largest and second largest wheat producers in the world (FAO, 2010). Evaluation of the O_3-induced wheat production loss in these two countries is important as it provides an input to policy makers to make considerations of how much emissions should be reduced when developing an economic development strategy.

In the last decade, many studies have made great effort to estimate the O_3-induced yield loss of wheat as well as other key staple crops on regional and global scales (Aunan et al., 2000; Avnery et al. 2011a, b; Van Dingenen et al., 2009; Wang & Mauzerall, 2004). The limitations of the previous studies, especially without use of the flux-based method were introduced in the Chapter 1. Stomatal O_3 flux depends not only on ambient [O_3] but also on stomatal conductance which is determined by the biological and environmental factors (Danielsson et al., 2003; Fuhrer, 2000). In consequence, the calculations of stomatal O_3 uptake are strongly dependent on the quality of the meteorological input data. An assessment of O_3 risk for vegetation in Europe indicated that a –43% bias on average in the estimated VPD (vapor pressure deficit) in their regional climate model caused a large overestimation of flux-based O_3 risk for the northern sites (Klingberg et al., 2011). Therefore, the uncertainties due to

the meteorological inputs should be especially concerned about when applying flux-based approaches to the yield loss estimation.

In this present study, both exposure-based and flux-based relationships derived from European OTC experiments and the FACE-O_3 experiment in Asia were applied to evaluate the O_3-induced wheat production loss (WPL) in China and India. Parallel use of both exposure- based and flux-based methods was intended to improve understanding of their reliability relative to one another. We focused on the aggravation of WPL from the base year (2000) to the near future (2020), since anthropogenic emissions of O_3 precursors have dramatically increased over these regions since 2000 as shown by both satellite observations and model estimations (Streets et al., 2005; Ohara et al., 2007; Kurokawa et al., 2009; Zhang et al., 2007, 2012). Present and future surface [O_3] were simulated by a high resolution (40 × 40 km) global–regional chemical transport model (CTM) system coupled with the Regional Emission inventory in Asia (REAS) (Ohara et al., 2007).

The objectives of this chapter are (1) to evaluate the magnitude and distribution of O_3-induced WPL in China and India using both exposure-based and flux-based methods and; (2) to analyze the uncertainties associated with the use of different O_3 dose metrics and the meteorological inputs for flux-based evaluations.

5.2. Materials and methods

5.2.1. Simulation of ozone concentration

A global–regional CTM system (WRF/Chem-CHASER) has been developed to simulate surface [O_3] over Asia. The global CTM is based on CHASER (CHemical Atmospheric general circulation model for Study of atmospheric Environment and Radiative forcing) (Sudo et al., 2002a, b; Takigawa et al., 2005), and the regional CTM is based on WRF (Weather Research and Forecasting) /Chem (Grell et al., 2005) using the dynamic cores of Advanced Research WRF (ARW) version 3.1. Gas–phase chemistry in the model uses RADM2 (Regional Acid Deposition Model Version 2) (Stockwell et al., 1990), and dust erosion is taken into account following Shaw et al.

(2008). Both of the regional and global CTMs are online, i.e., transport of chemical species is done using the same vertical and horizontal coordinates with the meteorological part of the model and using the same physics parameterization with no interpolation in time.

Anthropogenic emissions in Asia are taken from REAS, which is built upon consistent methodologies and data sources and employs specific information at regional, country, and province levels for Asia at a resolution of $0.5^{o} \times 0.5^{o}$ (longitude × latitude) (Ohara et al., 2007). REAS has three scenarios for emission control in China: REF (Reference Case), PSC (Policy Success Case), and PFC (Policy Failure Case); however, there is only one reference scenario (REF) for India for the prediction up to 2020. We chose the pessimistic scenario of PFC for China because the comparisons with satellite observations have indicated that the trends in Chinese anthropogenic emissions were mostly consistent with this scenario during the first decade of this century (Akimoto et al., 2006; Kurokawa et al., 2009; Wang et al., 2011; Zhang et al., 2007, 2012). The biomass burning emissions, especially from crop residue burning, are quite important as a source of O_3 precursors, and are parameterized using GFED2 (Global Fire Emission Database) inventories and AATSR (Advanced Along-Track Scanning Radiometer) hotspot data following Freitas et al. (2005). This study also applied EDGAR 2000 (Emission Database for Global Atmospheric Research) (Olivier & Berdowski, 2001) for emissions outside Asia, and GEIA (Global Emissions Inventory Activity) inventory (Guenther et al., 1995) for biogenic emissions. It should be noted that, for future emissions, we took into account the changes in REAS only for Asia, and left other emission inventories (e.g. EDGAR 2000 and GEIA) unchanged. Moreover, the meteorological conditions for the year 2000 were also used for 2020.

The WRF/Chem-CHASER model system is driven by meteorological data from the U.S. National Centers for Environmental Prediction (NCEP). The output of the global CTM is monotonically interpolated from the Gaussian latitude and longitude grid to the Lambert conformal conic projection for use in the regional CTM. The lateral

boundary is updated every 6 hours and linearly interpolated for each time step. Figure 5.1 shows the model domain for the regional CTM with a horizontal resolution of 40 km (199 × 149 grids). The regional CTM has 31 vertical layers up to 100 hPa with 11–12 layers across the heights of 0–2 km from the surface. As a result of the deposition of O_3 to the land surface, [O_3] shows a vertical gradient within the bottom layer of the CTM. To account for the [O_3] gradient, we converted the [O_3] at the reference height (approx. 25 m) to that at the canopy height (1 m) following the approach of Oue et al. (2009) when calculating the O_3 doses for WPL evaluations. This method has been shown to describe the [O_3] vertical variations well in a Chinese wheat field (Oue et al., 2009).

For years 2000 and 2020, each [O_3] simulation was integrated from January to December after a spinup calculation for one month, and the calculated values were recorded every hour.

5.2.2. Distribution of wheat production and phenology

Wheat is grown widely in China, and the main producing areas are located across central eastern China (CEC), particularly in the provinces of Henan, Shandong, Hebei, Jiangsu, and Anhui, which, combined together, account for more than 65% of the national wheat production (China Agricultural Yearbook Editorial Committee, 2000). In India, the major wheat production states are in the northern parts of the country with Uttar Pradesh, Punjab, Haryana, Madhya Pradesh and Rajasthan together contributing to almost 85% of the national wheat production (Central Statistical Organisation, 2000). In this study, the wheat production for each province/state of China and India was obtained from the respective national statistics (China Agriculture Yearbook Editorial Committee, 2000; Central Statistical Organisation, 2000). The provincial/state wheat production is subsequently distributed into each grid cell (40 × 40 km) (Fig. 5.1) according to the crop area map compiled by Monfreda et al. (2008). We did not consider the potential changes of wheat production from 2000 to 2020 in this study; hence the wheat production in 2020 in the absence of the effect of O_3 is assumed to be the same as that in 2000.

Calculation of both the exposure-based and flux-based O_3 doses requires accumulation of O_3 concentration or O_3 flux over a certain period of the growing season, with the critical stage of wheat being anthesis. For China, the statistical data of wheat phenology from more than 300 agro-meteorological stations, which were maintained by the Chinese Meteorological Administration, are interpolated into each grid cell within the domain using Kriging methods. For India and other regions within the CTM domain, however, we did not have the statistical data of wheat phenology, and used a phenological model to calculate the date of wheat anthesis as recommended in the Mapping Manual 2004 (LRTAP Convention, 2004). This model has also been applied successfully in a previous study (Van Dingenen et al., 2009), which crosschecked the modeled growing season against the national wheat growing season tables provided by USDA and LRTAP Convention (2004).

5.2.3. Dose–response functions

Among the exposure-based O_3 indices, AOT40 has been used most widely during the last two decades as it has been found to be closely related to the relative yield of many crop species (LRTAP Convention, 2004; Mills et al., 2007). Hence, the AOT40–response relationships for wheat derived from both the European OTC (Mills et al., 2007) and the Asian FACE (Zhu et al., 2011) experiments were chosen for the present study. The difference between these two studies is in the accumulation period for AOT40: 90 days in Mills et al. (2007) (herewith referred to as 90-days AOT40) and 75 days in Zhu et al. (2011) (herewith referred to as 75-days AOT40). We rescaled both AOT40–response functions so that the relative yield is equal to unity at zero AOT40, to eliminate any systematic bias in the estimate (Van Dingenen et al., 2009).

We also compared two stomatal O_3 flux–response relationships for wheat: POD_6 (phytotoxic O_3 dose, which is accumulated stomatal flux of O_3 above threshold of 6 nmol O_3 m^{-2} projected leaf area (PLA) s^{-1}) and POD_{12} (the same as POD_6 but for the threshold of 12 nmol O_3 m^{-2} PLA s^{-1}). The former was derived from European OTC experiments (Pleijel et al., 2007), and the latter was recently established at the Asian

FACE experiment (this study, Chapter 4). There are some differences between the POD_6 and POD_{12} approaches in the algorithm and parameterization of the multiplicative model to calculate stomatal conductance (g_{sto}). In comparison to the POD_6 approach, the POD_{12} approach uses a g_{sto} model with less restrictive VPD and O_3 functions and a more restrictive radiation function, and the temperature function is omitted.

The definition of these four O_3 dose metrics and their corresponding dose–response functions, which relate the O_3 doses to the relative yield, is given in Table 5.1.

5.2.4. Meteorological input and the associated uncertainties

The NCEP reanalysis dataset is one of the most widely used tools in meteorological, climatic and other related research, and is applied in this study as the meteorological input for the g_{sto} models. Temperature and relative humidity at 2 m height from NCEP with 6 h temporal resolution were linearly interpolated to obtain the hourly temporal resolution needed for the calculation of stomatal O_3 flux. Incoming downward short-wave radiation (SR) was converted to photosynthetic photon flux density (PPFD) by multiplying by a factor of 2 (Monteith & Unsworth, 2008).

It has been reported that the NCEP dataset tends to overestimate SR with an average bias of +20%, but underestimate both temperature and VPD with an average bias of –1.4 ºC and –25.7%, respectively (Zhao et al., 2006). Although these biases have large temporal and spatial variations (Aquila et al., 2005; Zhao et al., 2006; Liu et al., 2012), we adopted the simplest approach to the analysis of the uncertainty of the NCEP inputs for our POD_6 and POD_{12} calculations and the relative yield loss (RYL) estimations. Three sensitivity tests were conducted with perturbations of a 20% reduction in SR (SR × 0.8), a 3 ºC temperature increase (Temp + 3 ºC), and a 50% increase in VPD (VPD × 1.5) to the interpolated hourly meteorological output of the NCEP reanalysis. We tested for the individual effects of each variable, as well as a combined effect with the three perturbations applied together. The perturbations applied to temperature and VPD were based on the past studies that reported

particularly large underestimation by the NCEP dataset for our study domain (Zhao et al., 2006; Liu et al., 2012). Note, however, that we did not use the adjusted temperature to recalculate the accumulation period for stomatal O_3 uptake to account for the shift in plant phenology in response to the temperature change. We did not consider the sensitivity of photochemical production of O_3 to temperature either.

5.2.5. Crop loss assessment

We followed the approach adopted by Van Dingenen et al. (2009) (hereafter referred to as VD2009) and Avnery et al. (2011a, b) (hereafter referred to as A2011) to estimate the WPL. The respective exposure-based and flux-based O_3 doses were accumulated over their corresponding calculation periods for each of the 40 × 40 km grid cells, leading to a gridded relative yield loss (RYL_i) calculation. For each grid cell, the wheat production loss (WPL_i) was calculated from the RYL_i and the actual wheat production for the year 2000 within the grid cell (WP_i) as follows:

$$WPL_i = RYL_i / (1 – RYL_i) \times WP_i$$

The provincial/state and national WPL were obtained by summing up all WPL_i belonging to each province/state and country, and the provincial/state or national RYL were calculated by the aggregate WPL. The changes of WPL and RYL from the years 2000 to 2020 were then calculated as the difference between the two years.

5.3. Model evaluation against [O_3] observations

Although the CTM has been validated to perform well by comparisons of modelled [O_3] with ground–based observations at 251 stations in Japan (Takigawa et al., 2007) and Mount Tai in China (Takigawa et al., 2009), we further compared monthly [O_3] simulated with the WRF/Chem-CHASER model system used in this study against observations obtained from the literature over our study domain. Monthly observation data in China over the North China Plain (NCP), the Yangzi River Delta (YRD), and the Pearl River Delta (PRD) were from 1999 to 2006 with the exception of Jiangdu site in YRD including [O_3] data from 2007 to 2011 (this study, Chapter 2). In three diagnostic regions of India (Northern, Central and Southern India), the [O_3]

observations were conducted from 1997 to 2006 except for one older dataset from 1993 to 2000 (Naja et al., 2003) and another in 2008 (Reddy et al., 2010). Most of the observations were conducted at rural or suburban sites, but observations at some urban sites were also included where the available data were sparse especially in Northern and Central India. The simulated monthly [O_3] for the year 2000 were averaged across the grid cells where the observation sites were located, whereas the monthly values of the observed [O_3] were averaged across the observation sites and years within each region (Fig. 5.2). The region boundaries and the sources of the observation data for each region are listed in Table 5.2.

In general, magnitudes and seasonal variations of monthly [O_3] in the selected regions are simulated reasonably well with mixing ratios mostly falling within one standard deviation of the observations. However, simulated [O_3] for NCP and YRD tend to be underestimated by approximately 3–9 ppb for the monthly averages during the highest O_3 period in June. This may be caused by the inaccurate description of the temporal and spatial distribution of agricultural residue burning after winter crop harvest (e.g. wheat), which serves as a major O_3 precursor in this region (Li et al., 2007; Yamaji et al., 2008; Tang et al., 2013). The rapid increases in anthropogenic emission over this regions since 2000 (Ohara et al., 2007; Zhang et al., 2012) should have also contributed to the model underestimation. For PRD and India, on the other hand, the model apparently overestimates the [O_3] by approximately 5–10 ppb in several months particularly in summer. We ascribe this discrepancy partly for the insufficient resolution over time (6 h) and space (2.5º×2.5º) in NCEP data to reproduce meteorological fields in the rainy season, when the frequent precipitations may depress the local [O_3]. In addition, at some of the northern and central Indian observation sites located in densely populated areas, the [O_3] may have been suppressed by local NO_x titration, which contributed to the overestimation of [O_3]. This has been suggested in the previous studies (Van Dingenen et al., 2009; Avnery et al., 2011a).

It must be noted, nevertheless, that the accumulation period for AOT40 and POD_Y

calculations spans mainly from February to April and from March to May in major wheat producing areas of India and China, respectively, and that the model exhibited a good performance for these periods. Therefore, the overestimates and underestimates of [O_3] after these periods may not have significant effects on our estimation in the O_3-induced wheat yield loss.

5.4. Results

5.4.1. Distribution of exposure-based and flux-based O_3 doses

Spatial distributions of the exposure-based O_3 doses of 90-days AOT40 and 75-days AOT40 were consistent with each other for 2000 (Fig. 5.3a, b, left panels) and 2020 (Fig. 5.3a, b, middle panels). They indicated greater O_3 exposure in the regions of CEC (central Eastern China including North China Plain and Yangzi River Delta), the Pearl River Delta, and Tibet for China, and around the northernmost regions, Indo-Gangetic Plain, and mega cities for India. In 2000, across the major wheat producing areas of CEC and Indo-Gangetic Plain, the 90-days AOT40 exceeded the critical level of 3 ppm h that was established in Europe for the protection of crops (LRTAP Convention, 2004). With a large future increase in [O_3], some areas in the Yangzi River Delta and northernmost India will experience more than 15 ppm h of 90-days AOT40 in 2020. The extremely high O_3 exposure doses in the Tibetan plateau (Fig. 5.3a, b left and middle panels) may be caused by air exchange between stratosphere and troposphere (Ding & Wang, 2006), and will be unaffected by anthropogenic emissions, as shown by the little change in that region in AOT40 from 2000 to 2020 (Fig. 5.3a, b, right panels).

The geographical pattern of the flux-based POD_6 (Fig. 5.3c) is somewhat different from that of the exposure-based O_3 doses. In both 2000 and 2020, POD_6 is close to naught in the Tibetan plateau but elevated in southern and central India. This contrast is caused by stomatal closure in cold climates and opening in warm climates, since the effect of temperature on g_{sto} is accounted for in POD_6 (Pleijel et al., 2007). In POD_{12}, by comparison, the direct effect of temperature on stomatal opening is not considered,

whereas the influence of temperature is exerted via its effect on VPD (this study, Chapter 4). The spatial distribution of POD_{12} (Fig. 5.3d) is thus similar to that of AOT40. Furthermore, the increase in POD_{12} from 2000 to 2020 is significant in some high [O_3] areas but less dramatic than that in POD_6 (Fig. 5.3c, d, right panels).

5.4.2. Wheat production loss in 2000

As the main wheat producing areas (Fig. 5.1) overlap with areas of high exposure/flux O_3 doses (Fig. 5.3), the largest WPL is projected for the regions over CEC of China and northern India across all the O_3 dose metrics (Fig. 5.4). The top five wheat production provinces/states listed in Table 5.3 together account for more than 83% and 90% of the total WPL of China and India, respectively. On a provincial/state scale, Henan and Jiangsu in China have the greatest WPL (1.9–4.7 Mt) and RYL (11.5–23.5%), respectively, while Punjab in India shows the largest values of WPL (3.0–6.4 Mt) and RYL (17.4–30.7%). The countrywide WPL (RYL) for China and India are 7.8–20.0 Mt (6.4–14.9%) and 6.4–20.5 Mt (8.2–22.3%), respectively, depending on the O_3 dose metrics used.

In general, POD_6 gave a greater RYL than the other O_3 dose metrics for most of the provinces/states except a few cold-climate provinces (See Tables A1–A4 in Appendix for WPL and RYL in all the provinces/states of China and India). This discrepancy is especially large in some warm states of India with low O_3 exposure, e.g. Madhya Pradesh and Rajasthan which have a POD_6-based RYL of 13.5% and 8.5%, respectively, in contrast to an RYL of less than 2% estimated by the exposure-based O_3 dose metrics (Table 5.3). RYL estimates by POD_{12} were also a little higher than those by the exposure-based O_3 dose metrics, while 90-days AOT40 gave the lowest estimates.

5.4.3. Increase of wheat production loss from years 2000 to 2020

We projected a further 1.5–13.5% additional production loss ($RYL_{2020} - RYL_{2000}$) for the major wheat producing provinces/states by 2020, with the highest average increase of RYL in Anhui (12.3%) for China and Punjab (8.4%) for India across all

the O_3 dose metrics (Table 5.4, see Appendix for other provinces/states). At a national scale, the average increase in RYL from 2000 to 2020 is estimated to be 8.7% (with a range of 8.1–9.4%) for China and 6.7% (with a range of 5.4–7.7%) for India. The projected increase in WPL from 2000 to 2020 was significantly greater for China (10.2–11.5 Mt) than India (5.0–6.0 Mt) due to greater RYL increase and greater wheat production in China than in India.

All the O_3 dose metrics gave comparable estimates of increase in RYL from 2000 to 2020 (Table 5.4). The standard deviation of the projected RYL increase across the O_3 dose metrics was 0.6% and 0.9% for China and India, respectively, which was much smaller than that of RYL itself in 2000: 3.9% for China and 6.7% for India.

5.4.4. Relationships of RYL estimated by different O_3 dose metrics

The comparisons of the RYL estimates by 90-days AOT40 with the estimates by the other O_3 dose metrics for each province/state of China and India are presented in Fig. 5.5. The RYL by 75-days AOT40 showed close and linear relationships with 90-days AOT40 ($r^2 > 0.98$) (Fig. 5.5a, d) with the intercepts being close to zero and the slopes being ca. 1.1. This means that the RYL estimates by 75-days AOT40 are 1.1 times those by 90-days AOT40.

The two flux-based metrics: POD_6 and POD_{12} predict greater RYL than 90-days AOT40 in 2000 (Fig. 5.5b, c) with slopes greater than 1. In 2020, however, the fit lines came closer to the line of equality (x = y) for both POD_6 and POD_{12} (Fig. 5.5e, f). This is because the both O_3 dose metrics are based on g_{sto} models with a f_{O3} function to reflect the O_3-induced stomatal closure which constrains the O_3 uptake. Being exposure-based, 90-days AOT40 has no such constraint, and hence the deviation from the flux-based RYL diminishes as $[O_3]$ increases from 2000 to 2020. The f_{O3} function for POD_6 is more restrictive than that for POD_{12} as shown in Fig. 5.6 (see Pleijel et al. (2007) and Chapter 4 for further details), thus the decline of the slopes for POD_6 (from 1.259 to 0.851 in Fig. 5.5b, e) is greater than that for POD_{12} (from 1.173 to 1.013 in Fig. 5.5c, f).

The positive intercepts of the fit lines for POD_6 (Fig. 5.5b, e) could be explained as follows. Since the threshold of 6 nmol m^{-2} s^{-1} is approximately 18 ppb under the optimal conditions for O_3 uptake, the $[O_3]$ lower than 40 ppb could contribute to the flux-based dose to produce non-zero RYL at zero AOT40. With POD_{12}, on the other hand, the threshold of 12 nmol m^{-2} s^{-1} is approximately 37 ppb under the optimal conditions for O_3 uptake, and, hence, the near-zero RYL at zero AOT40 (Fig. 5.5c, f).

5.4.5. Uncertainties associated with the meteorological inputs

As shown in Figure 5.6, an increase of temperature by 3ºC increased RYL with POD_6 by +5.5% for China, but reduced that for India by –1.93%. Despite the lack of f_{temp} function in POD_{12}, the temperature rise increased VPD, which reduced stomatal opening and, hence, RYL. A 50% increase in VPD reduced RYL for both China and India to a greater extent with POD_6 (–1.1% for China and –4.2% for India) than POD_{12} (–0.4% for China and –2.4% for India). However, RYL was little changed by the 20% decrease in SR with either of the two flux-based metrics.

Overall, the combined perturbations to the three meteorological factors changed the estimated RYL by +3.4% (from 14.9% to 18.3%) and –1.1% (from 10.3% to 9.2%) for POD_6 and POD_{12}, respectively, for China, and by –7.9% (from 22.3% to 14.4%) and –3.8% (from 9.7% to 5.9%) for POD_6 and POD_{12}, respectively, for India. It should be noted that the same perturbations to the NCEP inputs for the year 2020 change RYL to a similar extent as noted above for 2000 (data not shown). Our estimated changes of RYL from 2000 to 2020 were, therefore, little affected by the NCEP input perturbations, with biases occurring only in the range of –0.2% and –1.0%, depending on the perturbation, O_3 dose metrics, and country.

5.4.6. Variations in the response functions of g_{sto} models

Analyses of the variations in the response functions (f_{temp}, f_{VPD} and f_{light}) with corresponding climatic variables averaged for each province/state (Fig. 5.8) show that +3 ºC increase in temperature may reduce the restriction of f_{temp} on g_{sto} for China, thus increase the O_3 uptake. In contrast, temperatures in India are already within the

optimal range, further elevation in temperature may lead to stomatal closure hence decrease the O_3 uptake (Fig. 5.8a, d).

The reduction in RYL by 50% increase in VPD is greater for India than that for China, which could be due to the multiplicative restriction of f_{VPD} on g_{sto} in India as the daytime average VPD in most of the states of India are higher than that of China (Fig. 5.8b, e). Considering the more restrictive VPD response function in the g_{sto} model of POD_6 (see Pleijel et al. (2007) and Chapter 4 for further details) results in sharper decline in f_{VPD} than that of POD_{12}, the larger changes in RYL is thus estimated by using POD_6 than that by using POD_{12}.

We found seldom changes of RYL with 20% decrease in SR. This may be because the exponential functions of f_{light} are insensitive to our change of SR, despite the more restrictive parameterizations for POD_{12} (Fig. 5.8c, f). For instance, a 20% decrease in the hourly mean SR at 500 W m^{-2} (approx. 1000 μmol m^{-2} s^{-1} PPFD by our recalculation) lead to only 4.6% decrease in f_{light} for POD_{12} (i.e. from 0.945 to 0.902), while nearly no change in f_{light} for POD_6. The deviation in f_{light} by SR decrease could become larger at low-level SR, but the consequent bias on O_3 uptake calculation may be small, as $[O_3]$ is also usually low in that situation.

5.5 Discussion

This study estimated that the ozone-induced wheat RYL in 2000 was 6–15% for China and 8–22% for India, respectively. These ranges of RYL in 2000 overlap with those in previous studies (VD2009 and A2011, the two global evaluations of the crop loss to O_3 with exposure-based O_3 metrics) (Table 5.5). However, our RYL estimates by 90-days AOT40 (our lower boundary estimates in Table 5.5) are smaller than those in the previous assessments with the same O_3 dose metrics (their upper boundary estimates in Table 5.5) for both China and India. This discrepancy could be ascribed to differences in agricultural datasets, emission inventories, the CTM, and the conversion of $[O_3]$ from CTM output to that at the canopy height. With the high spatial resolution and the emission inventory developed specifically for Asia, our

CTM performed well in terms of [O_3] simulation in Asia (Takigawa et al., 2007, 2009, and Fig. 5.2). By comparison, both VD2009 and A2011 significantly overestimated [O_3] during the wheat season in Northern India (Van Dingenen et al., 2009; Avnery et al. 2011a). Moreover, the [O_3] at the canopy height in a Chinese wheat field was better estimated with the method of Oue et al. (2009) (slope = 1.10, r^2 = 0.65) than with either of the methods recommended in LRTAP Convention (2004) (slope of 1.32, r^2 of 0.51 for method A, and slope = 1.22, r^2 = 0.55 for method B) that were adopted in VD2009 (Takigawa, unpublished data). In A2011, furthermore, the direct use of the [O_3] output of the CTM should have led to a significant overestimation of canopy [O_3] and hence RYL. When we directly used the [O_3] at a reference height of approx. 25 m, our RYL estimates with 90-days AOT40 rose to 15.6% and 19.0% for China and India, respectively, approaching the numbers in A2011.

Under the future anthropogenic emissions of REAS, the projected increase in wheat RYL from 2000 to 2020 for China (8.1–9.4%) is greater than the estimate in VD2009 and close to the upper boundary of the A2011 estimates for the increase in RYL from 2000 to 2030 (Table 5.5). For India, on the other hand, our projection of RYL increase (5.4–7.7%) is smaller than the upper boundary estimates of VD2009 and A2011 for the change in RYL between 2000 and 2030. This is primarily because we have assumed a very large increase (128%) of NO_x emission in China according to the pessimistic scenario (PFC) for Chinese emission control, whereas, for India, we assumed a modest increase (49%) of NO_x emission under the reference scenario (Ohara et al., 2007). For China, as mentioned earlier, the PFC scenario is the closest among the 3 scenarios of REAS to the observed trend in recent years (Akimoto et al., 2006; Kurokawa et al., 2009; Wang et al., 2011; Zhang et al., 2007, 2012). For India, on the other hand, a recent inventory coupled with multi-satellite observations reported that NO_x emissions from the Indian power plants (the most important source of NO_x in India) increased by at least 70% during 1996−2010 (Lu & Streets, 2012). Another inventory (Cofala et al., 2006) also presented a greater increase (67%) in NO_x emissions than that in REAS (49%) from 2000 to 2020 under the Current Legislation

scenario (CLE) in India. Taking into account the possible underestimation of Indian NO_x emissions, our estimates of the increase in RYL from 2000 to 2020 for India may be conservative.

Among the O_3 dose metrics, the often-used 90-days AOT40 gave a smaller RYL than the 75-days AOT40, as presented in Table 5.3 and Fig. 5.5. The dose–response relationship with 90-days AOT40 has been derived from OTC experiments across Europe, whereas the relationship with 75-days AOT40 is based on the FACE experiment in the Yangzi River Delta of China. A comparison between these two relationships showed that the slope of the 75-days AOT40–response function was larger than that in 90-days AOT40, but that the difference was not statistically significant (Zhu et al., 2011). In the same study, an OTC study in northern China (Feng et al., 2003) showed lower yield loss sensitivity, and an OTC study in India (Sarkar & Agrawal, 2010) showed higher yield loss sensitivity than the European results; both of these results were statistically significant (Zhu et al., 2011). On the other hand, a recent study with OTC experiments suggested that the wheat cultivars in the Yangzi River Delta may be more sensitive to O_3 than that used in European studies (Wang et al., 2012). A survey of the experimental data over Asia indicated a large difference in the sensitivity of wheat yield loss to O_3, both between and within individual studies, varying with location, experimental method, and cultivars (Emberson et al., 2009). It thus appears that we are not yet able to make a general statement on the comparison between the regions in regards to sensitivity to wheat yield loss to O_3.

It is noteworthy that the flux-based approach of POD_6 from European studies gave substantially greater aggregate RYL than that of the 90-days AOT40 for China and India by a factor of 2.3 and 2.7, respectively for the year 2000 (Table 5.3). One possible explanation is that the lower threshold of POD_6 (approx. 18 ppb under the optimal conditions for O_3 uptake) may include contributions from $[O_3]$ lower than 40 ppb to produce higher RYL. Most importantly, a more frequent occurrence of environmental conditions optimal for O_3 uptake in our study regions, compared to

those in Europe, could have resulted in the larger RYL estimates on POD_6 as compared with those based on AOT40. There is evidence of these effects in our study, as seen in the discrepancy in RYL estimates between POD_6 and AOT40, which is enlarged in some warm states of India (Table 5.3). Indeed, many reports have shown an enhanced stomatal uptake of O_3 in warmer and more humid environments (such as in subtropical Asia) compared to cool climates (such as in northern Europe) (Danielsson et al., 2003; Mills et al., 2011). An assessment of O_3 impacts on crops in Europe for the year 2000 also showed a discrepancy between POD_6-based and AOT40-based wheat yield loss estimates, and, at most locations investigated, the flux-based estimate was greater than the exposure-based estimate (Holland et al., 2006).

In contrast to the large difference in the estimates of RYL and WPL between 90-days AOT40 and POD_6 (both of which are based on European studies), the estimates between 75-days AOT40 and POD_{12} from the Asian study exhibited a smaller difference. This might be because the dose–response functions of 75-days AOT40 and POD_{12} were derived from experiments at the same site in different years (Zhu et al., 2011; Chapter 4, this study). The omission of a temperature function in the g_{sto} model of POD_{12} may have also lessened the influence of climatic differences among locations on O_3 uptake and, hence, between the O_3 impact estimates. Furthermore, the threshold of POD_{12} (approx. 37 ppb under the optimal conditions for O_3 uptake) was close to that for AOT40.

In the future projections, the increase in RYL from 2000 to 2020 was comparable between the different O_3 dose metrics (Table 5.4). The 75-days AOT40 gave proportionately higher RYL than 90-days AOT40 by a factor of 1.1 for both 2000 and 2020, and, hence, resulted in a proportionately greater increase in RYL for 75-days AOT40 compared to 90-days AOT40. Why, then, has the discrepancy in the estimated RYL for the year 2000 between the AOT40-based and flux-based approaches disappeared in the RYL increases? With AOT40, the yield loss estimate increases in proportion to the increase of O_3 exposure, which is not the case in the flux-based

estimate. Exposure to high [O_3] causes a reduction in g_{sto} (Gelang et al., 2000; Danielsson et al., 2003; Feng et al., 2008), which would limit stomatal O_3 uptake, and diminish further increases of O_3 flux and yield loss. The lower threshold [O_3] (for POD_6) and favorable climate contribute to the higher RYL estimates for POD_Y in 2000, but do so to a lesser degree in the differential RYL between 2000 and 2020.

Furthermore, our sensitivity tests suggested that the POD_Y calculations are strongly affected by the quality of the meteorological inputs. The possible underestimation of temperature and VPD in the NCEP reanalysis dataset may have caused a large deviation in the estimated RYL. Since we applied the same inputs for 2000 and 2020, the effect of perturbations in meteorological factors on our estimated change in RYL is small (with biases only in the range between –0.2% and –1.0%). If the climate changes in the future, however, the O_3-induced RYL of wheat may increase or decrease to a large extent depending on the climatic region.

5.6. Conclusions

In this study, we evaluated O_3-induced WPL for China and India by using both exposure-based and flux-based approaches derived from European OTC and the FACE-O_3 experiments. Reduction in wheat production in 2000 was estimated to be 6.4–14.9% for China, and 8.2–22.3% for India. POD_6 predicted greater RYL, especially for the warm regions of India, whereas the 90-days AOT40 gave the lowest estimates. For the future projection, all the O_3 dose metrics gave comparable estimates of increase in RYL from 2000 to 2020 in the ranges of 8.1–9.4% for China and 5.4–7.7% for India, respectively. The lower projected increase in RYL for India may be due to conservative estimation of the emission increase in 2020. Sensitivity tests of the model showed that the PODY-based estimates of RYL are highly sensitive to perturbations in the meteorological inputs, but that the estimated increase of RYL from 2000 to 2020 is much more robust.

Admittedly, there remain some additional sources of uncertainty in our projections, such as the possible shift of plant phenology, the effects of soil water potential on

stomatal conductance, and the effects of climate change on surface [O_3] (Fuhrer, 2009; Teixeira et al., 2011). Varietal differences, if any, in stomatal responses to the environmental variables and the maximum stomatal conductance would also be counted as sources of uncertainty in the crop yield loss projections. Despite these uncertainties, however, this study and the past studies (Van Dingenen et al., 2009; Avnery et al. 2011a) show an overlapping of their ranges of wheat yield reduction due to present-day [O_3] (Table 5.5) beyond the differences between the studies in the emission inventories, CTM, and O_3 dose metrics. The much higher RYL in 2000 with the flux-based methods than those based on AOT40 for some major wheat producing areas suggests even larger O_3 risks due to the specific environmental regimes in our study regions. Moreover, the greatest confidence can be placed on the projected WPL increase from 2000 to 2020, given the consistent estimates across the different O_3 dose metrics and the small sensitivity in the estimates using the flux-based methods to perturbations in the meteorological inputs. The substantial, if not panicking, reduction in wheat production in the near future poses a serious challenge to the global food security, given that the two countries are the largest and the second largest in the world in terms of the wheat production and population. We therefore strongly urge that measures to be taken to curb the rapid increase of surface [O_3] in the two countries as well as other countries with increasing emission of O_3 precursors.

Table 5.1 Overview of O_3 dose metrics and corresponding dose–response functions used to calculate relative yield loss of wheat in our study.

Experiment	O_3 index	Accumulation period	Function (y = relative yield, x = O_3 dose)	Reference
European OTC	90-days AOT40	90 days, centering on the anthesis date.	y = –0.0163x + 1	Mills et al., 2007, corrected for offset (see text)
Asian FACE	75-days AOT40	75 days, from 44 days before to 30 days after the anthesis date.	y = –0.0205x + 1	Zhu et al., 2011, corrected for offset (see text)
European OTC	POD_6	970˚C days, starting 270˚C days before anthesis.	y = –0.048x + 1	Pleijel et al., 2007
Asian FACE	POD_{12}	800˚C days, starting 200˚C days before anthesis.	y = –0.082x + 1	This study, Chapter 4

Table 5.2 List of the regional boundaries, number of observational sites, and data sources of the observed [O_3] for each defined region.

Region	Minimum lon, lat	Maximum lon, lat	Number of stations	Reference
NCP China	115, 36	118, 41	5	Li et al., 2007; Lin et al., 2008, 2009; Shan et al., 2008; Wang et al., 2010
YRD China	118, 30	121, 32	7	Wang et al., 2006; Tu et al., 2007; Jiangdu site, Chapter 2
PRD China	112, 22	117, 25	16	Zheng et al., 2010
North India	72, 23	77, 29	4	Naja et al., 2003; Satsangi et al., 2004; Mittal et al., 2007; Ghude et al., 2008
Central India	72, 17	76, 20	6	Debaje & Kakade, 2006, 2009; Beig et al., 2007; Debaje et al., 2010
South India	77, 8	80, 15	6	Nair et al., 2002; Naja & Lal, 2002; Debaje et al., 2003; Ahammed et al., 2006; Beig et al., 2007; Reddy et al., 2010

Table 5.3 Aggregate wheat production loss (WPL) in 2000 estimated by different O_3 dose metrics for the top five wheat producing provinces/states in China and India as well as for the countries as a whole. The relative yield loss (RYL) is shown in parentheses.

	WPL (10^4 metric tons) and RYL (%) in 2000			
Province/ State	90-days AOT40	75-days AOT40	POD_6	POD_{12}
Henan	185.1 (7.5%)	205.8 (8.2%)	473.2 (17.1%)	269.6 (10.5%)
Shandong	151.2 (6.7%)	173.9 (7.6%)	416.0 (16.4%)	271.8 (11.4%)
Hebei	100.3 (7.3%)	111.8 (8.0%)	249.7 (16.3%)	180.4 (12.3%)
Jiangsu	138.5 (11.5%)	169.8 (13.7%)	328.3 (23.5%)	247.7 (18.8%)
Anhui	74.0 (8.0%)	85.1 (9.1%)	219.7 (20.5%)	120.6 (12.4%)
Whole China	777.9 (6.4%)	888.6 (7.2%)	1995.1 (14.9%)	1301.2 (10.3%)
Uttar Pradesh	158.8 (6.4%)	163.2 (6.6%)	647.0 (21.8%)	165.4 (6.7%)
Punjab	304.3 (17.4%)	343.7 (19.2%)	641.6 (30.7%)	360.8 (20.0%)
Haryana	99.9 (10.4%)	107.8 (11.1%)	329.5 (27.7%)	147.1 (14.6%)
Madhya Pradesh	12.1 (1.4%)	12.6 (1.5%)	129.7 (13.5%)	13.7 (1.6%)
Rajasthan	4.2 (0.6%)	4.8 (0.7%)	64.0 (8.5%)	6.9 (1.0%)
Whole India	639.3 (8.2%)	698.8 (8.9%)	2049.7 (22.3%)	768.7 (9.7%)

Table 5.4 Increase of aggregate wheat production loss (WPL) from 2000 to 2020 estimated by different O_3 dose metrics for the top five wheat production provinces/states in China and India as well as for the countries as a whole. Increase of the relative yield loss (RYL) is shown in parentheses.

	Increases of WPL (10^4 metric tons) and RYL (%)			
Province/ State	90-days AOT40	75-days AOT40	POD_6	POD_{12}
Henan	262.2 (10.6%)	293.8 (11.8%)	289.8 (10.5%)	270.8 (10.6%)
Shandong	173.5 (7.6%)	199.9 (8.7%)	216.1 (8.5%)	195.2 (8.2%)
Hebei	70.1 (5.1%)	83.0 (6.0%)	92.0 (6.0%)	80.3 (5.5%)
Jiangsu	118.8 (9.8%)	145.2 (11.7%)	116.4 (8.3%)	140.1 (10.6%)
Anhui	110.2 (11.9%)	126.5 (13.5%)	116.0 (10.8%)	124.3 (12.8%)
Whole China	1016.3 (8.4%)	1153.2 (9.4%)	1080.0 (8.1%)	1129.1 (8.9%)
Uttar Pradesh	160.2 (6.5%)	170.6 (6.9%)	154.6 (5.2%)	149.5 (6.0%)
Punjab	183.7 (10.5%)	204.7 (11.4%)	79.8 (3.8%)	143.0 (7.9%)
Haryana	77.1 (8.0%)	84.1 (8.7%)	53.5 (4.5%)	72.8 (7.2%)
Madhya Pradesh	35.6 (4.2%)	37.0 (4.4%)	73.8 (7.7%)	38.0 (3.9%)
Rajasthan	15.6 (2.3%)	16.7 (2.4%)	52.9 (7.0%)	11.1 (1.5%)
Whole India	549.6 (7.1%)	598.5 (7.7%)	496.0 (5.4%)	502.3 (6.4%)

Table 5.5 Comparison of relative yield loss (RYL) estimates in this study with those of other studies (VD2009: Van Dingenen et al. 2009; A2011: Avnery et al., 2011a, b) that are based on similar methodologies. The range of RYL across the various O_3 dose metrics is shown for each study.

	RYL in 2000 (%)			Change in RYL relative to 2000 (%)			
				2020	2030		
	This study	VD2009	A2011	This study [a]	VD2009 [b]	A2011 [c]	A2011 [d]
China	6–15	10–19	3–16	+ 8–9	- 2.3	+ 1–10	+ 0–2
India	8–22	13–28	9–30	+ 5–8	+ 10.7	+ 3–18	+ 1–7

[a] Estimates with PFC (Policy Failure Case) and REF (Reference) scenarios of REAS for China and India, respectively.

[b] RYL estimated with the 2030 CLE (Current Legislation) scenario and averaged across the M7 and AOT40 estimates.

[c] Estimates based on scaling up of the 1990 anthropogenic emissions of EDGAR 2.0 according to IPCC A2 scenario.

[d] Estimates based on scaling up of the 1990 anthropogenic emissions of EDGAR 2.0 according to IPCC B1 scenario.

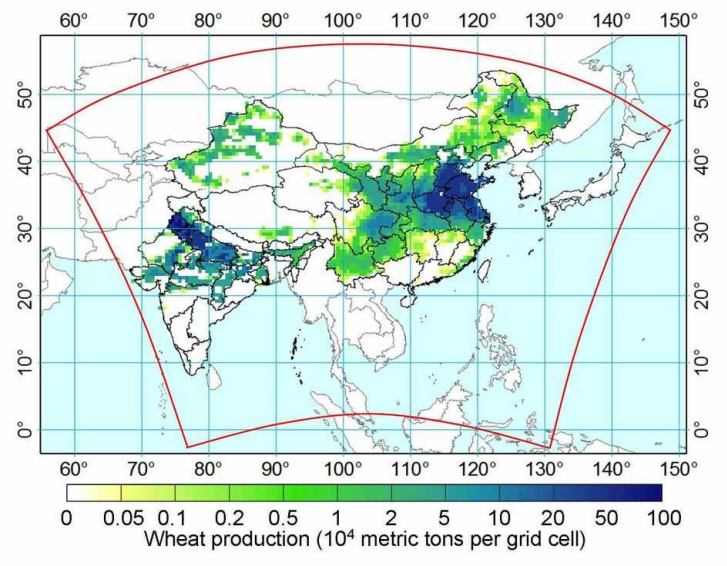

Fig. 5.1 Distribution of wheat production in China and India for the year 2000, Data in each grid cell (40 km × 40 km) were calculated from the statistics of provincial/state wheat production (China Agriculture Yearbook 2000 and Statistical Yearbook India 2000) with the distribution according to the crop area map for wheat compiled by Monfreda et al. (2008). Red line denotes the model domain boundary for the regional CTM part.

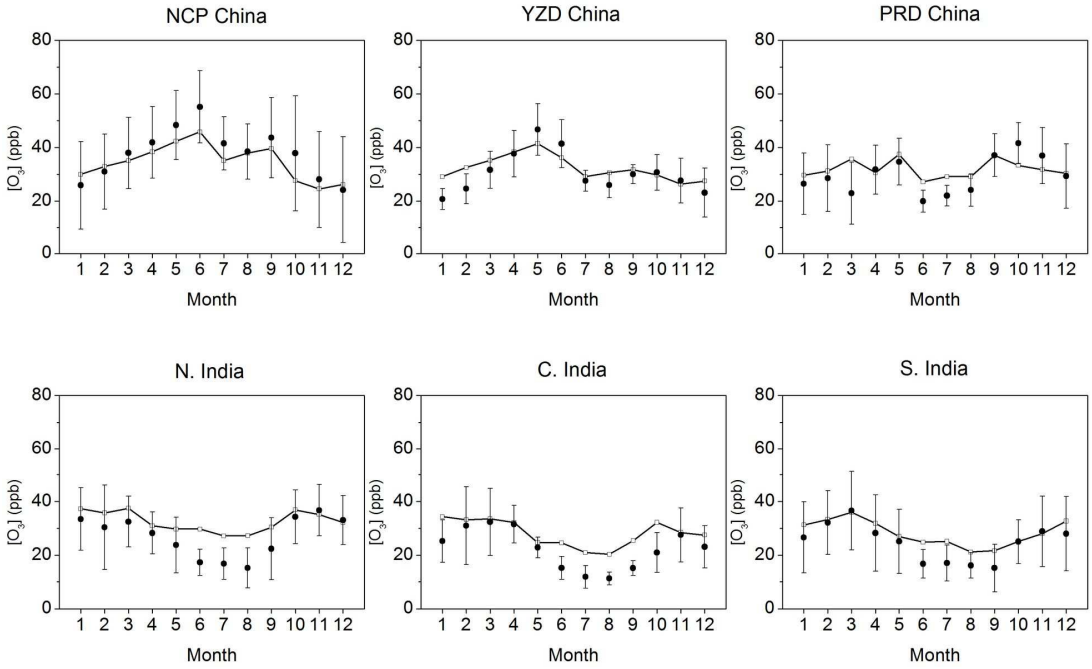

Fig. 5.2 Comparisons between monthly simulated [O_3] (lines) for year 2000 and measured [O_3] (dots) in each defined region. Monthly simulated values are averaged over the grid cells where the observational sites are located. The measured values and error bars represent the means and ± 1 standard deviations of the monthly [O_3] of the observational sites within each region.

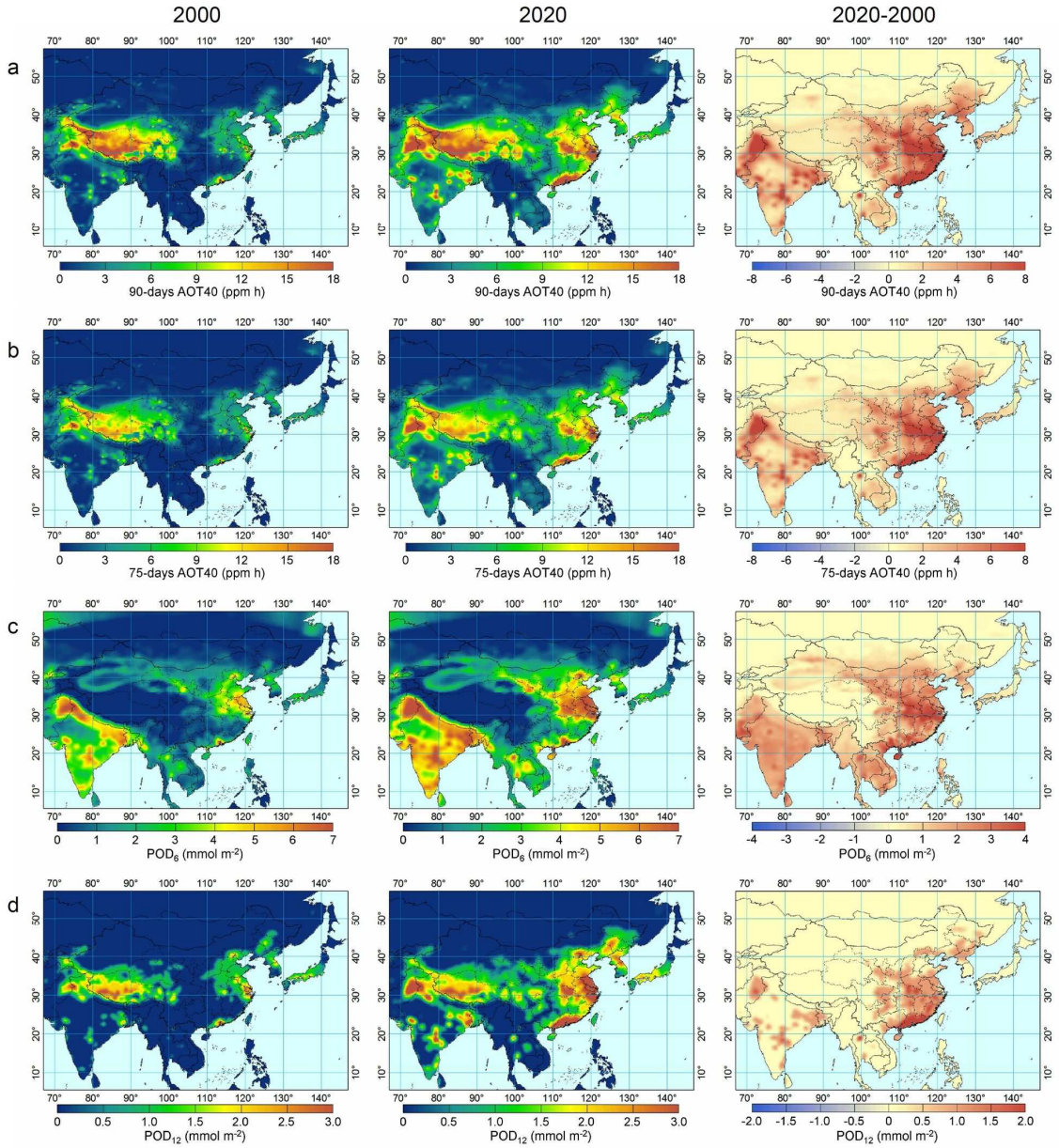

Fig. 5.3 Spatial distribution of 90-days AOT40 (a), 75-days AOT40 (b), POD_6 (c) and POD_{12} (d) over our study domain for years 2000 (left panels) and 2020 (middle panels), and their changes from 2000 to 2020 (right panels, 2020 minus 2000). See text for definition of the O_3 dose metrics and their calculations.

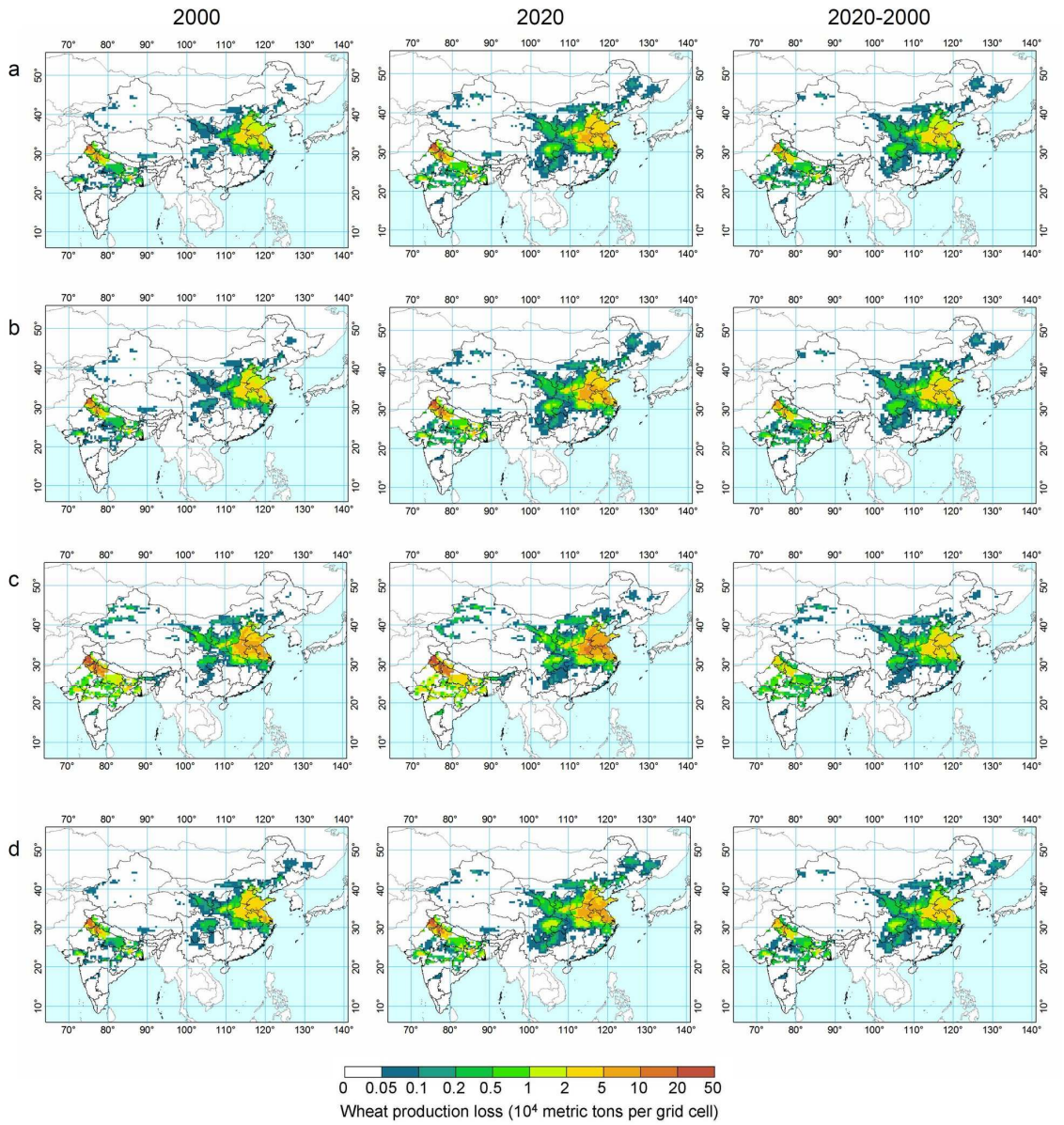

Fig. 5.4 Distribution of wheat production losses in China and India for years 2000 (left panels) and 2020 (middle panels), and their change from 2000 to 2020 (right panels, 2020 minus 2000) estimated by 90-days AOT40 (a), 75-days AOT40 (b), POD_6 (c), and POD_{12} (d). See text for definition of the O_3 dose metrics and their calculations.

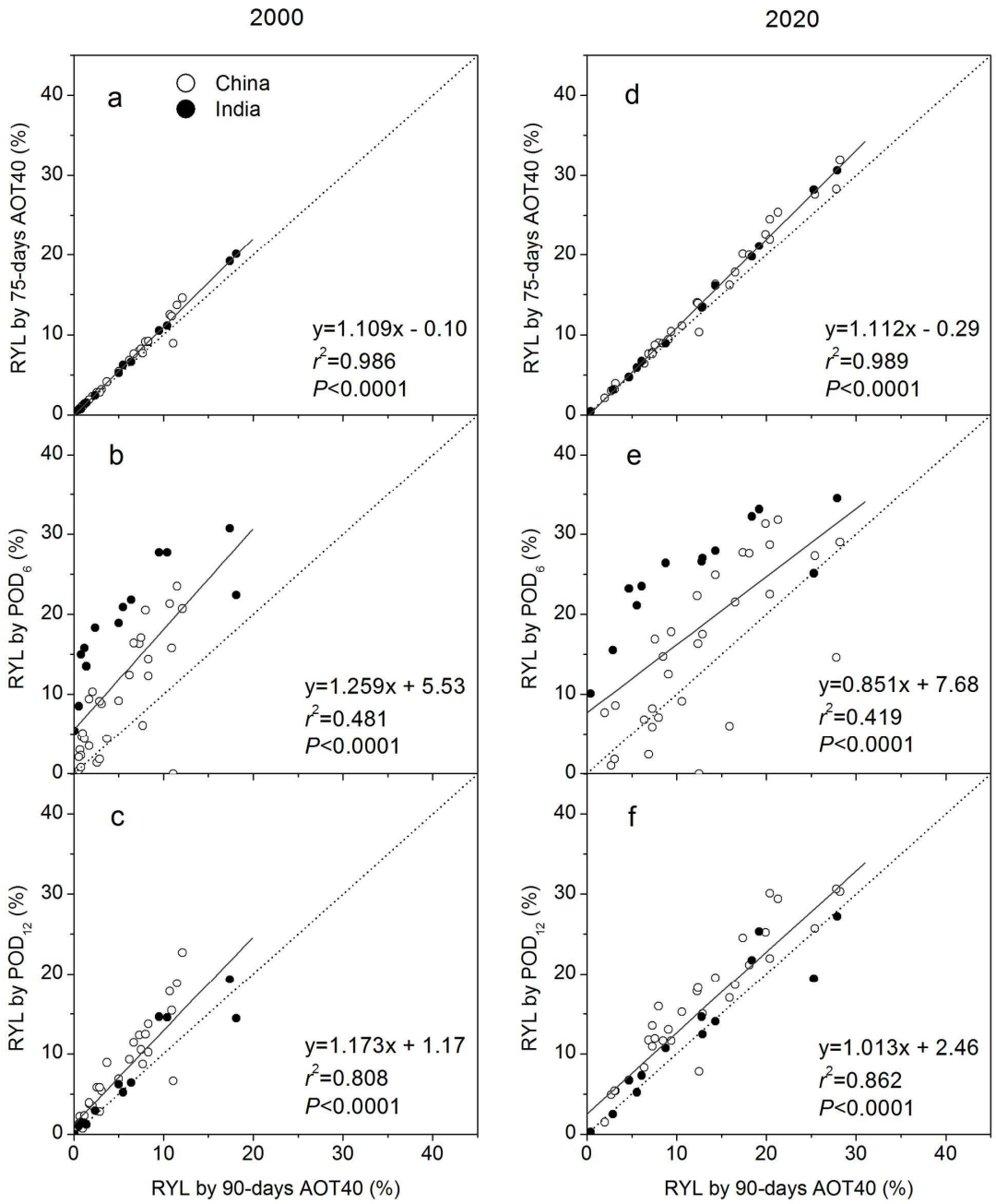

Fig. 5.5 Comparison of the relative yield loss (RYL) estimated by 90-days AOT40 with those by other O_3 metrics: 75-days AOT40 (a, d), POD_6 (b, e), and POD_{12} (c, f) in years 2000 (left panels) and 2020 (right panels). Their linear relationships were fitted for RYL at each province/state in China and India.

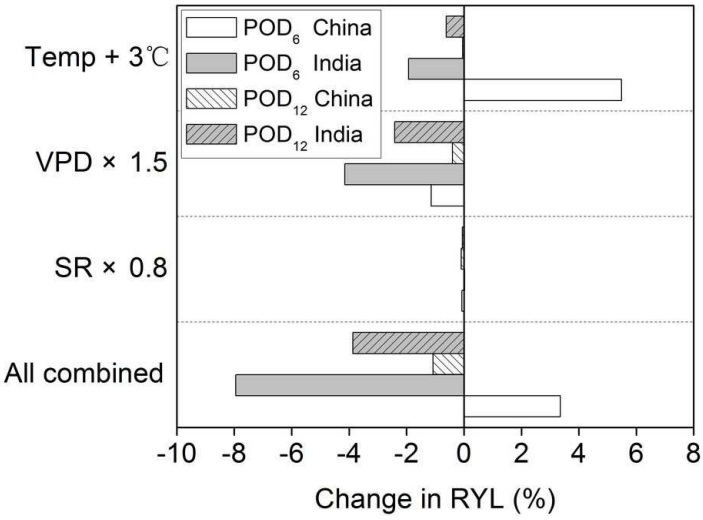

Fig. 5.6 Changes in the estimated national relative yield loss (RYL) of wheat for year 2000 with perturbations to the NCEP inputs of temperature (Temp + 3ºC), VPD (VPD × 1.5), short-wave radiation (SR × 0.8), and their combination, by using both POD_6 and POD_{12} methods.

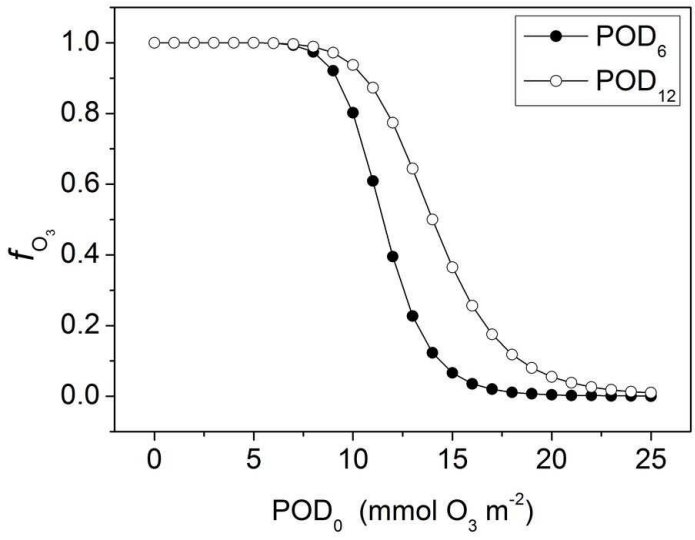

Fig. 5.7 Comparison of the function used to describe O_3-induced reduction in stomatal conductance (g_{sto}) in POD_6 (Pleijel et al., 2007) with that in POD_{12} (this study, Chapter 4). f_{O3} represents the ratio of g_{sto} under accumulated stomatal O_3 uptake relative to the g_{sto} without the O_3 effects. POD_0 is the accumulated stomatal O_3 flux with a zero threshold.

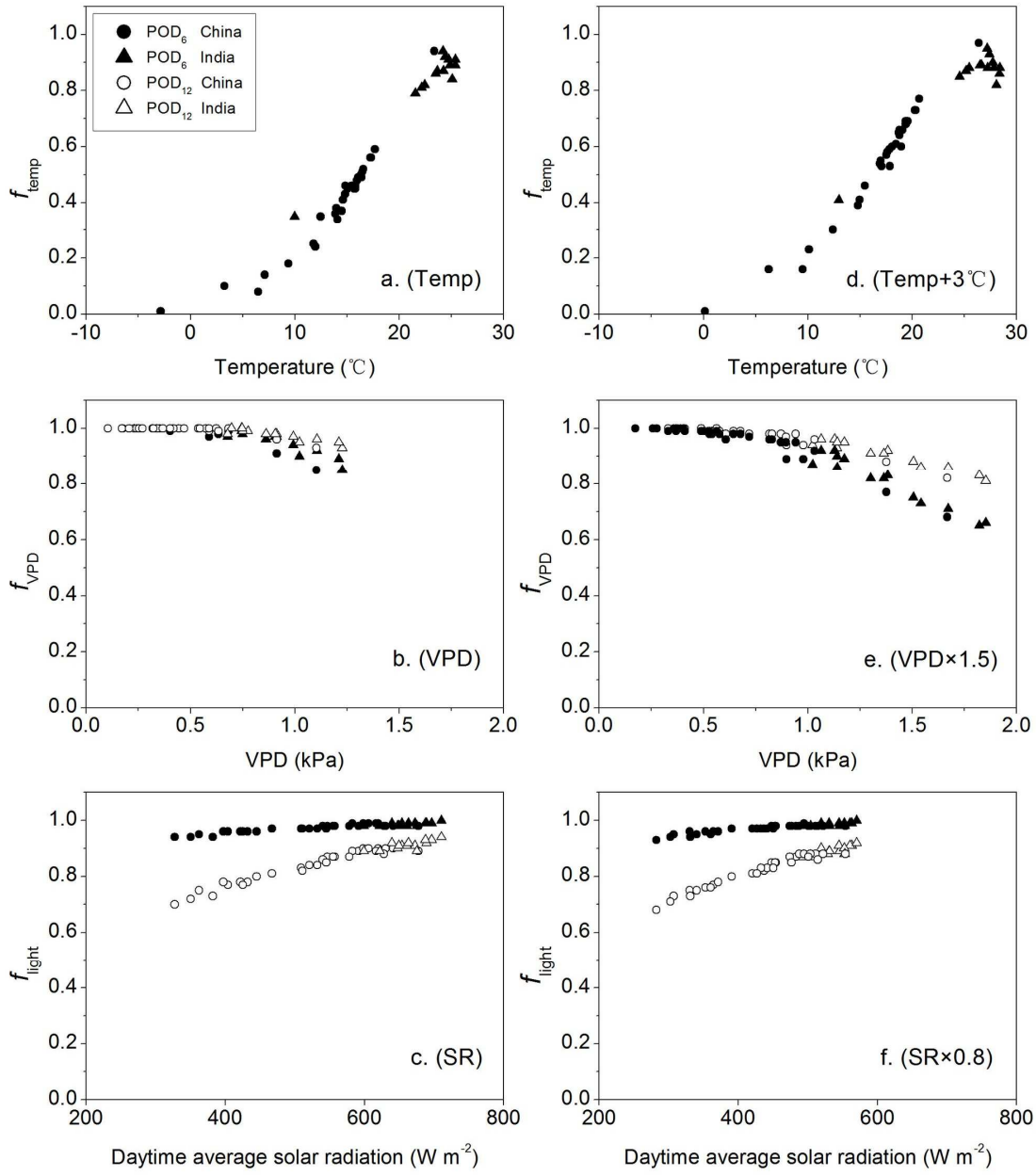

Fig. 5.8 Variations in the g_{sto} response functions of temperature (f_{temp}) (a, d), VPD (f_{VPD}) (b, e), and radiation (f_{light}) (c, f) with NCEP inputs (left panels) and adjusted NCEP inputs (right panels). The indicator values represent the relative terms of each response function (*y*-axis) and corresponding climatic factors (*x*-axis) for each province/state in China and India averaged for daytime across the POD_6/POD_{12} accumulation period.

CHAPTER 6

CONCLUSIONS AND IMPLICATIONS

Increasing food demand for a growing population in combination with changing consumption patterns (Schmidhuber & Tubiello, 2007; Smil, 2000) is sufficient to cause concerns about the future of food supply in Asia. Furthermore, the continuing increase of O_3 precursors emission due to rapid economic development, and, hence, the impacts of increasing surface [O_3] on crop production will add more concerns about the food supply in this region. Therefore, the question: "*How can we protect the crop production in Asia from the deleterious impact of ozone pollution in the near future*?" is urgent for crop producers, scientists, policy makers, and also consumers.

With this dissertation study, I tried to find an answer to the above question. To this end, I conducted the long-term observations to characterize O_3 pollution and its determinants in northern YRD, developed the FACE-O_3 system to investigate O_3 effects on rice and wheat plants, established the flux–response relationship for wheat to quantitatively estimate yield loss, and evaluated the wheat production losses in China and India due to present-day and future [O_3]. In this chapter, I summarize the findings and limitations of my study, and further discuss the wider implications of the findings.

6.1. Ozone pollution in agricultural fields of northern YRD is serious, and aggressive measures must be taken to restrict the open crop residue burning in addition to the controls over industrial and municipal emissions.

The results of in-situ surface [O_3] observations for five years (2007–2011) showed a frequent occurrence of high hourly [O_3] (exceeding the CAAQS Grade II, approx. 102 ppb) at an agricultural site in Jiangsu province. Although the Asian monsoon and associated long-range transports of maritime air mass caused depressions of high [O_3] in summer, the 3 month AOT40 for respective rice and wheat seasons greatly exceeded the critical level for protecting crop species from O_3 damage as defined in

Europe. Since the measurements were conducted within the typical agricultural land use, this study confirmed the serious situation of the current O_3 pollution in northern YRD.

Analysis of [O_3] variations in combination with the meteorological and satellite observations further revealed not only the industrial emissions from fossil fuel combustion, but also emissions from extensive open burning of crop residues as an important source of the O_3 pollution. There was an evidence of the effects that higher [O_3] and poorer air quality (higher API) were observed at and around the study site, respectively, during the high fire activities in the surrounding regions.

The contributions of biomass burning (forest fires, agricultural waste burning, and vegetable fuel combustion) to regional and global air pollution have been demonstrated by many previous studies (Andreae & Merlet, 2001; Galanter et al., 2000; Streets et al., 2003; Yamaji et al., 2010). Most recently, People's Daily (http://english.people.com.cn/index.html, accessed on 31 January 2013) reported that half of China continued to be plagued by Atmospheric Brown Cloud (ABC), observed as widespread layers of brownish haze that caused severe air pollution and low visibility. ABCs are regional scale plumes of air pollutants, consisting of mainly aerosol particles, such as black carbon (BC), and precursor gases (producing ozone and aerosols). These air pollutants are emitted from biomass burning, motor vehicles and industrial processes with incomplete combustion, and significantly affect the regional climate, hydrological cycle, glacial melting, agriculture and human health (UNEP & C^4, 2002). Radiocarbon measurements of aerosols in ABCs have determined that biomass combustion produced two-thirds of the bulk carbonaceous aerosols, as well as one-half and two-thirds of two BC subfractions, respectively (Gustafsson et al., 2009). However, effective measures to restrict the open crop residue burning have not been well executed in China by now.

The special strict policy against open straw burning as well as other emissions for the sake of Beijing Olympic Games in 2008 has been proved to have significantly reduced the boundary layer O_3 and other pollutants over the Central Eastern China

(Wang et al., 2009b). This effect was also demonstrated by the lower [O_3] observations in 2008 at our study site. Therefore, I suggest that aggressive measures to restrict the open crop residue burning can be and must be executed in China immediately, which would be beneficial not only for the reduction of surface O_3 to protect crop production, but for a better air quality in general: a basic requirement for human health and wellbeing.

6.2. FACE-O_3 is an ideal means to investigate ozone effects on crops as well as efficacy of countermeasures against the ozone impacts.

The FACE-O_3 system developed in this study was demonstrated to be capable of elevating canopy [O_3] under fully open-air field condition with a reliable performance. Both temporal and spatial controls were comparable to or better than other existing O_3 fumigation systems. Comparison of O_3 exposure regime as characterized by M7 and AOT40 indicated that artificial addition of ozone with this system only altered O_3 regime in the experimental plots to a modest extent that is comparable to the alteration by open-top chambers. The FACE-O_3 system can thus provide a realistic experimental platform closely reproducing the future situation with elevated [O_3] levels.

FACE and OTC are currently the prevailing approaches to studying plant responses to elevated [O_3] as well as other atmospheric components such as CO_2. Method-inherent characteristics of either method distinctly influence their applicability and results. Taking advantage of relatively simpler facilities and lower costs, experiments with OTC could accommodate more [O_3] levels and combinations with other treatments than those with FACE. Using the charcoal-filtered air (CF) in OTC, it is also possible to have sub-ambient [O_3] plots, which is so far lacking in the open-air fumigation experiments. On the other hand, FACE provides a microclimate close to the real world, thus leading to ecologically more meaningful results. The effects of elevated [O_3] on crops in a FACE study can be observed in relation to a wider range of natural variations and their interactions, such as changing weather conditions, soil moisture and [O_3] itself.

In contrast to other trace gases e.g. CO_2 with only modest fluctuations in the atmosphere, surface [O_3] shows pronounced seasonal and diurnal variations, which may have implications for the crop response to O_3 (Heath et al., 2009). In the present FACE-O_3 system, ozone was added according to instantaneous [O_3] measured at A-O_3, and the [O_3] variation at E-O_3 thus could represent the natural seasonal distribution in the field, with relatively high levels around flowering stage (May) for wheat, and spikelet formation stage (July) for rice. These high [O_3] periods were consistent with the critical stages to O_3 of wheat and rice plants, respectively, as indicated by other studies conducted in the FACE-O_3 (Shi et al., 2009; Wang et al., 2012c; Zhu et al., 2011). I suppose that the seasonal cycle of [O_3] at our study site may thus partly contributed to the differential O_3 sensitive stage between wheat and rice, and suggested the importance of taking O_3 exposure pattern into account when comparing crop response to O_3 among different experimental conditions.

In addition to the minimal alterations to microclimate and [O_3] regime, the FACE-O_3 field experiments allowed a much larger area for varietal and agronomic trials than was possible within chambers. The varietal difference in the yield and yield component responses to elevated O_3 have been found in wheat (Feng et al., 2011; Zhu et al., 2011) and rice (Shi et al., 2009; Wang et al., 2012c), respectively. These results indicated a possibility of breeding for higher tolerance to elevated [O_3] in crops. The physiological and biochemical traits associated with the varietal difference observed in FACE-O_3 experiments could serve as useful indicators of inherited O_3 tolerance for the breeding efforts. Recently, agronomic trials such as different fertilization and planting density were carried out with the FACE-O_3 system. The preliminary results revealed that appropriate agronomic managements might be another potential way to protect crop yield from O_3 damage (Zhu, personal communication).

My dissertation study as well as other studies have thus confirmed that field experiment with FACE-O_3 would be an ideal means to investigate the realistic O_3 effects on crop production, and explore adaptive efforts to this challenge.

6.3. The established flux–response relationship is suitable for wheat in YRD, but a network field experiments is needed for an improved assessment of ozone impact on crops over Asia.

In this study, I parameterized a multiplicative g_{sto} model of wheat from LRTAP using g_{sto} measurements from the FACE-O_3 experiments. The revised model exhibited superior performance on g_{sto} simulation in a subtropical region than the European models. A stomatal O_3 uptake index POD_{12} was judged as reasonable for an O_3 flux–response relationship for wheat in YRD, and produced a good fit to measured yield reductions. Both flux-based and AOT40-based response relationships indicated that the wheat cultivars used here were more sensitive to O_3 than European cultivars. It could be inferred that the g_{sto} model and corresponding flux–response relationship established in this study were more suitable to predict O_3 risk for wheat production in YRD rather than those from Europe.

On the other hand, when flux-based methods were applied to a large-scale evaluation of wheat yield loss in China and India, the European flux dose metric POD_6 showed a greater response to the climatic influences on stomatal O_3 uptake than POD_{12} did. This might be because, as compared with the European g_{sto} model parameterizations, I omitted temperature function and made the VPD function to be less restrictive based on the local observations. However, it is well known that most physiological responses may vary with the prevailing environmental condition (Larcher, 2003; Körner, 2006). Different wheat stomatal response functions to large climatic variables over Asia is thus likely. Mapping a more credible O_3 flux risk to wheat in Asia requires measurements of g_{sto} at many other sites in the major producing areas to improve the current g_{sto} model.

The same argument holds for the application of the dose–response relationships to Asian crops. Ideally, such relationships would be derived from coordinated standardized experimental campaigns assessing crop response to a range of O_3 concentrations (Unsworth & Geissler, 1992). To date, the geographical distribution of such crop effect studies have been lacking in Asia. The existing dose–response

relationships (mostly exposure-based O_3 doses) for Asian crops were entirely based on local investigations with a few cultivars. Different experimental methods used in these studies made it hard to compare the results with each other various designs of e.g. OTCs. Until now, a general statement is not feasible yet on the comparison between the regions in crop yield loss sensitivity to O_3 in Asia. Therefore, there is an uncertainty in my estimations of wheat production loss for China and India by using dose–response functions derived from the FACE-O_3 experiment at single site.

The above shortages in the current studies could be overcome by conducting network field experiments. Such programs have already been done in North America (National Crop Loss Assessment Network, reviewed by Heck et al., 1988) and Europe (European Open Top Chamber Programme, reviewed by Jäger et al., 1992), and have been proved to promote the research on O_3 risk for vegetation both on regional and global scale. Since Asian countries are projected to experience some of the highest surface [O_3] increase in the next several decades, improved assessments of O_3 impact on wheat and other major crops require a network field experiments across Asia.

6.4. Wheat production loss in China and India due to increasing [O_3] is substantial, and further studies are warranted on the interactions between ozone pollution and climate change for the future food security.

With [O_3] field simulated by a high resolution (40 × 40 km) chemical transport model coupled with the Regional Emission inventory in Asia (REAS), this study estimated that wheat production in China and India have been reduced by 6.4–14.9% and 8.2–22.3%, respectively, due to current O_3 level in 2000. A further decline in wheat yields is projected to be 8.1–9.4% for China and 5.4–7.7% for India by 2020 if O_3 precursor emissions continue to increase. Because I applied both exposure-based and flux-based approaches derived from European OTC and our FACE-O_3 experiments, and converted the [O_3] from the model outputs to that at the canopy height, the present results should be more credible than the previous estimations with the exposure-based O_3 metrics derived from US or European OTC experiments. It is

especially true for the projected increase in wheat production loss from 2000 to 2020 as the estimates across different O_3 dose metrics were comparable and the uncertainties in the flux-based evaluations from perturbations in the meteorological inputs was small.

It should be noted that this evaluation was based on the premise that the climatic condition in 2020 is the same as that in 2000, both for [O_3] simulation and stomatal O_3 uptake calculation. Although the short-term climatic changes may not be significant, the long-term trends are assured and should make influences on the crop responses to O_3. For example, increase in atmospheric CO_2 concentration may reduce stomatal conductance (Ainsworth, 2008), hence reduce stomatal O_3 uptake. Change in meteorology (e.g. temperature, humidity, soil water content) may affect the growing season, crop distribution, and stomatal dose itself (Fuhrer, 2009). Recently, such effects are being taken into account for an assessment of future O_3 risk. In the assessment for three 30-years' time-windows (1961–1990, 2021–2050, 2071–2100), the flux-based risk of O_3 damage to vegetation was predicted to remain unchanged or decrease at most sites of central and southern Europe, despite a projected substantial increase in future [O_3]. This is mainly due to reductions in stomatal conductance under elevated CO_2 concentrations (Klingberg et al., 2011). In Chapter 5 of this thesis, a 3 ºC and 50% increase in temperature and VPD, respectively, from the NCEP dataset significantly affected the flux-based estimates of wheat production loss in China and India. Both positive and negative effects were observed depending on the meteorological variables and climatic region.

In addition, elevated temperature may increase biogenic emissions of reactive species, which favours O_3 production (Sanderson et al., 2003; Zeng et al., 2008). The formation and destruction processes of O_3 are also controlled by the meteorological factors such as radiation, temperature and humidity (local weather), and by the long-range transport of pollutants (synoptic weather), all of which are sensitive to changes in climate (Chen et al., 2008; Steiner et al., 2010). Although these changes were not considered in the current study, they have to be addressed for more

comprehensive projections of the O_3 impacts in the future.

Climate change impacts are exerted over a long-term, whereas the O_3 pollution impacts are immediate but continuous (IPCC, 2007). They share some of the anthropogenic causes and both dramatically affect the agroecosystems. However, current research on their interactions and the secondary effects on global biogeochemical cycles are still limited (Long, 2012). There is an urgent need to develop more holistic approaches to linking the effects of ozone, climate, and nutrient and water availability, on individual plants, species interactions and ecosystem functions.

6.5. How can we protect the crop production in Asia from the deleterious impact of ozone pollution in the near future?

Surface [O_3] will increase dramatically in developing countries in Asia over the next several decades, and may become a major risk in food production and ecosystem functions. Scientific research could help the countries to combat the damages by increased surface [O_3]. Agronomic countermeasures, e.g. breeding and nutrient management, against the O_3 damage to crops would be one direction of scientific research (Avnery et al., 2013). Such studies have been impractical in the small land areas available in OTC and other existing facilities. The FACE-O_3 system established in this study would serve as a very powerful platform for the study of agronomic countermeasures as mentioned above, and thereby contribute to the mitigation of the O_3 damages.

More importantly than the adaptive efforts, however, stricter emission controls of O_3 precursors must be urgently imposed or strengthened to curb the rapid increase in surface [O_3] in Asia. This is because surface O_3 is a major risk not only for crops and natural vegetation but for human health as well. Aggressive restrictive measures on industrial, municipal and agricultural (such as biomass burning) emissions are required. Taking these measures has indeed greatly improved the air quality in Europe over the last several decades (Jonson et al., 2006; Vestreng et al., 2004). The scientific

efforts for the assessment of O_3 impacts on vegetation and human health should have helped the implementation of air quality management over Europe (LRTAP Convention, 2004, 2010). In Asia also, a better prediction of the increasing O_3 impacts should help the policy makers and the society to realize this approaching risk and take actions against it. The expected network experiments with FACE-O_3 system could support the scientific efforts for the improved prediction of O_3 impacts on vegetation across Asian countries.

Only with these efforts, we will be able to protect the crop production, as well as natural vegetation and human health from the deleterious impact of ozone pollution in the near future.

REFERENCES

Adams,R.M., Glyer, D.J.,McCarl, B.A.,1987. The NCLAN economic assessment: approach, findings and implications. In: Heck, W.W., Taylor, O.C., Tingey, D.T. (Eds.), Assessment of Crop Losses from Air Pollutants. Elsevier Applied Science, London.

Adams, R.M., Glyer, J.D., Johnson, S.L., McCarl, B.A., 1989. A reassessment of the economic effects of ozone on United States agriculture. Journal of the Air Pollution Control Association 39, 960–968.

Ahammed, Y.N., Reddy, R.R., Gopal, K.R., Narasimhulu, K., Basha, D.B., Reddy, L.S.S., Rao, T.V.R., 2006. Seasonal variation of the surface ozone and its precursor gases during 2001–2003, measured at Anantapur (14.62ºN), a semi-arid site in India. Atmospheric Research 80, 151–164.

Akimoto, H., 2003. Global air quality and pollution, Science 302, 1716–1719.

Ainsworth, E.A., 2008. Rice production in a changing climate: a meta-analysis of responses to elevated carbon dioxide and elevated ozone concentration. Global Change Biology 14, 1642–1650.

Andreae, M.O., Merlet, P., 2001. Emissions of trace gases and aerosols from biomass burning. Global Biogeochemical Cycles 15, 955–966.

Aunan, K., Berntsen, T.K., Seip, H.M., 2000. Surface ozone in China and its possible impact on agricultural crop yields. Ambio 29, 294–301.

Aquila, A.D., Lucarini, V., Ruti, P.M., Calmanti, S., 2005. Hayashi spectra of the northern hemisphere mid-latitude atmospheric variability in the NCEP–NCAR and ECMWF reanalyses. Climate Dynamics 25, 639–652.

Avnery, S., Mauzerall, D.L., Liu, J., Horowitz, L.W., 2011a. Global crop yield reductions due to surface ozone exposure: 1. Year 2000 crop production losses and economic damage. Atmospheric Environment 45, 2284–2296.

Avnery, S., Mauzerall, D.L., Liu, J., Horowitz, L.W., 2011b. Global crop yield reductions due to surface ozone exposure: 2. Year 2030 potential crop production losses and economic damage under two scenarios of O_3 pollution. Atmospheric Environment 45, 2297–2309.

Avnery, S., Mauzerall, D.L., Fiore, A.M., 2013. Increasing global agricultural production by reducing ozone damages via methane emission controls and ozone-resistant cultivar selection. Global Change Biology 19, 1285–1299.

Ashmore, M.R., 2005. Assessing the future global impacts of ozone on vegetation. Plant, Cell and Environment 28, 949–964.

Ashmore, M.R., Emberson, L., Karlsson, P.E., Pleijel, H., 2004. New directions: a new generation of ozone critical levels for the protection of vegetation in Europe. Atmospheric Environment 38, 2213–2214.

Barbero, R., Moron, V., Mangeas, M., and Despinoy, M., 2011. Relationships between MODIS and ATSR fires and atmospheric variability in New Caledonia (SW Pacific). Journal of Geophysical Research 116, D21110, doi:10.1029/2011JD015915.

Beig, G., Gunthe, S., Jadhav, D.B., 2007. Simultaneous measurements of ozone and its precursors on a diurnal scale at a semi urban site in India. Journal of Atmospheric Chemistry 57, 239–253.

Betzelberger, A.M., Gillespie, K.M., Mcgrath, J.M., Koester, R.P., Nelson, R.L., Ainsworth, E.A., 2010. Effects of chronic elevated ozone concentration on antioxidant capacity, photosynthesis and seed yield of 10 soybean cultivars. Plant, Cell and Environment 33, 1569–1581.

Biswas, D.K., Xu, H., Li, Y.G., Sun, J.Z., Wang, X.Z., Han, X.G., Jiang, G.M., 2008. Genotypic differences in leaf biochemical, physiological and growth responses to ozone in 20 winter wheat cultivars released over the past 60 years. Global Change Biology 14, 46–59.

Black, V.J., Black, C.R., Roberts, J.A., Stewart, C.A., 2000. Impact of ozone on the reproductive development of plants. New Phytologist 147, 421–447.

Booker, F., Muntifering, R., McGrath, M., Burkey, K., Decoteau, D., Fiscus, E., Manning, W., Krupa, S., Chappelka, A., Grantz, D., 2009. The ozone component of global change: potential effects on agricultural and horticultural plant yield, product quality and interactions with invasive species. Journal of Integrative Plant Biology 51, 337–351.

Bridgham, S.D., Pastor, J., Updegraff, K., Malterer, T.J., Johnson, K., Harth, C., Chen, J., 1999. Ecosystem control over temperatures and energy flux in northern peatlands. Ecological Applications 9, 1345–1358.

Campbell, G.S., Norman, J.M., 1998. Introduction to Environmental Biophysics. Springer-Verlag, New York, Berlin, Heidelberg.

Central Statistical Organisation, 2000. Statistical Abstract, India 2000. Central Statistical Organisation, Ministry of Statistics & Programme Implementation, Government of India, New Delhi, India.

China Agricultural Yearbook Editorial Committee, 2000. China Agricultural Yearbook 2000. China Agriculture Press, Beijing, China (in Chinese).

Chen, Z.H., Cheng, S.Y., Li, J.B., Guo, X.R., Wang, W.H., Chen, D.S., 2008. Relationship between atmospheric pollution processes and synoptic pressure patterns in northern China. Atmospheric Environment 42, 6078–6087.

Cheung, V.T.F., Wang, T., 2001. Observational study of ozone pollution at a rural site in the Yangtze Delta of China. Atmospheric Environment 35, 4947–4958.

Clarke, B.B., Greenhalgh-Weidman, B., Brennan, E.G., 1990. An assessment of the impact of ambient ozone on field-grown crops in New Jersey using the EDU method: part 1 white potato (Solanum tuberosum). Environmental Pollution 66, 351–360.

Cofala, J., Amann, M., Mechler, R., 2006. Scenarios of world anthropogenic

emissions of air pollutants and methane up to 2030, Interim Report IR-06-023. available at: http://webarchive.iiasa.ac.at/rains/global_emiss/.

Colls, J.J., Weigel, H.J., Geissler, P.A., 1993. Microclimate in open-top chambers. In: Jäger, H.J. et al., (Ed.) Effects of air pollution on agricultural crops in Europe. Brussels, European Commission (Air Pollution Research Report, No. 46), pp. 175–191.

Davies, D.K., Ilavajhala, S., Wong, M.M., and Justice, C.O., 2009. Fire Information for Resource Management System: Archiving and Distributing MODIS Active Fire Data. IEEE Transactions on Geoscience and Remote Sensing 47, 72–79.

Danielsson, H., Karlsson, G.P., Karlsson, P.E., Pleijel, H., 2003. Ozone uptake modelling and flux-response relationships—an assessment of ozone-induced yield loss in spring wheat. Atmospheric Environment 37, 475–485.

Debaje, S.B., Kakade, A.D., 2006. Measurements of Surface Ozone in Rural Site of India. Aerosol and Air Quality Research 6, 444–465.

Debaje, S.B., Kakade, A.D., 2009. Surface ozone variability over western Maharashtra, India. Journal of Hazardous Materials 161, 686–700.

Debaje, S.B., Kakade, A.D., Jeyakumar, S.J., 2010. Air pollution effect of O_3 on crop yield in rural India. Journal of Hazardous Materials 183, 773–779.

Debaje, S.B., Johnson, S.J., Ganesan, K., Jadhav, D.B., Seetaramayya, S., 2003. Surface ozone measurements at tropical rural coastal station Tranquebar, India. Atmospheric Environment 37, 4911–4916.

De Temmerman, L., Wolf, J., Colls, J., Bindi, M., Fangmeier, A., Finnan, J., Ojanperä , K., Pleijel, H., 2002. Effect of climatic conditions on tuber yield (Solanum tuberosum L.) in the European ‘CHIP’ experiments. European Journal of Agronomy 17, 243–255.

Ding, A., Wang, T., 2006. Influence of stratosphere–to–troposphere exchange on the seasonal cycle of surface ozone at Mount Waliguan in western China. Geophysical

Research Letters 33, doi:10.1029/2005GL024760.

Draxler, R.R., Hess, G.D., 1998. An overview of the HYSPLIT_4 modeling system of trajectories, dispersion, and deposition. Australian Meteorological Magazine 47, 295–308.

Emberson, L.D., Ashmore, M.R., Cambridge, H.M., Simpson, D., Tuovinen, J.P., 2000. Modelling stomatal ozone flux across Europe. Environmental Pollution 109, 403-413.

Emberson, L.D., Büker, P., Ashmore, M.R., et al. 2009. A comparison of North American and Asian exposure-response data for ozone effects on crop yields. Atmospheric Environment 43, 1945–1953.

EPA, 1996. Air quality criteria for ozone and related photochemical oxidants. United States Environmental Protection Agency (EPA).

Erbs, M., Fangmeier, A., 2005. A chamberless field exposure system for ozone enrichment of short vegetation. Environmental Pollution 133, 91–102.

FAO, 2010. Food and Agricultural Organization of the United Nations, FAOSTAT. available at: http://faostat.fao.org/

Feng, Z., Jin, M., Zhang, F., Huang, Y., 2003. Effects of ground-level ozone (O_3) pollution on the yields of rice and winter wheat in the Yangtze River Delta. Journal of Environmental Sciences 15, 360–362.

Feng, Z., Kobayashi, K., 2009. Assessing the impacts of current and future concentrations of surface ozone on crop yield with meta-analysis. Atmospheric Environment 43, 1510–1519.

Feng, Z., Kobayashi, K., Ainsworth, E.A., 2008. Impact of elevated ozone concentration on growth, physiology and yield of wheat (Triticum aestivum L): a meta-analysis. Global Change Biology 14, 2696–2708.

Feng, Z., Pang, J., Kobayashi, K., Zhu, J., Ort, D.R., 2011. Differential responses in

two varieties of winter wheat to elevated ozone concentration under fully open-air field conditions. Global Change Biology 17, 580–591.

Feng, Z., Pang, J., Nouchi, I., Kobayashi, K., Yamakawa, T., Zhu, J., 2010. Apoplastic ascorbate contributes to the differential ozone sensitivity in two varieties of winter wheat under fully open-air field conditions. Environmental Pollution 158, 3539–3545.

Fiscus, E.L., Booker, F.L., Burkey, K.O., 2005. Crop responses to ozone: uptake, modes of action, carbon assimilation and partitioning. Plant, Cell and Environment 28, 997–1011.

Freitas, S.R., Longo, K.M., Dias, M.A.F.S., Dias, P.L.S., Chatfield, R., Prins, E., Artaxo, P., Grell, G., Recuero, F.S., 2005. Monitoring the transport of biomass burning emissions in South America. Environmental Fluid Mechanics 5, 135–167.

Fuhrer, J., 1994a. Effects of ozone on managed pasture: I. Effects of open-top chambers on microclimate, ozone flux, and plant growth. Environmental Pollution 86, 297–305.

Fuhrer, J., 1994b. The critical level for ozone to protect agricultural crops–an assessment of data from European open-top chamber experiments. In: Fuhrer, J., Achermann, B. (eds.), Critical Levels for Ozone. A UNECE Workshop Report. Schriftenreihe der FAC, Liebefeld, vol. 16, pp. 42–57.

Fuhrer, J., 2000. Introduction to the special issue on ozone risk analysis for vegetation in Europe. Environmental Pollution 109, 359–360.

Fuhrer, J., 2003. Agroecosystem responses to combinations of elevated CO_2, ozone, and global climate change. Agriculture, Ecosystems and Environment 97, 1–20.

Fuhrer, J., 2009. Ozone risk for crops and pastures in present and future climates. Naturwissenschaften 96, 173–194.

Fuhrer, J., and Booker, F., 2003. Ecological issues related to ozone: agricultural issues. Environment International 29, 141–154.

Fuhrer, J., Skärby, L., Ashmore, M.R., 1997. Critical levels for ozone effects on vegetation in Europe. Environmental Pollution 97, 91–106.

Galanter, M., Levy, H., and Carmichael, G., 2000. Impacts of biomass burning on tropospheric CO, NO_x and O_3. Journal of Geophysical Research 105, 6633–6653.

Gelang, J., Pleijel, H., Sild, E., Danielsson, H., Younis, S., Selldén, G., 2000. Rate and duration of grain filling in relations to flag leaf senescence and grain yield in spring wheat (Triticum aestivum) exposed to different concentrations of ozone. Physiologia Plantarum 110, 366–375.

Geng, F., Tie, X., Xu, J., Zhou, G., Peng, L., Gao, W., Tang, X., and Zhao, C., 2008. Characterizations of ozone, NO_x, and VOCs measured in Shanghai, China. Atmospheric Environment 42, 6873–6883.

Ghude, S.D., Jain, S.L., Arya, B.C., Beig, G., Ahammed, Y.N., Kumar, A., Tyagi, B., 2008. Ozone in ambient air at a tropical megacity, Delhi: characteristics, trends, and cumulative ozone exposure indices. Journal of Atmospheric Chemistry 60, 237–252.

Giglio, L., Descloitres, J., Justice, C. O., and Kaufman, Y., 2003. An enhanced contextual fire detection algorithm for MODIS. Remote Sensing of Environment 87, 273–282.

Grell, G.A., Peckham, S.E., Schmitz, R., McKeen, S.A., Frost, G., Skamarock, W.C., Eder, B., 2005. Fully coupled “online” chemistry within the WRF model. Atmospheric Environment 39, 6957–6975.

Gustafsson, Ö., Krusa, M., Zencak, Z., Sheesley, R.J., Granat, L., Engström, E., Praveen, P.S., Rao, P.S.P., Leck, C., Rodhe, H., 2009. Brown Clouds over South Asia: Biomass or Fossil Fuel Combustion? Science 323, 495–498.

Harper, L.A., Baker, D.N., Box, J.E., Hesketh, J.D., 1973. Carbon dioxide and the photosynthesis of field crops: A metered carbon dioxide release in cotton under field conditions. Agronomy Journal 65, 7–11.

He, Y., Uno, I., Wang, Z., Pochanart, P., Li, J., and Akimoto, H., 2008. Significant impact of the East Asia monsoon on ozone seasonal behavior in the boundary layer of Eastern China and the west Pacific region. Atmospheric Chemistry and Physics 8, 7543–7555.

Heath, R.L., 1987. The biochemistry of ozone attack on the plasma membrane of plant cells. Recent Advances in Phytochemistry 21, 29–54.

Heath, R.L., Lefohn, A.S., Musselman, R.C., 2009. Temporal processes that contribute to nonlinearity in vegetation responses to ozone exposure and dose. Atmospheric Environment 43, 2919–2928.

Heck, W.W., Taylor, O.C., Tingey, D.T., 1988. Assessment of Crop Loss from Air Pollutants. In: Proceedings of the International Conference. Elsevier Applied Science, Raleigh, North Carolina, USA, London.

Holland, M., Kinghorn, S., Emberson, L., Cinderby, S., Ashmore, M., Mills, G., Harmens, H., 2006. Development of a framework for probabilistic assessment of the economic losses caused by ozone damage to crops in Europe. CEH Project No. C02309NEW. Report to U.K. Department of Environment, Food and Rural affairs under contract 1/2/170 1/3/205.

Hoshika, Y., Paoletti, E., Omasa, K., 2012. Parameterization of Zelkova serrata stomatal conductance model to estimate stomatal ozone uptake in Japan. Atmospheric Environment 55, 271–278.

IPCC (Intergovernmental Panel on Climate Change), 2007. Climate Change 2007: The Physical Science Basis. Contribution of Working Group I to the Fourth Assessment Report of the Intergovernmental Panel on Climate Change. Cambridge University Press, Cambridge, UK.

Ishii, S., Marshall, F.M., Bell, J.N.B., Abdullah, A.M., 2004. Impact of ambient air pollution on locally grown rice cultivars (*Oryza sativa* L.) in Malaysia. Water, Air and Soil Pollution 154, 187–201.

Jäger, H.J., Unsworth, M., De Temmermann, L., Mathy, P. (Eds.), 1992. Effects of Air Pollution on Agricultural Crops in Europe – Results of the European Open-Top Chamber Project. Commission of the European Communities, Brussels Air Pollution Research Report 46.

Jarvis, P.G., 1976. The interpretation of the variations in leaf water potential and stomatal conductance found in canopies in the field. Philosophical Transactions of the Royal Society, London B 273, 593–610.

Jetten, T.H., 1992. Physical description of transport processes inside an open top chamber in relation to field conditions. Doctoral thesis, Wageningen Agricultural University. ISBN: 90-5485-011-6

Jonson, J.E., Simpson, D., Fagerli, H., and Solberg, S., 2006. Can we explain the trends in European ozone levels? Atmospheric Chemistry and Physics 6, 51–66.

Kahl, J.D.W., 1996. On the prediction of trajectory model error. Atmospheric Environment 30, 2945–2957.

Karlsson, P.E., Braun, S., Broadmeadow, M., Elvira, S., Emberson, L., Gimeno, B.S., Le Thiec, D., Novak, K., Oksanen, E., Schaub, M., Uddling, J., Wilkinson, M., 2007. Risk assessments for forest trees: the performance of the ozone flux versus the AOT concepts. Environmental Pollution 146, 608–616.

Kaufman, Y.J., Justice, C.O., Flynn, L.P., Kendall, J.D., Prins, E.M., Giglio, L., Ward, D.E., Menzel, W.P., and Setzer, A.W., 1998. Potential global fire monitoring from EOS-MODIS. Journal of Geophysical Research 103, 32215–32238.

Kimball, B.A., Conley, M.M.,Wang, S., Lin, X., Luo, C., Morgan, J., and Smith, D., 2008. Infrared heater arrays for warming ecosystem field plots. Global Change Biology 14, 309–320.

Kimball, B.A., Kobayashi, K., Bindi, M., 2002. Responses of agricultural crops to free-air CO_2 enrichment. Advances in Agronomy 77, 293–368.

Kiple, K.F., and Ornelas, K.C., (Eds.) 2000. The Cambridge World History of Food,

Vol 1. Cambridge University Press, UK.

Klingberg, J., Engardt, M., Uddling, J., Karlsson, P.E., Pleijel, H., 2011. Ozone risk for vegetation in the future climate of Europe based on stomatal ozone uptake calculations. Tellus 63A, 174–187.

Kobayashi, K., 1992. Modeling and assessing the impact of ozone on rice growth and yield. In: Berglund, R.L., (Ed.) Tropospheric Ozone and the Environment II. Air and Waste Management Association, Pittsburgh, USA, pp. 537–551.

Kobayashi, K., Okada, M., Nouchi, I., 1995. Effects of ozone on dry matter partitioning and yield of Japanese cultivars of rice (Oryza sativa L.). Agriculture, Ecosystems and Environment 53, 109–122.

Körner, C., 2006. Significance of temperature in plant life. In: Plant Growth and Climate Change (eds Morison JIL, Morecraft MD) pp. 48–69. Blackwell Publishing, Oxford, UK.

Krupa, S.V., Nosal, M., Legge, A.H., 1994. Ambient ozone and crop loss: establishing a cause-effect relationship. Environmental Pollution 83, 269–276.

Krupa, S.V., Nosal, M., Legge, A.H., 1998. A numerical analysis of the combined open-top chamber data from the USA and Europe on ambient ozone and negative crop responses. Environmental Pollution 101, 157–160.

Kumar, R., Naja, M., Satheesh, S.K., Ojha, N., Joshi, H., Sarangi, T., Pant, P., Dumka, U.C., Hegde, P., and Venkataramani, S., 2011. Influences of the springtime northern Indian biomass burning over the central Himalayas. Journal of Geophysical Research 116, D19302, doi:10.1029/2010JD015509.

Kurokawa, J., Yumimoto, K., Uno, I., Ohara, T., 2009. Adjoint inverse modeling of NO_x emissions over eastern China using satellite observations of NO_2 vertical column densities. Atmospheric Environment 43, 1878–1887.

Lam, K.S., Wang, T., Wu, C., And Li, Y., 2005. Study on an ozone episode in hot season in Hong Kong and transboundary air pollution over Pearl River Delta

region of China. Atmospheric Environment 39, 1967–1977.

Larcher, W., (Ed.) 2003. Physiological Plant Ecology. 4th Edition, Springer-Verlag, Berlin, Germany, 513 pp.

Lefohn, A.S., Foley, J.K., 1992. NCLAN results and their application to the standard-setting process: protecting vegetation from surface ozone exposures. Journal of the Air and Waste Management Association 62, 1046–1052.

Lefohn, A.S., Laurence, J.A., Kohut, R.J., 1988. A comparison of indices that describe the relationship between exposure to ozone and reduction in the yield of agricultural crops. Atmospheric Environment 22, 1229–1240.

Lefohn, A.S., Shadwick, D., Oltmans, S.J., 2010. Characterizing changes in surface ozone levels in metropolitan and rural areas in the United States for 1980–2008 and 1994–2008. Atmospheric Environment 44, 5199–5210.

Legge, A.H., Grunhage, L., Noal, M., Jager, H.J., Krupa, S.V., 1995. Ambient ozone and adverse crop response: an evaluation of north American and European data as they relate to exposure indices and critical levels. Journal of Applied Botany 69, 192–205.

Lesser, V.M., Rawlings, J.O., Spruill, S.E., Somerville, M.C., 1990. Ozone effects on agricultural crops: statistical methodologies and estimated dose-response relationships. Crop Science 30, 148–155.

Li, J., Wang, Z., Akimoto, H., Gao, C., Pochanart, P., and Wang, X., 2007. Modeling study of ozone seasonal cycle in lower troposphere over east Asia. Journal of Geophysical Research 112, D22S25. doi:10.1029/2006JD008209.

Lin, W., Xu, X., Ge, B., Zhang, X., 2009. Characteristics of gaseous pollutants at Gucheng, a rural site southwest of Beijing. Journal of Geophysical Research 114, D00G14, doi:10.1029/2008JD010339.

Lin, W., Xu, X., Zhang, X., Tang, J., 2008. Contributions of pollutants from North China Plain to surface ozone at the Shangdianzi GAW Station. Atmospheric

Chemistry and Physics 8, 5889–5898.

Liu, J.J., Jones, D.B.A., Worden, J.R., Noone, D., Parrington, M., and Kar, J., 2009. Analysis of the summertime buildup of tropospheric ozone abundances over the Middle East and North Africa as observed by the Tropospheric Emission Spectrometer instrument. Journal of Geophysical Research 114, D05304, doi:10.1029/2008JD010993.

Liu, Z., Xu, Z., Yao, Z., Huang, H., 2012. Comparison of surface variables from ERA and NCEP reanalysis with station data over eastern China. Theoretical and Applied Climatology 107, 611–621.

Logan, J.A., 1989. Ozone in rural areas of the United States. Journal of Geophysical Research 94 (D6), 8511–8532.

Long, S.P., 2012. Virtual Special Issue on food security – greater than anticipated impacts of near-term global atmospheric change on rice and wheat. Global Change Biology 18, 1489–1490.

Long, S.P., Ainsworth, E.A., Leakey, A.D.B., Nösberger, J., Ort, D.R., 2006. Food for thought: lower-than-expected crop yield stimulation with rising CO_2 concentrations. Science 312, 1918–1921.

Long, S.P., Ainsworth, E.A., Rogers, A., Ort, D.R., 2004. Rising atmospheric carbon dioxide: plants FACE the future. Annual Review of Plant Biology 55, 591–628.

Long, S.P., Naidu, S.L., 2002. Effects of oxidants at the biochemical, cell and physiological levels. In: Treshow, M., (Ed.) Air Pollution and Plants. John Wiley, London, UK, pp. 69–88.

Lu, Z., Streets, D.G., 2012. Increase in NO_x Emissions from Indian Thermal Power Plants during 1996−2010: Unit-Based Inventories and Multisatellite Observations. Environmental Science & Technology 46, 7463–7470.

LRTAP Convention 2004. Manual on methodologies and criteria for modelling and mapping critical loads and levels and air pollution effects, risks and trends.

Chapter 3. Mapping critical levels for vegetation (2007 revision). International Cooperative Programme on Mapping and Modelling under the UNECE Convention on Long-Range Transboundary Air Pollution.

LRTAP Convention 2010. Manual on methodologies and criteria for modeling and mapping critical loads & levels and air pollution effects, risk and trends. Chapter 3. Mapping critical levels for vegetation (2010 revision). (Available at http://icpvegetation.ceh.ac.uk)

Luo, C., John, St.J.C., Zhou, X., Lam, K.S., Wang, T., and Chameides, W.L., 2000. A nonurban ozone air pollution episode over eastern China: observations and model simulations. Journal of Geophysical Research 105, 1889–1908.

Mauzerall, D.L., Wang, X., 2001. Protecting agricultural crops from the effects of tropospheric ozone exposure-reconciling science and standard setting. Annual Review of Energy and Environment 26, 237–268.

McLeod, A.R., 1995. An open-air system for exposure of young forest trees to sulphur dioxide and ozone. Plant, Cell and Environment 18, 215–225.

McLeod, A.R., Roberts, T.M., Alexander, K., Cribb, D.M., 1991. The yield of winter cereals exposed to sulphur dioxide under field conditions. Agriculture, Ecosystems and Environment 33, 193–213.

McLeod, A.R., Long, S.P., 1999. Free-air carbon dioxide enrichment (FACE) in global change research: a review. Advances in Ecological Research 28, 1–55.

Meehl, G.A., Stocker, T.F., Collins, W.D., Friedlingstein, P., Gaye, A.T., Gregory, J.M., Kitoh, A., Knutti, R., Murphy, J.M., Noda, A., Raper, S.C.B., Watterson, I.G., Weaver, A.J., Zhao, Z.C., 2007. Global climate projections. In: Solomon, S., Qin, D., Manning, M., Chen, Z., Marquis, M., Averyt, K.B., Tignor, M., Miller, H.L. (Eds.), Climate Change 2007: The Physical Science Basis. Contribution of Working Group I to the Fourth Assessment Report of the Intergovernmental Panel on Climate Change. Cambridge University Press, Cambridge, UK and New York,

USA.

Meyer, U., Köllner, B., Willenbrink, J., Krause, G.H.M., 1997. Effects of ozone on agricultural crops in Germany. I. Different ambient ozone exposure regimes affect photosynthesis and assimilate allocation in spring wheat. New Phytologist 136, 645–652.

Mills, G., Buse, A., Gimeno, B., Bermejo, V., Holland, M., Emberson, L., Pleijel, H., 2007. A synthesis of AOT40-based response functions and critical levels of ozone for agricultural and horticultural crops. Atmospheric Environment 41, 2630-2643.

Mills, G., Hayes, F., Simpson, D., Emberson, L., Norris, D., Harmens, H., Buker, P., 2011a. Evidence of widespread effects of ozone on crops and (semi-)natural vegetation in Europe (1990–2006) in relation to AOT40- and flux-based risk maps. Global Change Biology 17, 592–613,

Mills, G., Pleijel, H., Braun, S., Büker, P., Bermejo, V., Calvo, E., Danielsson, H., Emberson, L., Fernandez, I.G., Grünhage, L., Harmens, H., Hayes, F., Karlsson, P.E., Simpson, D., 2011b. New stomatal flux-based critical levels for ozone effects on vegetation. Atmospheric Environment 45, 5064–5068.

Mittal, M.L., Hess, P.G., Jain, S.L., Arya, B.C., Sharma, C., 2007. Surface ozone in the Indian region. Atmospheric Environment 41, 6572–6584.

Mollah, M., Norton, R., Huzzey, J., 2009. Australian grains free-air carbon dioxide enrichment (AGFACE) facility: design and performance. Crop & Pasture Science 60, 697–707.

Monfreda, C., Ramankutty, N., Foley, J.A., 2008. Farming the planet: 2. Geographic distribution of crop areas, yields, physiological types, and net primary production in the year 2000. Global Biogeochemical Cycles 22, GB1022. doi:10.1029/2007GB002947.

Monks, P.S., 2000. A review of the observations and origins of the spring ozone maximum. Atmospheric Environment 34, 3545–3561.

Monteith, J., and Unsworth, M.H., 2008. Principles of Environmental Physics. 3rd Edition. Academic Press, London, 418 pp.

Musselman, R.C., Lefohn, A.S., Massman, W.J., Heath, R.L., 2006. A critical review and analysis of the use of exposure- and flux-based ozone indices for predicting vegetation effects. Atmospheric Environment 40, 1869–1888.

Morgan, P.B., Ainsworth, E.A., Long, S.P., 2003. How does elevated ozone impact soybean? A meta-analysis of photosynthesis, growth and yield. Plant, Cell and Environment 26, 1317–1328.

Morgan, P.B., Bernacchi, C.J., Ort, D.R., Long, S.P., 2004. An in vivo analysis of the effect of season-long open-air elevation of ozone to anticipated 2050 levels on photosynthesis in soybean. Plant Physiology 135, 2348–2357.

Morgan, P.B., Mies, T.A., Bollero, G.A., Nelson, R.L., Long, S.P., 2006. Season-long elevation of ozone concentration to projected 2050 levels under fully open-air conditions substantially decreases the growth and production of soybean. New Phytologist 170, 333–343.

Nair, P.R., Chand, D., Lal, S., Naja, M., Parameswaran, K., Ravindran, S., Venkataramani, S., 2002. Temporal variations in surface ozone at Thumba (8.6°N, 77°E) – a tropical coastal site in India. Atmospheric Environment 36, 603–610.

Naja, M., Akimoto, H., 2004. Contribution of regional pollution and long-range transport to the Asia-Pacific region: Analysis of long-term ozonesonde data over Japan. Journal of Geophysical Research 109, D21306, doi:10.1029/2004JD004687.

Naja, M., Lal, S., 2002. Surface ozone and precursor gases at Gadanki (13.5ºN, 79.2ºE), a tropical rural site in India. Journal of Geophysical Research 107, doi:10.1029/2001JD000357.

Naja, M., Lal, S., Chand, D., 2003. Diurnal and seasonal variabilities in surface ozone at a high altitude site Mt Abu (24.6°N, 72.7°E, 1680 m asl) in India. Atmospheric

Environment 37, 4205–4215.

Nakatani, A., Kondo, S., Hayashida, S., Nagashima, T., Sudo, K., Liu, X., Chance, K., and Hirota, I., 2012. Enhanced Mid-Latitude Tropospheric Column Ozone over East Asia: Coupled Effects of Stratospheric Ozone Intrusion and Anthropogenic Sources. Journal of the Meteorological Society of Japan 90, 207–222.

Nali, C., Pucciariello, C., Lorenzini, G., 2002. Ozone distribution in central Italy and its effect on crop productivity. Agriculture, Ecosystems and Environment 90, 277–289.

Nussbaum, S., Fuhrer, J., 2000. Difference in ozone uptake in grassland species between open-top chambers and ambient air. Environmental Pollution 109, 464–471.

Ohara, T., Akimoto, H., Kurokawa, J., Horii, N., Yamaji, K., Yan, X., and Hayasaka, T., 2007. An Asian emission inventory of anthropogenic emission sources for the period 1980–2020. Atmospheric Chemistry and Physics 7, 4419–4444.

Okada, M., Lieffering, M., Nakamura, H., Yoshimoto, M., Kim, H.Y., Kobayashi, K., 2001. Free-air CO_2 enrichment (FACE) using pure CO_2 injection: system description. New Phytologist 150, 251–260.

Olszyk, D.M., Tibbitts, T.W., Hertzberg, W.M., 1980. Environment in open-top field chambers utilized for air pollution studies. Journal of Environmental Quality 9, 610–615.

Oue, H., Feng, Z., Pang, J., Miyata, A., Mano, M., Kobayashi, K., Zhu, J., 2009. Modeling the stomatal conductance and photosynthesis of a flag leaf of wheat under elevated O_3 concentration. Journal of Agricultural Meteorology 65, 239–248.

Oue, H., Kobayashi, K., Zhu, J.G., Guo, W.S., Zhu, X.K., 2011. Improvements of ozone dose response functions for predicting the yield loss of wheat due to elevated ozone. Journal of Agricultural Meteorology 67, 21–32.

Pang, J., Kobayashi, K., Zhu, J., 2009. Yield and photosynthetic characteristics of flag leaves in Chinese rice (Oryza sativa L) varieties subjected to free-air release of ozone. Agriculture Ecosystems and Environment 132, 203–211.

Piikki, K., De Temmerman, L., Högy, P., Pleijel, H., 2008. The open-top chamber impact on vapour deficit and its consequences for stomatal ozone uptake. Atmospheric Environment 42, 6513–6522.

Pleijel, H., Danielsson, H., Emberson, L.D., Ashmore, M.R., Mills, G., 2007. Ozone risk assessment for agricultural crops in Europe: Further development of stomatal flux and flux-response relationships for European wheat and potato. Atmospheric Environment 41, 3022–3040.

Pleijel, H., Danielsson, H., Karlsson, G.P., Gelang, J., Karlsson, P.E., Sellden, G., 2000. An ozone flux-response relationship for wheat. Environmental Pollution 109, 453–462.

Pleijel, H., Danielsson, H., Ojanpera, K., De Temmerman, L., Högy, P., Badiani, M., Karlsson, P.E., 2004. Relationships between ozone exposure and yield loss in European wheat and potato—a comparison of concentration- and flux-based exposure indices. Atmospheric Environment 38, 2259–2269.

Pleijel, H., Danielsson, H., Vandermeiren, K., Blum, C., Colls, J., Ojanper.a, K., 2002. Stomatal conductance and ozone exposure in relation to potato tuber yield—results from the European CHIP programme. European Journal of Agronomy 17, 303–317.

Pleijel, H., Skärby, L., Wallin, G., Sellden, G., 1995. A process-oriented explanation of the non-linear relationship between grain yield of wheat and ozone exposure. New Phytologist 131, 241–246.

Pleijel, H., Wallin, G., Karlsson, P.E., Skarby, L., Sellden, G., 1994. Ozone deposition to an oat crop (*Avena sativa* L.) grown in open-top chambers and in the ambient air. Atmospheric Environment 28, 1971–1979.

Pochanart, P., Akimoto, H., Kinjo, Y., and Tanimoto, H., 2002. Surface ozone at four remote island sites and the preliminary assessment of the exceedances of its critical level in Japan. Atmospheric Environment 36, 4235–4250.

Pochanart, P., Akimoto, H., Kajii, Y., Potemkin, V.M., and Khodzher, T.V., 2003. Regional background ozone and carbon monoxide variations in remote Siberia/East Asia. Journal of Geophysical Research 108, 4028, doi:10.1029/2001JD001412.

Reddy, B.S.K., Kumar, K.R., Balakrishnaiah, G., Gopal, K.R., Reddy, R.R., Ahammed, Y.N., Narasimhulu, K., Reddy, L.S.S., Lal, S., 2010. Observational studies on the variations in surface ozone concentration at Anantapur in southern India. Atmospheric Research 98, 125–139.

Riahi, K., Grübler, A., Nakićenović, N., 2007. Scenarios of long-term socio-economic and environmental development under climate stabilization. Technological Forecasting and Social Change 74, 887–935.

Sanderson, M.G., Jones, C.D., Collins, W.J., Johnson, C.E., Derwent, R.G., 2003. Effect of climate change on isoprene emissions and surface ozone levels. Geophysical Research Letters 30, 1936 doi:10.1029/2003GL017642

Sarkar, A., Agrawal, S.B., 2010. Elevated ozone and two modern wheat cultivars: An assessment of dose dependent sensitivity with respect to growth, reproductive and yield parameters. Environmental and Experimental Botany 69, 328–337.

Satsangi, G.S., Lakhani, A., Kulshrestha, P.R., Taneja, A., 2004. Seasonal and diurnal variation of surface ozone and a preliminary analysis of exceedance of its critical levels at a semi-arid site in India. Journal of Atmospheric Chemistry 47, 271–286.

Schmidhuber, J., Tubiello, F.N., 2007. Global food security under climate change. Proceedings of National Academy of Science USA 104,19703–19708.

Sikder, H.A., Suthawaree, J., Kato, S., Kajii, Y., 2011. Surface ozone and carbon monoxide levels observed at Oki, Japan: Regional air pollution trends in East Asia.

Journal of Environmental Management 92, 953–959.

Simpson, D., Ashmore, M.R., Emberson, L., Tuovinen, J.P., 2007. A comparison of two different approaches for mapping potential ozone damage to vegetation. A model study. Environmental Pollution 146, 715–725.

Shan, W., Yin, Y., Zhang, J., and Ding Y., 2008. Observational study of surface ozone at an urban site in East China. Atmospheric Research 89, 252–261.

Shaw, W.J., Allwine, K.J., Fritz, B.G., Rutz, F.C., Rishel, J.P., Chapman, E.G., 2008. An evaluation of the wind erosion module in DUSTRAN. Atmospheric Environment 42, 1907–1921.

Shi, G., Yang, L., Wang, Y., Kobayashi, K., Zhu, J., Tang, H., Pan, S., Chen, T., Liu, G., Wang, Y., 2009. Impact of elevated ozone concentration on yield of four Chinese rice cultivars under fully open-air field conditions. Agriculture, Ecosystems and Environment 131, 178–184.

Smil, V., 2000. Feeding the World: A challenge for the Twenty-First Century. The MIT Press, Cambridge, Massachusetts, London, England.

Solomon, P., Cowling, E., Hidy, G., Furiness, C., 2000. Comparison of scientific findings from major ozone field studies in North America and Europe. Atmospheric Environment 34, 1885–1920.

Steiner, A.L., Davis, A.J., Sillman, S., Owen, R.C., Michalak, A.M., Fiore, A.M., 2010. Observed suppression of ozone formation at extremely high temperatures due to chemical and biophysical feedbacks. Proceedings of National Academy of Science USA 107,19685–19690.

Stockwell, W.R., Middleton, P., Chang, J.S., Tang, X., 1990. The second-generation regional acid deposition model chemical mechanism for regional air quality modeling. Journal of Geophysical Research 95, 16343–16367.

Stohl, A., 1998. Computation, accuracy and applications of trajectories: a review and bibliography. Atmospheric Environment 32, 947–966.

Streets, D.G., Hao, J., Wu, Y., Jiang, J., Chan, M., Tian, H., Feng, X., 2005. Anthropogenic mercury emissions in China. Atmospheric Environment 39, 7789–7806.

Streets, D.G., Waldhoff, S.T., 2000. Present and future emissions of air pollutants in China: SO_2, NO_x and CO. Atmospheric Environment 34, 363–374.

Streets, D.G., Yarber, K.F.,Woo, J.H., and Carmichael, G.R.,2003. Biomass burning in Asia: annual and seasonal estimates and atmospheric emissions. Global Biogeochemical Cycles 17, doi:10.1029/2003GB002040.

Sudo, K., Takahashi, M., Akimoto, H., 2002a. CHASER: A global chemical model of the troposphere 2. Model results and evaluation. Journal of Geophysical Research 107, D21, 4586, doi:10.1029/2001JD001114.

Sudo, K., Takahashi, M., Kurokawa, J., Akimoto, H., 2002b. CHASER: A global chemical model of the troposphere 1. Model description. Journal of Geophysical Research 107, D17, 4339, doi:10.1029/2001JD001113.

Suthawaree, J., Kato, S., Takami, A., Kadena, H., Toguchi, M., Yogi, K., Hatakeyama, S., and Kajii, Y., 2008. Observation of ozone and carbon monoxide at Cape Hedo, Japan: Seasonal variation and influence of long-range transport. Atmospheric Environment 42, 2971–2981.

Takigawa, M., Niwano, M., Akimoto, H., Takahashi, M., 2007. Development of a one–way nested global–regional air quality forecasting model. SOLA 3, 81–84.

Takigawa, M., Niwano, M., Akimoto, H., Takahashi, M., and Kobayashi, K., 2009. Projection of surface ozone over East Asian in 2020. Journal of Agricultural Meteorology 65, 161–166.

Takigawa, M., Sudo, K., Akimoto, H., Kita, K., Takegawa, N., Kondo, Y., Takahashi, M., 2005. Estimation of the contribution of intercontinental transport during PEACE campaign by using a global model. Journal of Geophysical Research 110, D21313, doi:10.1029/2005JD006226.

Tanimoto, H., 2009. Increase in springtime tropospheric ozone at a mountainous site in Japan for the period 1998–2006. Atmospheric Environment 43, 1358– 1363.

Teixeira, E., Fischer, G., van Velthuizen, H., van Dingenen, R., Dentener, F., Mills, G., Walter, C., and Ewert, F., 2011. Limited potential of crop management for mitigating surface ozone impacts on global food supply. Atmospheric Environment 45, 2569–2576.

The Royal Society, 2008. Ground-level ozone in the 21st century: future trends, impacts and policy implications. Science Policy Report 15/08. The Royal Society, London.

Tingey, D.T., Hogsett, W.E., Lee, E.H., Herstrom, A.A., Azevedo, S.H., 1991. An evaluation of various alternative ambient ozone standards based on crop yield loss data. In: Bergland, R.L., Lawson, D.R., McKee, D.J. (Eds.), Tropospheric Ozone and the Environment, Journal of the Air and Waste Management Association, Pittsburgh, pp. 272–288.

Tu, J., Xia, Z., Wang, H., and Li, W., 2007. Temporal variations in surface ozone and its precursors and meteorological effects at an urban site in China. Atmospheric Research 85, 310–337.

Uddling, J., Gunthardt-Goerg, M.S., Matyssek, R., Oksanen., E., Pleijel, H., Sellden G., Karlsson, P.E., 2004. Biomass reduction of juvenile birch is more strongly related to stomatal uptake of ozone than to indices based on external exposure. Atmospheric Environment 38, 4709–4719.

Uddling, J., Pleijel, H., 2006. Changes in stomatal conductance and net photosynthesis during phenological development in spring wheat: implications for gas exchange modelling. International Journal of Biometeorology 51, 37-48.

United Nations Environment Programme (UNEP) and the Center for Clouds, Chemistry and Climate (C^4), 2002. The Asian Brown Cloud: Climate and Other Environmental Impacts UNEP, Nairobi. ISBN 92-807-2240-9, available at:

http://www.rrcap.ait.asia/abc/pub.cfm

Unsworth, M.H., Geissler, P., 1992. Results and achievements of the European Open Top Chamber Network. In: Jäger, H.J., Unsworth, M., De Temmerman, L., Mathy, P. (Eds.), Effects of Air Pollution on Agricultural Crops in Europe Air Pollution Research Report 46.

Vestreng, V., 2001. Emission data reported to UNECE/EMEP: Evaluation of spatial distribution of emissions. EMEP/MSC-W Note 1/01, Norwegian Meteorological Institute, Oslo.

Vestreng, V., Adams, M., and Goodwin, J.: Inventory review 2004: Emission data reported to CLRTAP and under the NEC directive, EMEP/MSC-W status report 1/04, The Norwegian Meteorological Institute, Oslo, Norway, 2004.

Van Aardenne, J.A., Carmichael, G.R., Levy, H., Streets, D.G., and Hordijk, L., 1999. Anthropogenic NO_x emissions in Asia in the period 1990– 2020. Atmospheric Environment 33, 633–646.

Van Dingenen, R., Dentener, F.J., Raes, F., Krol, M.C., Emberson, L., Cofala, J., 2009. The global impact of ozone on agricultural crop yields under current and future air quality legislation. Atmospheric Environment 43, 604–618.

Vingarzan, R., 2004. A review of surface ozone background levels and trends. Atmospheric Environment 38, 3431–3442.

Volk, M., Geissmann, M., Blatter, A., Contat, F., Fuhrer, J., 2003. Design and performance of a free-air exposure system to study long-term effects of ozone on grasslands. Atmospheric Environment 37, 1341–1350.

Wahid, A., Maggs, R., Shamsi, S.R.A., Bell, J.N.B., Ashmore, M.R., 1995. Air pollution and its impacts on wheat yield in the Pakistan Punjab. Environmental Pollution 88, 147–154.

Wang, H., Kiang, C.S., Tang, X., Zhou, X., and Chameides, W.L., 2005. Surface ozone: A likely threat to crops in Yangtze delta of China. Atmospheric

Environment 39, 3843–3850.

Wang, H., Zhou, L., and Tang, X., 2006. Ozone concentrations in rural regions of the Yangtze Delta in China. Journal of Atmospheric Chemistry 54, 255–265.

Wang, S., Xing, J., Chatani, S., Hao, J., Klimont, Z., Cofala, J., Amann, M., 2011. Verification of anthropogenic emissions of China by satellite and ground observations. Atmospheric Environment 45, 6347–6358.

Wang, T., Cheung, V.T.F., Anson, M., and Li, Y., 2001. Ozone and related gaseous pollutants in the boundary layer of eastern China: Overview of the recent measurements at a rural site. Geophysical Research Letters 28, 2373–2376.

Wang, T., Wei, X., Ding, A., Poon, C.N., Lam, K.S., Li, Y., Chan, L., and Anson, M., 2009a. Increasing surface ozone concentrations in the background atmosphere of Southern China, 1994–2007. Atmospheric Chemistry and Physics 9, 6217–6227.

Wang, X., Manning, W.J, Feng, Z., Zhu, Y., 2007a. Ground-level ozone in China: distribution and effects on crop yields. Environmental Pollution 147, 394–400.

Wang, X., Mauzerall, D.L., 2004. Characterizing distributions of surface ozone and its impact on grain production in China, Japan and South Korea: 1990 and 2020. Atmospheric Environment, 38, 4383–4402.

Wang, X., Zheng, Q., Feng, Z., Xie, J., Feng, Z., Ouyan, Z., Manning, W.J., 2008a. Comparison of a diurnal vs steady state ozone exposure profile on growth and yield of oilseed rape (Brassica napus L.) in open-top chambers in the Yangtze Delta, China. Environmental Pollution 156, 449–453.

Wang, X., Zheng, Q., Yao, F., Chen, Z., Feng, Z., Manning, W.J., 2007b. Assessing the impact of ambient ozone on growth and yield of a rice (*Oryza sativa* L.) and a wheat (*Triticum aestivum* L.) cultivar grown in the Yangtze Delta, China, using three rates of application of ethylenediurea (EDU). Environmental Pollution 148, 390–395.

Wang, X., Zhang, Q., Zheng, F., Zheng, Q., Yao, F., Zhan, C., Zhang, W., Hou, P.,

Feng, Z., Song, W., Feng, Z., Lu, F., 2012a. Effects of elevated O_3 concentration on winter wheat and rice yields in the Yangtze River Delta, China. Environmental Pollution 171, 118–125.

Wang, Y., Hao, J., McElroy, M.B., Munger, J.W., Ma, H., Chen, D., and Nielsen, C.P., 2009b. Ozone air quality during the 2008 Beijing Olympics: effectiveness of emission restrictions. Atmospheric Chemistry and Physics 9, 5237–5251.

Wang, Y., Hao, J., Mcelroy, M.B., Munger, J.W., Ma, H., Nielsen, C.P., Zhang, Y., 2010. Year round measurements of O_3 and CO at a rural site near Beijing: variations in their correlations. Tellus 62B, 228–241.

Wang, Y., McElroy, M.B., Munger, J.W., Hao, J., Ma, H., Nielsen, C.P., and Chen, D., 2008b. Variations of O_3 and CO in summertime at a rural site near Beijing. Atmospheric Chemistry and Physics 8, 6355–6363.

Wang, Y., Yang, L., Han, Y., Zhu, J., Kobayashi, K., Tang, H., Wang, Y., 2012b. The impact of elevated tropospheric ozone on grain quality of hybrid rice: A free-air gas concentration enrichment (FACE) experiment. Field Crops Research 129, 81–89.

Wang, Y., Yang, L., Kobayashi, K., Zhu, J., Chen, C.P., Yang, K., Tang, H., Wang, Y., 2012c. Investigations on spikelet formation in hybrid rice as affected by elevated tropospheric ozone concentration in China. Agriculture, Ecosystems and Environment 150, 63–71.

World Bank, 2007. World Development Report 2008: Agriculture for Development (World Bank, Washington DC).

Xu, W., Zhao, C., Ran, L., Deng, Z., Liu, P., Ma, N., Lin, W., Xu, X., Yan, P., He, X., Yu, J., Liang, W., Chen, L., 2011. Characteristics of pollutants and their correlation to meteorological conditions at a suburban site in the North China Plain. Atmospheric Chemistry and Physics 11, 4353–4369.

Xu, X., Lin, W., Wang, T., Yan, P., Tang, J., Meng, Z., Wang, Y., 2008. Long-term

trend of surface ozone at a regional background station in eastern China 1991–2006: enhanced variability. Atmospheric Chemistry and Physics 8, 2595–2607.

Xue, Y., Xu, H., Mei, L., Guang, J., Guo, J., Li, Y., Hou, T., Li, C., Yang, L., and He, X., 2012. Merging aerosol optical depth data from multiple satellite missions to view agricultural biomass burning in Central and East China. Atmospheric Chemistry and Physics 12, 10461–10492.

Yamaji, K., Li, J., Uno, I., Kanaya, Y., Irie, H., Takigawa, M., Komazaki, Y., Pochanart, P., Liu, Y., Tanimoto, H., Ohara, T., Yan, X., Wang, Z., and Akimoto, H., 2010. Impact of open crop residual burning on air quality over Central Eastern China during the Mount Tai Experiment 2006 (MTX2006). Atmospheric Chemistry and Physics 10, 7353–7368.

Yamaji, K., Ohara, T., Uno, I., Kurokawa, J., Pochanart, P., and Akimoto, H., 2008. Future prediction of surface ozone over east Asia using Models-3 Community Multiscale Air Quality Modeling System and Regional Emission Inventory in Asia. Journal of Geophysical Research 113, D08306, doi:10.1029/2007JD008663.

Yao, F.F., Wang, X.K., Lu, F., Feng, Z.W., Ouyang, Z.Y., 2008. Assessing the impact of ambient ozone on crop ecosystem: a case study in Yangtze Delta, China. Asian Journal of Ecotoxicology (in Chinese) 3, 189–195.

Zeng, G., Pyle, J.A., Young, P.J., 2008. Impact of climate change on tropospheric ozone and its global budgets. Atmospheric Chemistry and Physics 8, 369–387.

Zhan, C., Wang, X., Feng, Z., Zheng, F., Duan, X., Yang, W., 2008. Effects of elevated ozone on growth and yield of field-grown rice in Yangtze River Delta, China. Journal of Environmental Sciences 20, 320–325.

Zhang, Q., Geng, G., Wang, S., Richter, A., He, K., 2012. Satellite remote sensing of changes in NO_x emissions over China during 1996–2010. Chinese Science Bulletin 57, 2857–2864.

Zhang, Q., Streets, D.G., He, K., Wang, Y., Richter, A., Burrows, J.P., Uno, I., Jang, C.J., Chen, D., Yao, Z., Lei, Y., 2007. NO_x emission trends for China, 1995–2004: The view from the ground and the view from space. Journal of Geophysical Research 112, D22306, doi:10.1029/2007JD008684.

Zhao, C., Wang, Y., and Zeng, T., 2009. East China Plains: A “Basin” of Ozone Pollution. Environmental Science & Technology 43, 1911–1915.

Zhao, M., Running, S.W., Nemani, R.R., 2006. Sensitivity of Moderate Resolution Imaging Spectroradiometer (MODIS) terrestrial primary production to the accuracy of meteorological reanalyses. Journal of Geophysical Research 111, G01002, doi:10.1029/2004JG000004.

Zheng, J., Zhong, L., Wang, T., Louie, P.K.K., Li, Z., 2010. Ground-level ozone in the Pearl River Delta region: Analysis of data from a recently established regional air quality monitoring network. Atmospheric Environment 44, 814–823.

Zhu, X., Feng, Z., Sun, T., Liu, X., Tang, H., Zhu, J., Guo, W., Kobayashi, K., 2011. Effects of elevated ozone concentration on yield of four Chinese cultivars of winter wheat under fully open-air field conditions. Global Change Biology 17, 2697–2706.

APPENDIX

Table A1 Aggregate wheat production loss (WPL) in 2000 estimated by different O_3 dose metrics for each province of China. The relative yield loss (RYL) is shown in parentheses.

	WPL (10^4 metric tons) and RYL (%) in 2000			
	90-days AOT40	75-days AOT40	POD_6	POD_{12}
Heilongjiang	1.6 (0.6%)	1.7 (0.6%)	1.0 (0.4%)	3.6 (1.3%)
Jilin	0.4 (2.6%)	0.5 (2.8%)	0.2 (1.4%)	1.0 (5.8%)
Liaoning	2.3 (3.7%)	2.5 (4.1%)	2.7 (4.4%)	5.8 (8.9%)
Inner mongolia	2.5 (0.9%)	3.0 (1.1%)	13.2 (4.6%)	5.2 (1.9%)
Hebei	100.3 (7.3%)	111.8 (8.0%)	249.7 (16.3%)	180.4 (12.3%)
Beijing	11.5 (10.7%)	13.6 (12.5%)	25.9 (21.3%)	20.7 (17.8%)
Tianjin	6.5 (8.3%)	7.1 (9.1%)	10.0 (12.3%)	11.4 (13.7%)
Chongqing	0.7 (0.7%)	0.8 (0.8%)	3.3 (3.0%)	2.4 (2.2%)
Shandong	151.2 (6.7%)	173.9 (7.6%)	416.0 (16.4%)	271.8 (11.4%)
Jiangsu	138.5 (11.5%)	169.8 (13.7%)	328.2 (23.5%)	247.7 (18.8%)
Anhui	74.0 (8.0%)	85.1 (9.1%)	219.6 (20.5%)	120.6 (12.4%)
Henan	185.1 (7.5%)	205.8 (8.2%)	473.2 (17.1%)	269.6 (10.5%)
Shanghai	5.3 (12.1%)	6.6 (14.6%)	10.0 (20.7%)	11.3 (22.7%)
Zhejiang	8.8 (10.9%)	10.1 (12.3%)	13.5 (15.8%)	13.1 (15.4%)
Shanxi	17.7 (6.2%)	19.4 (6.8%)	37.7 (12.4%)	27.5 (9.3%)
Hubei	27.7 (8.3%)	31.0 (9.2%)	51.1 (14.4%)	34.5 (10.2%)
Jiangxi	0.5 (5.0%)	0.6 (5.4%)	1.0 (9.2%)	0.7 (6.9%)
Fujian	0.4 (2.9%)	0.4 (2.8%)	0.3 (1.8%)	0.4 (2.8%)
Guangdong	0.4 (7.7%)	0.4 (7.7%)	0.3 (6.1%)	0.4 (8.7%)
Hunan	0.3 (1.2%)	0.3 (1.3%)	1.0 (4.4%)	0.5 (2.3%)
Shaanxi	12.9 (3.1%)	13.6 (3.2%)	39.3 (8.8%)	23.2 (5.4%)
Guangxi	0.0 (0.8%)	0.0 (0.8%)	0.1 (2.3%)	0.0 (0.8%)
Guizhou	0.7 (0.6%)	0.7 (0.6%)	2.3 (2.1%)	1.2 (1.1%)
Sichuan	9.3 (1.7%)	10.3 (1.9%)	19.9 (3.5%)	21.2 (3.8%)
Yunan	1.3 (0.8%)	1.3 (0.8%)	1.3 (0.8%)	2.4 (1.5%)
Gansu	6.8 (2.1%)	7.5 (2.3%)	36.9 (10.3%)	12.4 (3.7%)
Ningxia	1.3 (1.7%)	1.5 (1.9%)	8.1 (9.4%)	3.2 (3.9%)
Qinghai	1.8 (2.9%)	1.7 (2.8%)	6.0 (9.1%)	3.6 (5.8%)
Xinjiang	4.3 (1.0%)	4.4 (1.0%)	23.2 (5.1%)	3.2 (0.7%)
Tibet	3.9 (11.1%)	3.0 (8.9%)	0.0 (0.0%)	2.2 (6.6%)
Whole China	777.9 (6.4%)	888.6 (7.2%)	1995.1 (14.9%)	1301.2 (10.3%)

Table A2 Aggregate wheat production loss (WPL) in 2020 estimated by different O_3 dose metrics for each province of China. The relative yield loss (RYL) is shown in parentheses.

	WPL (10^4 metric tons) and RYL (%) in 2020			
	90-days AOT40	75-days AOT40	POD_6	POD_{12}
Heilongjiang	7.7 (2.7%)	8.6 (3.0%)	2.9 (1.0%)	14.0 (4.9%)
Jilin	1.1 (6.9%)	1.3 (7.6%)	0.4 (2.4%)	2.0 (11.7%)
Liaoning	4.9 (8.0%)	5.5 (9.0%)	4.4 (7.1%)	10.3 (15.9%)
Inner mongolia	8.9 (3.2%)	10.6 (3.9%)	24.6 (8.6%)	15.4 (5.5%)
Hebei	170.4 (12.3%)	194.8 (14.0%)	341.7 (22.3%)	260.7 (17.8%)
Beijing	18.6 (17.4%)	22.0 (20.1%)	33.6 (27.7%)	28.5 (24.6%)
Tianjin	9.7 (12.4%)	11.0 (13.9%)	13.3 (16.3%)	15.1 (18.2%)
Chongqing	7.8 (7.3%)	8.3 (7.8%)	9.0 (8.2%)	14.6 (13.5%)
Shandong	324.7 (14.3%)	373.8 (16.3%)	632.1 (24.9%)	467.0 (19.5%)
Jiangsu	257.3 (21.3%)	315.0 (25.4%)	444.7 (31.8%)	387.8 (29.4%)
Anhui	184.2 (19.9%)	211.6 (22.6%)	335.7 (31.3%)	244.8 (25.2%)
Henan	447.4 (18.1%)	499.6 (20.0%)	763.0 (27.6%)	540.4 (21.1%)
Shanghai	8.9 (20.4%)	11.0 (24.5%)	13.9 (28.7%)	15.0 (30.1%)
Zhejiang	22.9 (28.2%)	26.3 (31.9%)	24.9 (29.0%)	25.9 (30.3%)
Shanxi	46.9 (16.5%)	50.9 (17.8%)	65.4 (21.5%)	54.6 (18.6%)
Hubei	84.4 (25.4%)	92.7 (27.6%)	97 (27.3%)	87.1 (25.7%)
Jiangxi	2.1 (20.4%)	2.2 (22.0%)	2.4 (22.5%)	2.3 (21.9%)
Fujian	2.4 (15.9%)	2.4 (16.2%)	0.9 (6.0%)	2.5 (17.0%)
Guangdong	1.3 (27.8%)	1.3 (28.3%)	0.7 (14.6%)	1.5 (30.6%)
Hunan	2.0 (9.1%)	2.1 (9.4%)	2.9 (12.5%)	2.9 (13.0%)
Shaanxi	54.0 (12.9%)	56.4 (13.5%)	77.8 (17.5%)	64.6 (15.1%)
Guangxi	0.2 (6.4%)	0.2 (6.4%)	0.2 (6.8%)	0.2 (8.3%)
Guizhou	7.9 (7.3%)	8.2 (7.6%)	6.5 (5.9%)	11.9 (10.9%)
Sichuan	58.4 (10.6%)	61.5 (11.1%)	51.4 (9.1%)	85.7 (15.2%)
Yunan	5.0 (3.1%)	5.1 (3.2%)	2.9 (1.8%)	8.7 (5.4%)
Gansu	30.7 (9.4%)	34.2 (10.4%)	63.7 (17.8%)	40.1 (12.1%)
Ningxia	6.0 (7.6%)	7.0 (8.7%)	14.6 (16.9%)	9.8 (12.0%)
Qinghai	5.2 (8.5%)	5.5 (8.9%)	9.6 (14.7%)	7.3 (11.6%)
Xinjiang	8.8 (2.0%)	9.1 (2.1%)	35.1 (7.7%)	6.9 (1.6%)
Tibet	4.4 (12.5%)	3.5 (10.3%)	0.0 (0.0%)	2.6 (7.8%)
Whole China	1794.2 (14.7%)	2041.7 (16.6%)	3075.1 (23.0%)	2430.2 (19.2%)

Table A3 Aggregate wheat production loss (WPL) in 2000 estimated by different O_3 dose metrics for each state of India. The relative yield loss (RYL) is shown in parentheses.

	WPL (10^4 metric tons) and RYL (%) in 2000			
	90-days AOT40	75-days AOT40	POD_6	POD_{12}
Uttar Pradesh	158.8 (6.4%)	163.2 (6.6%)	647.0 (21.8%)	165.4 (6.7%)
Madhya Pradesh	12.1 (1.4%)	12.6 (1.5%)	129.7 (13.5%)	13.7 (1.6%)
Rajasthan	4.2 (0.6%)	4.8 (0.7%)	64.0 (8.5%)	6.9 (1.0%)
Bihar	21.4 (5.5%)	24.1 (6.2%)	101.5 (20.9%)	25.1 (6.6%)
West Bengal	8.4 (9.5%)	9.3 (10.5%)	30.5 (27.7%)	14.1 (15.0%)
Assam	0.1 (0.1%)	0.1 (0.1%)	5.2 (5.4%)	0.0 (0.0%)
Orissa	0.0 (1.2%)	0.0 (1.4%)	0.1 (15.8%)	0.0 (1.6%)
Gujarat	10.4 (5.0%)	10.8 (5.2%)	45.4 (18.9%)	14.2 (6.8%)
Maharashtra	2.7 (2.4%)	2.7 (2.4%)	25.0 (18.3%)	4.3 (3.7%)
Haryana	99.9 (10.4%)	107.8 (11.1%)	329.5 (27.7%)	147.1 (14.6%)
Punjab	304.3 (17.4%)	343.7 (19.2%)	641.6 (30.7%)	360.8 (20.0%)
Karnataka	0.1 (0.8%)	0.1 (0.7%)	2.9 (15.0%)	0.3 (1.8%)
Himachal Pradesh	14.2 (18.1%)	16.2 (20.1%)	18.5 (22.4%)	12.3 (16.1%)
Jammu & Kashmir	2.7 (7.4%)	3.5 (9.5%)	8.7 (23.9%)	4.6 (12.5%)
Whole India	639.3 (8.2%)	698.8 (8.9%)	2049.7 (22.3%)	768.7 (9.7%)

Table A4 Aggregate wheat production loss (WPL) in 2020 estimated by different O_3 dose metrics for each state of India. The relative yield loss (RYL) is shown in parentheses.

	WPL (10^4 metric tons) and RYL (%) in 2020			
	90-days AOT40	75-days AOT40	POD_6	POD_{12}
Uttar Pradesh	319.0 (12.9%)	333.8 (13.5%)	801.7 (27.0%)	314.8 (12.7%)
Madhya Pradesh	47.7 (5.6%)	49.6 (5.9%)	203.5 (21.1%)	51.7 (6.1%)
Rajasthan	19.9 (2.9%)	21.5 (3.1%)	116.9 (15.5%)	18.0 (2.6%)
Bihar	57.5 (14.3%)	65.2 (16.1%)	137.5 (27.9%)	63.5 (16.1%)
West Bengal	16.9 (19.2%)	18.8 (21.1%)	36.4 (33.1%)	24.1 (25.7%)
Assam	0.3 (0.4%)	0.3 (0.4%)	9.6 (10.1%)	0.2 (0.3%)
Orissa	0.0 (6.1%)	0.0 (6.7%)	0.1 (23.5%)	0.0 (8.1%)
Gujarat	26.4 (12.8%)	27.5 (13.4%)	64.1 (26.6%)	34.7 (16.6%)
Maharashtra	10.0 (8.8%)	10.2 (8.9%)	36.1 (26.4%)	14.0 (12.1%)
Haryana	177.0 (18.4%)	191.9 (19.8%)	383.1 (32.2%)	219.9 (21.8%)
Punjab	488.0 (27.9%)	548.5 (30.6%)	721.5 (34.5%)	503.8 (27.9%)
Karnataka	0.8 (4.7%)	0.8 (4.7%)	4.5 (23.2%)	1.2 (7.2%)
Himachal Pradesh	19.8 (25.3%)	22.6 (28.2%)	20.8 (25.1%)	16.3 (21.4%)
Jammu & Kashmir	5.6 (15.2%)	6.6 (18.0%)	10.0 (27.3%)	8.6 (23.6%)
Whole India	1188.9 (15.3%)	1297.3 (16.6%)	2545.7 (27.7%)	1270.9 (16.1%)

THANKS FOR YOUR TIME!